U.PORTO

DOUTORAMENTO

FARMACOLOGIA E FARMACOTERAPIA

Preclinical Pharmacology of Novel Palladium-Based Antineoplastic Agents for Triple-Negative Breast Cancer

Martin Vojtek

D

2023

U.PORTO

Martin Vojtek. Preclinical Pharmacology of Novel Palladium-Based Antineoplastic Agents for Triple-Negative Breast Cancer

D.FFUP **2023**

Preclinical Pharmacology of Novel Palladium-Based Antineoplastic Agents for Triple-Negative Breast Cancer

Martin Vojtek

FACULDADE DE FARMÁCIA

U.PORTO
FACULDADE DE FARMÁCIA
UNIVERSIDADE DO PORTO

Preclinical Pharmacology of Novel Palladium-Based Antineoplastic Agents for Triple-Negative Breast Cancer

Martin Vojtek

Thesis of the 3rd Cycle of Studies Leading to the Doctoral Degree in Pharmaceutical Sciences – Specialty in Pharmacology and Pharmacotherapy

Work carried out under the supervision of:

Assistant Professor Carmen Diniz Pereira (supervisor)

Associate Professor Isabel Maria Pinto Leite Viegas Oliveira Ferreira (co-supervisor)

Associate Professor Helder Dias Mota-Filipe (co-supervisor)

Porto

May, 2023

This work was supported by the Portuguese Foundation for Science and Technology (FCT) and PhD Program in Medicines and Pharmaceutical Innovation (i3DU) through PhD Grant PD/BD/135460/2017 and COVID/BD/152492/2022 funded by the European Social Fund of the European Union and national funds FCT/MCTES.

The experimental work presented in this thesis was mainly performed at the Laboratory of Pharmacology of the University of Porto in Portugal. The Pd(II) compounds herein used were synthesized and characterized by the Molecular-Physical Chemistry R&D Group, Department of Chemistry, University of Coimbra in Portugal.

ACKNOWLEDGMENTS

I would like to take this opportunity to express my sincere gratitude to all those who have supported me throughout my research journey and took part in this chapter of my life.

Firstly, I would like to thank my supervisor, Professor Carmen Diniz, for her invaluable guidance, support, and encouragement. Her knowledge and insights have been instrumental in shaping this research project and helped me to navigate the challenges along the way. I am grateful for her patience, positivity, understanding and mentorship throughout all these years.

I would also like to extend my profound thanks to my co-supervisors, Professor Isabel M.P.L.V.O. Ferreira and Professor Helder Mota-Filipe, for their valuable contributions to this research. Their support and expertise have stimulated me with a broader perspective and enriched my scientific and professional outlook.

Many thanks also go out to Professor M.P.M. Marques who synthesised and characterised studied compounds, and thus made this project possible.

I sincerely thank to all my lab colleagues: Rita, Ana Filipa, Margarida, Dany, Rui, Liliana, Angela, Joana, Ana Lúcia, Tatiana, Dr. Miguel, Júlio, Edgar and Olga for their friendship, support, and collaboration. Their insights and contributions have been invaluable, and I am grateful for the stimulating and supportive research environment they have created. I also thank Anabela, Céu, Mónica, Margarida and Cátia that helped me to solve multiple challenges I have faced during my research and for providing me with their never-ending support.

I would like to extend my heartfelt thanks to many caring people that are part of my life: Pedro Pinto, Pedro Medeiros, José Águeda, Pedro Silva, Matias, Salomé, Bruno, Francisca, Sara, Riemer, Duarte, Daniel, Luís, Sofia, Martina, Lucka, Romana, Afonso, Mârcia and Jasmine. Thank you all for your friendship, inspiration, cheers, and enduring support that accompanied this journey.

I thank my parents, my grandparents, my sister and my brother-in-law for their unwavering love and endless support throughout all my life. Their encouragement and understanding were instrumental in my success.

Thank you all!

ABSTRACT

Breast cancer is a leading cancer among women and is responsible for 1 in 6 of all cancer deaths worldwide. By 2040, the incidence of new breast cancer cases is projected grow by 40%, reaching 3 million of new cases every year. Triple-negative breast cancer (TNBC) constitutes 10-30% of all breast cancer cases and is considered one of the most aggressive and fatal forms. Chemotherapy with platinum-(Pt)-based chemotherapeutics, such as cisplatin and carboplatin, is a common backbone for TNBC treatment but their indiscriminatory toxicity and loss of activity due to cancer drug resistance limit their effectivity. Therefore, treatment of TNBC still constitutes an unmet medical need to be addressed. One promising approach for the development of new TNBC treatments is focused on novel palladium-(Pd)-based compounds that share coordination chemistry with Pt-based compounds but present superior characteristics regarding their safety and resistance profiles.

This thesis aimed to evaluate the therapeutic potential of two new multi-nuclear Pd-based compounds with biogenic polyamine, Pd_2Spm (Spm=spermine) and Pd_3Spd_2 (Spd=spermidine), as promising drug candidates for TNBC. The study was conducted using *in vitro*, *in ovo* and *in vivo* models to determine the anticancer effects compared to reference Pt drug, cisplatin. The *in vitro* screening studies were performed in MDA-MB-231 cells, Pt-resistant MDA-MB-231/R cells, and non-neoplastic breast MCF-12A cells to select most promising Pd compound regarding antiproliferative activity, ability to overcome resistance to Pt drugs and selectivity. Various putative pharmacological targets were assessed aiming to provide mechanistic clues on action of the most promising Pd-based. *In vivo* studies in mice were also conducted to evaluate the pharmacokinetics and *in vivo* antitumour efficacy of selected Pd compound.

The *in vitro* results demonstrated that both Pd_2Spm and Pd_3Spd_2 elicit similar antiproliferative effects in Pt-sensitive (Pd_2Spm IC_{50}: 7.3–8.3 μM and Pd_3Spd_2 IC_{50}: 7.9–8.4 μM) and Pt-resistant (Pd_2Spm IC_{50}: 11.3–12.1 μM and Pd_3Spd_2 IC_{50}: 10.6–13.3 μM) TNBC cells. Pd_2Spm showed superior selectivity index (>7.9) towards cancer cells with lower impact on non-neoplastic cells than Pd_3Spd_2. For this reason, further focus of this work was given to Pd_2Spm.

A fast, reliable, and cost-effective alternative to microwave-assisted digestion was developed and validated for ICP-MS quantification of the Pd/Pt content in animal tissues and biofluids (LODs of 0.001 μg/L and accuracy > 95% for all biologic matrices except adipocyte tissue). Applying this methodology, Pd_2Spm showed excellent *in vivo* therapeutic

application due to higher terminal half-life of free Pd in serum and lower accumulation in tissues (except for the kidney) as compared to cisplatin. Additionally, Pd_2Spm treatment (5 mg/kg/day, for 5 consecutive days) has reduced the tumour growth by 43.3% compared to vehicle-treated animals and was coupled to minimal systemic toxicity. Cisplatin-treated animals (2 mg/kg/day, for 5 consecutive days), on the other hand, reduced tumour volume by 56.6% but has caused weight loss, diarrhoea and haematotoxicity.

While Pd_2Spm and cisplatin induced similar reduction of cancer invasiveness and *in vivo* tumour growth, the two compounds do not share same mechanism of action. Mechanistically, ERK 1/2 activation and autophagy were triggered by Pd_2Spm differently to cisplatin and seem to contribute to cell death mechanisms in both sensitive and resistant cells treated with this Pd agent.

Altogether, findings of this preclinical study constitute the first *in vivo* evidence and proof-of-principle of therapeutic potential of Pd_2Spm as a novel chemotherapeutic for TNBC given its different mode of action, superior selectivity, ability to overcome resistance, and minimal toxicity compared to cisplatin. Moreover, the study provided insights into mechanism of action of Pd_2Spm and established a foundation for further investigation and development of palladium compounds with biogenic polyamines for the treatment of TNBC and its Pt-resistant forms.

Keywords: TNBC, Pd(II)-based complexes, cisplatin, *in vivo*, antitumoral

RESUMO

O cancro da mama é um dos principais cancros entre as mulheres e é responsável por 1 em cada 6 mortes por cancro em todo o mundo. Em 2040, prevê-se que a incidência de novos casos de cancro da mama aumente em 40%, atingindo 3 milhões de novos casos por ano. O cancro da mama triplo-negativo (TNBC) constitui 10-30% de todos os casos de cancro da mama e é considerado uma das formas mais agressivas e fatais. A quimioterapia com quimioterápicos baseados em platina (Pt), como a cisplatina e a carboplatina, é uma abordagem comum para o tratamento de TNBC, mas a sua toxicidade indiscriminatória e a perda de atividade devido à resistência a fármacos limitam a sua efetividade. Portanto, o tratamento de TNBC ainda constitui uma necessidade médica a ser abordada. Uma abordagem promissora para o desenvolvimento de novos tratamentos para TNBC concentra-se em compostos novos à base de paládio (Pd) que compartilham a química de coordenação com compostos à base de Pt, mas apresentam características superiores em relação à sua segurança e perfis de resistência.

Esta tese teve como objetivo avaliar o potencial terapêutico de dois novos compostos multinucleares à base de Pd com poliamina biogénica, Pd_2Spm (Spm = espermina) e Pd_3Spd_2 (Spd = espermidina), como promissores candidatos a fármacos para TNBC. O estudo foi conduzido utilizando modelos *in vitro, in ovo* e *in vivo* para determinar os efeitos anticancerígenos em comparação com a droga de referência à base de Pt, a cisplatina. Os estudos de *screening in vitro* foram realizados em células MDA-MB-231, células MDA-MB-231/R resistentes à Pt e células mamárias não neoplásicas MCF-12A para selecionar o composto Pd mais promissor em relação à atividade antiproliferativa, capacidade de superar a resistência aos fármacos à base de Pt e seletividade. Foram avaliados vários alvos farmacológicos putativos com o objetivo de fornecer indicações mecanísticas sobre a ação do composto à base de Pd mais promissor. Estudos *in vivo* em ratos também foram realizados para avaliar a farmacocinética e a eficácia antitumoral *in vivo* do composto Pd selecionado.

Os resultados *in vitro* demonstraram que tanto Pd_2Spm quanto Pd_3Spd_2 provocam efeitos antiproliferativos semelhantes em células TNBC sensíveis à Pt (IC_{50} de Pd_2Spm: 7,3-8,3 µM e IC_{50} de Pd_3Spd_2: 7,9-8,4 µM) e resistentes à Pt (IC_{50} de Pd_2Spm: 11,3-12,1 µM e IC_{50} de Pd_3Spd_2: 10,6-13,3 µM). Pd_2Spm demonstrou um índice de seletividade superior (> 7,9) para células cancerosas com um impacto menor em células não neoplásicas do que Pd_3Spd_2. Por esta razão, este trabalho concentrou-se mais em Pd_2Spm.

Foi desenvolvida e validada uma alternativa rápida, fidedigna e económica à digestão assistida por micro-ondas para a quantificação por ICP-MS do teor de Pd/Pt em tecidos animais e biofluídos (LODs de 0,001 µg/L e precisão> 95% para todas as matrizes biológicas, exceto tecido adiposo). Aplicando esta metodologia, Pd_2Spm mostrou excelente aplicação terapêutica *in vivo* devido a uma meia-vida terminal mais alta do Pd livre no soro e uma menor acumulação nos tecidos (exceto no rim) em comparação com a cisplatina. Além disso, o tratamento com Pd_2Spm (5 mg/kg/dia, por 5 dias consecutivos) reduziu o crescimento tumoral em 43,3% em comparação com animais tratados com veículo e foi associado a toxicidade sistêmica mínima. Os animais tratados com cisplatina (2 mg/kg/dia, por 5 dias consecutivos), por outro lado, reduziram o volume tumoral em 56,6%, mas causaram perda de peso, diarreia e hematotoxicidade nestes animais.

Embora Pd_2Spm e cisplatina induzam uma redução similar da invasividade do cancro e do crescimento tumoral *in vivo*, os dois compostos não compartilham o mesmo mecanismo de ação. Mecanicamente, a ativação do ERK 1/2 e a autofagia foram desencadeadas por Pd_2Spm de forma diferente da cisplatina e parecem contribuir para os mecanismos de morte celular em células sensíveis e resistentes tratadas com este agente de Pd.

Em conjunto, os resultados deste estudo pré-clínico constituem a primeira evidência *in vivo* e fornecem um *proof-of-principle* do potencial terapêutico de Pd_2Spm como uma nova possibilidade quimioterapêutica para TNBC, dada a sua ação diferenciada, seletividade superior, capacidade de superar resistência e toxicidade mínima em comparação com a cisplatina. Além disso, o estudo forneceu indicações sobre o mecanismo de ação do Pd_2Spm e estabeleceu uma base para investigação e desenvolvimento adicional de compostos de paládio com poliaminas biogênicas para o tratamento de TNBC e suas formas resistentes ao Pt.

Palavras-chave: TNBC, complexos baseados em Pd(II), cisplatina, *in vivo*, antitumoral

LIST OF PUBLICATIONS

The author declares that present thesis includes 1 review article and 4 original articles previously published in peer-reviewed international journals, in **chapters I, III, IV**, and **V**. The permission to reproduce the articles were obtained from respective publishers, when required. For the open access journals distributed under the terms and conditions of the Creative Commons Attribution (CC BY) license, the copyright is retained by the author. The author participated in the work conception and design, conducted the experiments, data validation and analysis and wrote the original drafts of all articles included in this thesis.

PUBLICATIONS INCLUDED IN THIS THESIS

Vojtek M, Marques MPM, Ferreira IMPLVO, Mota-Filipe H, Diniz C. Anticancer activity of palladium-based complexes against triple-negative breast cancer. Drug Discovery Today. 2019; 24(4):1044–1058. doi:10.1016/j.drudis.2019.02.012

Vojtek M, Pinto E, Gonçalves-Monteiro S, Almeida A, Marques MPM, Mota-Filipe H, Ferreira IMPLVO, Diniz C. Fast and reliable ICP-MS quantification of palladium and platinum-based drugs in animal pharmacokinetic and biodistribution studies. Analytical Methods. 2020;12(39):4806–4812. doi:10.1039/d0ay01328e

Vojtek M, Gonçalves-Monteiro S, Pinto E, Kalivodová S, Almeida A, Marques MPM, Batista de Carvalho ALM, Martins CB, Mota-Filipe H, Ferreira IMPLVO, Diniz C. Preclinical Pharmacokinetics and Biodistribution of Anticancer Dinuclear Palladium(II)-Spermine Complex (Pd_2Spm) in Mice. Pharmaceuticals. 2021;14(2):173. doi:10.3390/ph14020173

Vojtek M, Gonçalves-Monteiro S, Šeminská P, Valová K, Bellón L, Dias-Pereira P, Marques F, Marques MPM, Batista de Carvalho ALM,, Mota-Filipe H, Ferreira IMPLVO, Diniz C. Pd_2Spermine Complex Shows Cancer Selectivity and Efficacy to Inhibit Growth of Triple-Negative Breast Tumors in Mice. Biomedicines. 2022;10(2):210. doi:10.3390/biomedicines10020210

Vojtek M, Martins CB, Ramos R, Duarte SG, Ferreira IMPLVO, Batista de Carvalho ALM,, Marques MPM, Diniz C. Pd(II) and Pt(II) Trinuclear Chelates with Spermidine: Selective Anticancer Activity towards TNBC-Sensitive and -Resistant to Cisplatin. Pharmaceutics. 2023;15(4):1205. doi:10.3390/pharmaceutics15041205

MANUSCRIPT IN PREPARATION

Vojtek M, Batista de Carvalho ALMB, Ferreira IMPLVO, Mota-Filipe H, Marques MPM, Diniz C. Palladium(II) dinuclear chelate with spermine, Pd_2Spm, overcomes resistance of triple-negative breast cancer cells to platinum(II) drugs through autophagy and involving ERK 1/2 pathway.

ORAL COMMUNICATIONS

Martin Vojtek, Inês Lamego, Edgar Pinto, Agostinho A. Almeida, Isabel M.P.L.V.O. Ferreira, Ana L.M. Batista de Carvalho, M.P.M. Marques, Helder Mota-Filipe, Carmen Diniz. "Anticancer Metal Complexes with Polyamines Against Breast Cancer: Cellular Drug Uptake and Selective Cytotoxicity". XLVIII Annual Meeting of Portuguese Pharmacological Society, XXXVI Clinical Pharmacology, XVII Toxicology. February 5–6 2018, Lisbon, Portugal.

Martin Vojtek, Edgar Pinto, Salomé Gonçalves-Monteiro, Agostinho A. Almeida, Helder Mota-Filipe, Isabel M.P.L.V.O. Ferreira, Carmen Diniz. "Novel cost-effective ICP-MS method for pharmaco-toxicokinetic studies of platinum and palladium-based drugs in variety of animal tissues". XLIX Annual Meeting of Portuguese Pharmacological Society, XXXVII Clinical Pharmacology, XVIII Toxicology. February 6–9 2019, Porto, Portugal.

Martin Vojtek, Salomé Gonçalves-Monteiro, Patrícia Dias-Pereira, Franklim Marques, A.L.M. Batista de Carvalho, M.P.M. Marques, Helder Mota-Filipe, Isabel M.P.L.V.O Ferreira, Carmen Diniz. "Anticancer palladium-spermine complex: In vivo activity against anticancer triple negative breast cancer". L Annual Meeting of Portuguese Pharmacological Society, XXXVIII Clinical Pharmacy, XIX Toxicology. February 5–7 2020, Coimbra, Portugal.

POSTER COMMUNICATIONS

Martin Vojtek, Inês Lamego, Edgar Pinto, Agostinho A. Almeida, Isabel M.P.L.V.O. Ferreira, Ana L.M. Batista de Carvalho, M.P.M. Marques, Hélder Mota-Filipe, Carmen Diniz. Anticancer Metal-Polyamine Complexes Against Breast Cancer. 11th Meeting of Young Researchers – University of Porto. Porto, Portugal, 7–9 February 2018

Martin Vojtek, Salomé Gonçalves-Monteiro, Edgar Pinto, Patrícia Dias-Pereira, Franklim Marques, A.L.M. Batista de Carvalho, M.P.M. Marques, Helder Mota-Filipe, Agostinho Almeida, Isabel M.P.L.V.O Ferreira, Carmen Diniz. Anticancer activity of palladium-spermine complex against triple-negative breast cancer. 8th European Virtual Congress of Pharmacology (EPHAR 2021), Online, 6–8 December 2021.

Martin Vojtek, A.L.M. Batista de Carvalho, M.P.M. Marques, Helder Mota-Filipe, Isabel M.P.L.V.O Ferreira, Carmen Diniz. Palladium-spermine complex (Pd2Spm) triggers autophagy and caspase-independent cell death in triple-negative breast cancer cells. The 8th International Electronic Conference on Medicinal Chemistry (ECMC 2022), Online, 01-30 November 2022.

TABLE OF CONTENTS

LIST OF FIGURES

List of Tables

LIST OF ABBREVIATIONS

ALT	Alanine aminotransferase
ANOVA	Analysis of variance
AST	Aspartate aminotransferase
AUC	Area under the curve
BALB/c	Bagg Albino inbread mice strain
BC	Breast cancer
BRCA	Breast cancer associated
BW	Body weight
ca.	Circa (around)
CAM	Chorioallantoic membrane
CCD	Central composite design
CDK	Cyclin-Dependent Kinase
CK	Cytokeratin
CL/F	Rate of total clearance
C_{max}	Peak plasma concentration
CTR	Copper transporter
DMEM-HG	Dulbecco's Modified Eagle Medium – High Glucose
DMFO	Difluoromethylornithine
DMSO	Dimethyl sulfoxide
DNA	Deoxyribonucleic acid
EC_{50}	Half maximal effective concentration
ECACC	European Collection of Cell Cultures
EDTA	Ethylene diamine tetra acetic acid
EGFR	Epidermal growth factor receptor
EMA	European Medicine Agency
ER	Oestrogen receptor
ERK	Extracellular signal-regulated kinase
EU	European Union
FBS	Foetal bovine serum
H&E	Haematoxylin and eosin
Hb	Haemoglobin

HBSS	Hank’s balanced salt solution
hEGF	Human epidermal growth factor
HER2	Human epidermal growth factor receptor-type 2
HRP	Horseradish peroxidase
HS	Horse serum
Htc	Haematocrit
i.p.	Intraperitoneal
i.v.	Intravenous
IC_{50}	Half maximal inhibitory concentration
ICP-MS	Inductively Coupled Plasma Mass Spectrometry
IHC	Immunohistochemistry
IM	Immunomodulatory
LAR	Luminal androgen receptor/luminal-like
LC3	Microtubule-associated protein 1A/1B-light chain 3
LOD	Limits of detection
Log	Logarithmic
LOQ	Limits of quantitation
M	Metastasis
MAP	Mitogen-activated protein kinase
m/z	Mass-to-charge ratio
MCV	Mean corpuscular volume
MDC	Monodansylcadaverine
MSL	Mesenchymal-stem cell-like
mTOR	Mammalian target of rapamycin
MW	Molecular weight
N	Nodes
Nec-1	Necrostatin 1
NF- κB	Nuclear factor kappa-light-chain-enhancer of activated B cells
NMWL	Nominal molecular weight limit
ORR	Overall response rate
OS	Overall survival
p.o.	per os
PAM	Prediction analysis of microarray

PARP	Poly (ADP-ribose) polymerase
PAS	Periodic acid–schiff
PBS	Phosphate Buffered Saline
pCR	Pathological complete response
PD-L1	Programmed death-ligand 1
PFS	Progression-free survival
PI3K	Phosphoinositide 3-kinases
PK	Pharmacokinetics
PR	Progesterone receptor
pSIVA	Polarity Sensitive Indicator of Viability & Apoptosis
Pd	Palladium
Pt	Platinum
Put	Putrescine
RBC	Red blood cells
RNA	Ribonucleic acid
ROS	Reactive oxygen species
SEM	Standard error of the mean
Spd	Spermidine
Spm	Spermine
T	Tumour
$T_{1/2}$	Half-life
TdT	Terminal deoxynucleotidyl transferase
t_{max}	Time to reach c_{max}
TNBC	Triple-negative breast cancer
TUNEL	Terminal deoxynucleotidyl transferase biotin-dUTP nick end labeling
VEGF	Vascular endothelial growth factor
VEGFR	Vascular endothelial growth factor receptor
Vs	Versus
Vz	Distribution volume
%CV	Coefficient of variation
λz	Lambda-z; elimination rate constant

THESIS OUTLINE

The present thesis is organized in six main chapters:

Chapter I – General Introduction

A general introduction to TNBC and key challenges with current treatment options are presented to provide a framework for the experimental part of the work. The chapter also includes a review article of Pd-based compounds and their activity towards TNBC.

Chapter II – General Scope and Aims of the Work

The chapter provides study basis, hypothesis and study goals.

Chapter III – Material and Methods

The third chapter describes materials and methodology used for the subsequent experiments.

Chapter IV – Results and Discussion

Chapter IV presents and discusses experimental work that was organized from *in vitro* assays in human cells to *in vivo* experiments in mice.

Chapter V – General Discussion

The chapter V presents a combined discussion of all the experimental work described in Chapter IV.

Chapter VI – Conclusions and Future Perspectives

Chapter VI provides conclusions of the thesis and highlights the most relevant achievements and knowledge obtained. Also, some aspects of the future work in the field are outlined.

At the end the list of all the references cited in the thesis is included as well as supplementary material of this thesis.

CHAPTER I: INTRODUCTION

Parts of this chapter are available in the following publication:

Vojtek M, Marques MPM, Ferreira IMPLVO, Mota-Filipe H, Diniz C. Anticancer activity of palladium-based complexes against triple-negative breast cancer. Drug Discovery Today. 2019; 24(4):1044–1058.

I.1 Overview of Breast Cancer

Breast cancer is the most common cancer type in the world, with 2.26 million new cases being diagnosed in 2020 that represent 24.5% of all cancer cases in females. Although it is the 5th leading cause of cancer deaths overall worldwide, breast cancer is the primary cause of death in women, accounting for 15.5% of all cancer deaths worldwide [1]. However, some exceptions are observed in Australia/New Zealand, Northern Europe, Northern America, and China (part of Eastern Asia) where breast cancer deaths are preceded by lung cancer, and in sub-Saharan Africa where cervical cancer-related deaths rank the first in women [1]. Breast cancer incidence rates vary significantly worldwide, ranging from 26.2 cases per 100,000 habitants South-Central Asia to 95.5 cases per 100,000 habitants in Australia and New Zealand (**Figure 1**) [1]. According to the projections, the global burden of new breast cancer cases is expected to increase by 40% by 2040, rising from 2.26 million new cases per year in 2020 to 3.2 million new cases per year in 2040 [1].

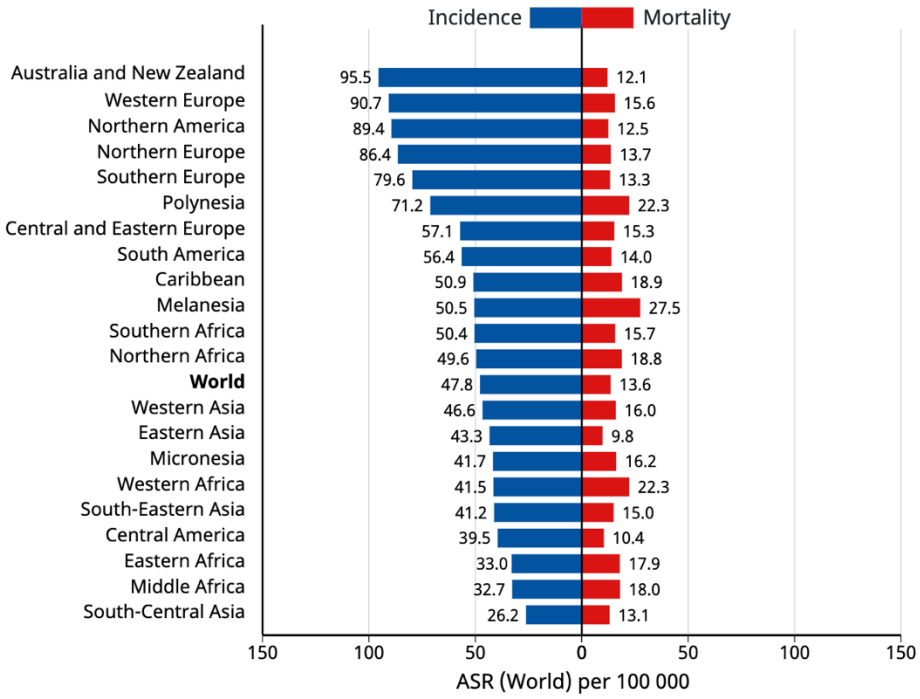

Figure 1. Breast cancer worldwide mortality and incidence rates (age standardized).

Adapted from [1]. Age standardized rate (ASR).

While breast cancer has most favourable survival rates in high-incidence developed regions of the world, the survival rate is the least favourable in Africa (**Figure 2)**. Mortality

rates from breast cancer have remained relatively unchanged over the years, with only slight decreases since 1990 in the Unites States of America, Canada and many European countries, mainly attributed to earlier detection and advances in treatment [2]. While the 5-year survival rate of invasive breast cancer has been shown to increase, from 74.8% (1977) to 89.7% (2013) [3], the median survival rate of the most advanced stage IV breast cancer that has metastasized remains low, between 2 to 3 years [4,5]. Additionally, approximately 30% of women develop advanced metastatic breast cancer as recurring disease, and 5-10% of all patients are being diagnosed already in metastatic stage of breast cancer, *de novo* metastatic breast cancer disease [6], which is still considered an incurable disease [7].

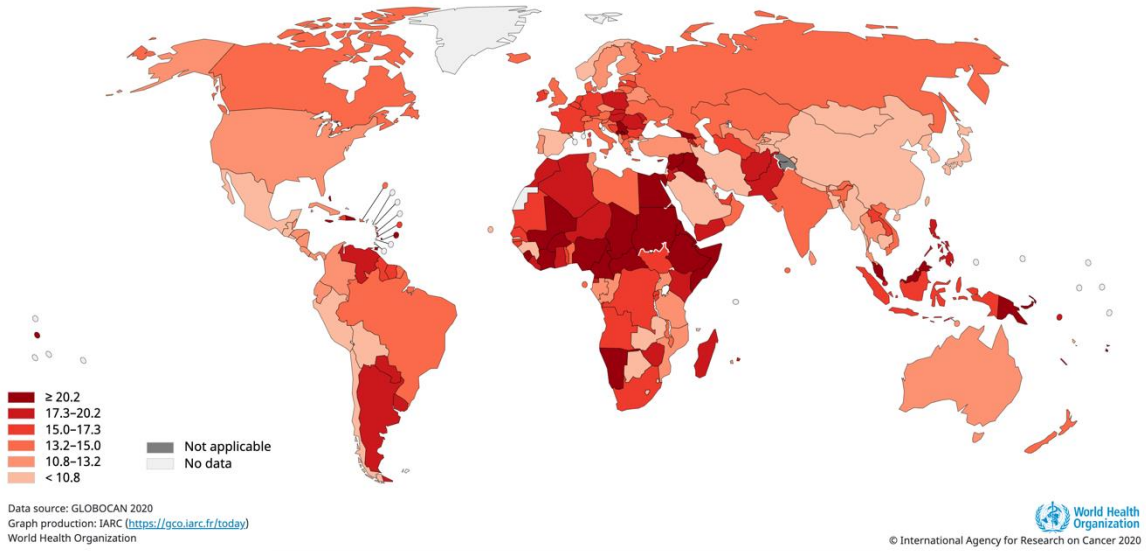

Figure 2. Mortality rates across world regions (age standardized)

Adapted from [1].

The aetiology of breast cancer is still not entirely understood, and multiple factors contribute to their development. The most pronounced risk factors for breast cancer are increasing age, particularly after reaching the age of 40 years. Other factors associated to breast cancer include family history of breast cancer at a young age, early menarche, late menopause, older age at first live childbirth, prolonged hormone replacement therapy, previous exposure to therapeutic chest wall irradiation, benign proliferative breast disease, and genetic mutations, such as mutation of the tumour suppressor breast cancer associated

(BRCA) genes BRCA1/2. Additionally, breast cancer is almost exclusively reported in women, while less than 1% of all cases are reported in male gender [8].

I.1.1 Breast Anatomy and Physiology

The female breast is a complex pair organ that consists of various tissue types, including exocrine mammary glands (one in each breast), adipose tissue, connective tissue, blood vessels, nerves and lymph nodes. The glandular tissue is organized into 10-20 milk-secreting lobes, which are arranged around the nipple **Figure 3**. Each lobe consists of 20-40 lobules formed by aggregation of small alveoli. The lobes are connected to the nipple by converging lactiferous duct that transport milk to the nipple. While the male breast also contain mammary gland, the physiological function of breastfeeding is limited to female gender [9].

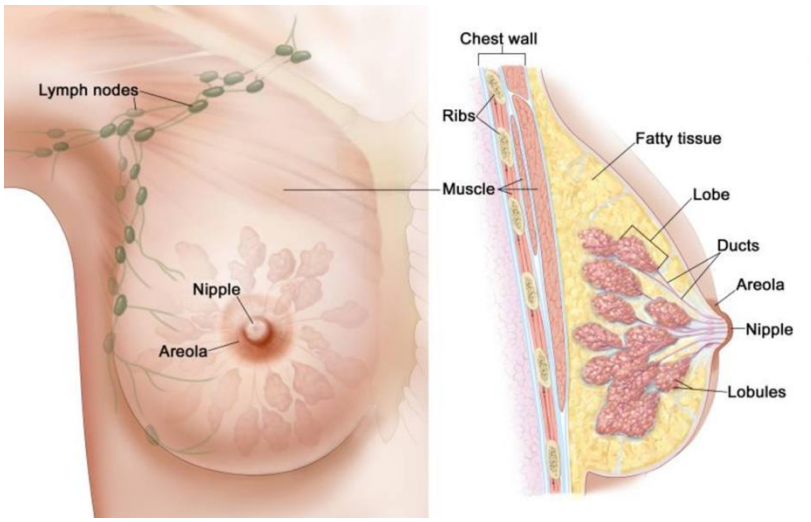

Figure 3. The anatomy of female breast.

Adapted from [10].

The mammary ducts and lobes are lined with layer of epithelial cells that consist of two main cell types. (**Figure 4**). The cuboidal luminal cells (cytokeratin (CK)-8/18, CK-7 and CK-19 positive) surround a central lumen, while the highly elongated myoepithelial/basal cells (CK-5/6, CK-14 and CK-17 positive) are located in a basal position adjacent to the basement membrane [11]. The mammary epithelium exists in a highly dynamic state, undergoing profound changes during the morphogenetic cycle, which starts at puberty. Oestrogen stimulates the accumulation of adipose tissue within the connective tissue and

the growth of the ductal system. Once ovulation and menstruation begin, progesterone promotes the formation of milk-secreting lobes. During the lactation, prolactin stimulates milk production in the alveolar luminal cells, while oxytocin contracts the myoepithelial cells, resulting in the ejection of milk from the alveolar lumen into the lactiferous ducts [12].

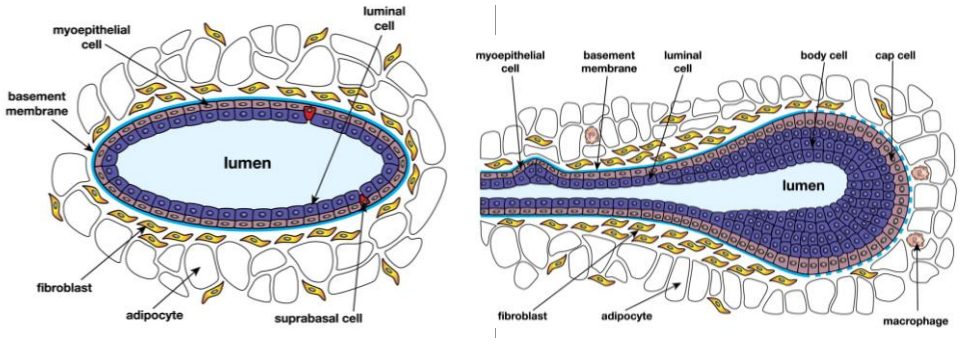

Figure 4. Schematic representation of epithelial layers of mammary gland.

Adapted from [13].

I.1.2 Breast Cancer Pathophysiology and Staging

Breast cancer arises from the epithelial lining of the mammary ducts or lobes. In situ carcinoma, also known as non-invasive breast carcinoma, does not spread from the lactiferous ducts or lobes, whereas invasive breast carcinoma is more common and breaches the basement membrane into surrounding normal tissue (**Figure 5).** Breast cancer can occur simultaneously in the mammary ducts and lobes, creating mixed tumours, or there may be more than one tumour arising from the same tumour or creating new ones, known as multifocal and multicentric tumours, respectively [14]. The vast majority of breast cancer tumours are invasive ductal carcinomas or invasive lobular carcinomas, accounting about 75% and 15%, respectively [15]. Other specific subtypes include invasive tubular, cribriform, metaplastic, apocrine, mucinous, papillary, and micropapillary carcinoma, as well as carcinoma with medullary, neuroendocrine, and salivary gland/skin adnexal type features [16].

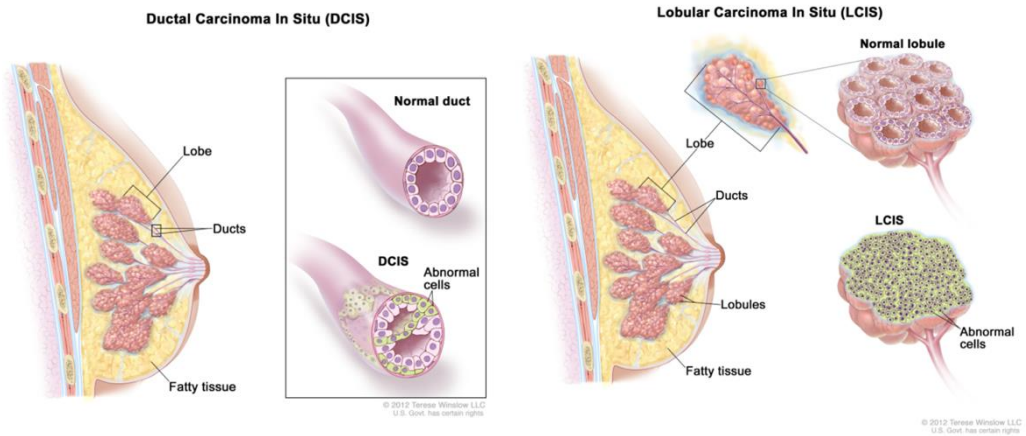

Figure 5. Illustration of ductal and lobular carcinomas.

Adapted from [10].

In the past, breast cancer classification relied solely on the histopathological appearance, which had limited impact on treatment decisions. However, current classification takes into clinical, molecular and genetic heterogeneity. Current gold standard for guiding therapy decision-making involves clinicopathological parameters such as histological grade, tumour size, lymph node metastasis and predictive biomarkers, such as expression of oestrogen receptor (ER), progesterone receptor (PR) and human epidermal growth factor receptor 2 (HER2) status [17].

Breast cancer staging provides clinical standardization tool for the treatment selection and prognosis. Based on a primary tumour size (T 1-4), number of metastasis in lymphatic nodes (N 0-3) and detection of distant metastasis (M 0-1), the American Joint Committee on Cancer created anatomic stage/prognostic groups spanning from Stage 0 to Stage 4 as summarized in **Table 1** [18].

Table 1. Breast Cancer Staging System

Stage	Description	1-year survival after diagnosis	5-year survival after diagnosis
Stage 0	Non-invasive BC (in situ)	100%	100%
Stage 1	Invasive BC, small tumour or tumours up to 2mm in breast or lymph nodes	100%	86%
Stage 2	Tumour 2-5cm or larger than 2mm tumours spread in 1-3 axillary lymph nodes	97%	69%

Stage	Description	1-year survival after diagnosis	5-year survival after diagnosis
Stage 3	Tumour larger than 5cm and 1-3 axillary lymph nodes affected, or cancer in 4-9 axillary lymph nodes	89%	51%
Stage 4	Metastatic cancer that invaded other organs (lungs, distant lymph nodes, bones, liver, brain)	60%	32%

Source of survival prognosis: [19]

A histologic grade should be assigned to invasive breast carcinomas. The grade for a tumour is determined by Nottingham combined histologic grading system that assign a value from 1 (favourable) to 3 (unfavourable) for each of the three following morphologic features: tubule formation, nuclear pleomorphism, and calibrated mitotic count. The combined score from all features is designated as histologic grade. The low histologic grade (favourable) Grade 1 has score of 3-5 points, while intermediate histologic grade (moderately favourable) Grade 2 has score of 6–7 points and high histologic grade (unfavourable) and Grade 3 has score of 8–9 points. The use of subjective grading alone is not recommended [20,21].

I.1.3 Breast Cancer Subtypes

The molecular classification of breast cancers comprises the evaluation of the specific biomarkers that define the cancer subtypes with distinct clinical prognosis and susceptibility to treatment. Using immunohistochemistry (IHC) methods on paraffin-embedded tissues, the evaluation of expression of ER, PR, and HER2 is used for the individualization of the therapeutic approach, prediction of both the treatment outcome and overall patient prognosis [22,23]. Combined evaluation of the three biomarkers (ER/PR/HER2) divides the breast cancers based on the receptor status in ER^+ positive ($ER^+/HER2^-$), $HER2^+$ positive ($ER^-/HER2^+$), triple negative ($ER^-/PR^-/HER2^-$) and triple positive ($ER^+/PR^+/HER2^+$) [24]. The patients with tumours ER^+ and/or $HER2^+$ subtypes can be treated with targeted therapies, only effective in these subsets of patients. However, approximately 10-30% of all breast cancer tumours lack of expressions of ER, PR or HER2, being classified as triple negative breast carcinoma (TNBC) [25].

Besides the IHC classification, the prediction analysis of microarray (PAM) 50 has identified intrinsic breast cancer subtypes based on the gene expression profiling of 50 genes. The subsequent adaptation of microarray-based PAM50 to quantitative real-time PCR allowed also analysis of RNA extracted from formalin-fixed paraffin-embedded samples. Using hierarchical clustering, Perou and colleagues identified five intrinsic breast cancer subtypes (Luminal A, Luminal B, HER2-enriched, Basal-like and Claudin low) and normal breast-like subtype [26–28]. These subtypes of breast cancer presented distinct genetic signatures **(Figure 6)** and revealed substantial differences in incidence, survival and response to treatment [28].

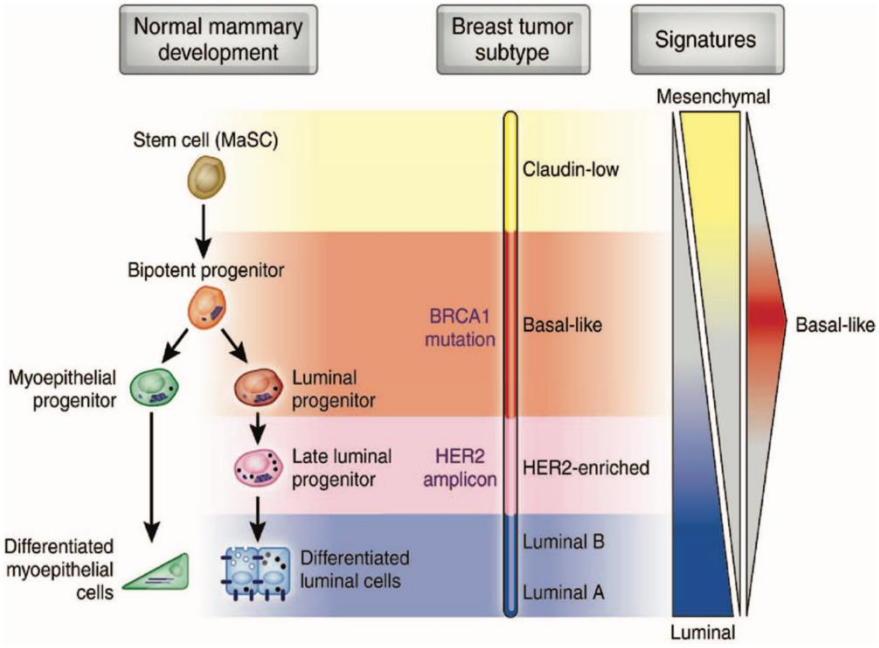

Figure 6. Mammary epithelial development and its putative relationship to intrinsic subtypes. Adapted from [27].

To further classify and understand the difference in therapeutic approach, the St. Gallen Consensus Conference on Breast Cancer in 2011 has established the approximation of the intrinsic subtypes to IHC classification as summarized in **Table 2** [29].

Table 2. Breast cancer intrinsic subtypes

	ER	PR	HER2	Recommended treatment	Grade	Outcome	Prevalence
Luminal A	+	±	-	Endocrine	1-2	Good	~27%
Luminal B	+	±	-	Endocrine ± chemotherapy	2-3	Intermediate	~20%
	+	±	+	Endocrine + chemotherapy + anti-HER2		Poor	
HER2 enriched (non-luminal)	-	-	+	Chemotherapy + anti-HER2	2-3	Poor	~14%
Basal	-	-	-	Chemotherapy	3	Poor	~18%
Claudin-low	-	-	-	Chemotherapy	3	Poor	~12%
Normal-like	+/-		-		1-3	Intermediate	~8%

Source of prevalence [30].

Additionally, they have also characterized a recommended systemic treatment for each of the subtypes were provided, including the endocrine therapy alone for Luminal A; endocrine ± cytotoxic therapy for luminal B (HER2 negative); cytotoxic + anti-HER2 + endocrine therapy for luminal B (HER2 positive); cytotoxic + anti-HER2 for HER2 positive (non-luminal); and cytotoxic for triple-negative [29]. **Luminal A** breast cancer is hormone-receptor positive (ER^+ and/or PR^+), HER2 negative, and has low levels of the protein Ki-67, which helps to control how fast cancer cells grow. Luminal A cancers tend to be a low-grade with slow growth and the best clinical prognosis. The targeted endocrine therapy includes selective oestrogen receptor modulators (tamoxifen) and aromatase inhibitors (anastrozole, exemestane, letrozole). The addition of adjuvant chemotherapy to treatment regime did not show any additional clinical benefit [31]. **Luminal B** breast cancer is hormone-receptor positive (ER^+ and/or PR^+), and either HER2 positive or HER2 negative with high levels of Ki-67. Luminal B cancers generally grow slightly faster than luminal A cancers and their prognosis is slightly worse [23]. **HER2-enriched** breast cancer is non-luminal hormone-receptor negative (ER^- and PR^-) and HER2 positive. HER2-enriched cancers tend to grow faster than luminal cancers and can have a worse prognosis, but they are often successfully treated with HER2-targeted therapies (trastuzumab, pertuzumab, lapatinib) [23]. **Basal-like** breast cancer is hormone-receptor negative (ER^- and PR^-) as well as HER2 negative. This type of cancer is more common in younger, African-American patients and patients with BRCA1/2 gene mutations [25]. Another particularity of basal-like tumours is their high proliferation rate and mutation of pro-apoptotic nuclear transcription factor p53 [27].

Claudin-low breast cancer subtype is the most recently identified subgroup. Exhibiting low expression of claudin genes (claudin 3,4 and 7) involved in epithelial cell tight-tight junctions. Furthermore, these tumours lack E-cadherin, another epithelial cell interaction protein. Although these tumours are similar to basal-like tumours, they differ having the stem cell features, features of epithelial-mesenchymal transition and tumour-initiating cell signature only present in this breast cancer subtype [27]. **Normal-like** breast cancer is similar to luminal A cancer, being hormone-receptor positive (ER^+ and/or PR^+), HER2 negative, and having low levels of protein Ki-67. While normal-like breast cancer has a good prognosis, its prognosis is slightly worse than for luminal A breast cancer [32].

Although the clinical designation obtained from IHC can be used to approximate the intrinsic subtype, the subtypes do not always fall into the IHC designation as already demonstrated by Parker and colleagues [33], having an overall 79% concordance rate between PAM50 vs IHC **Figure 7** [34].

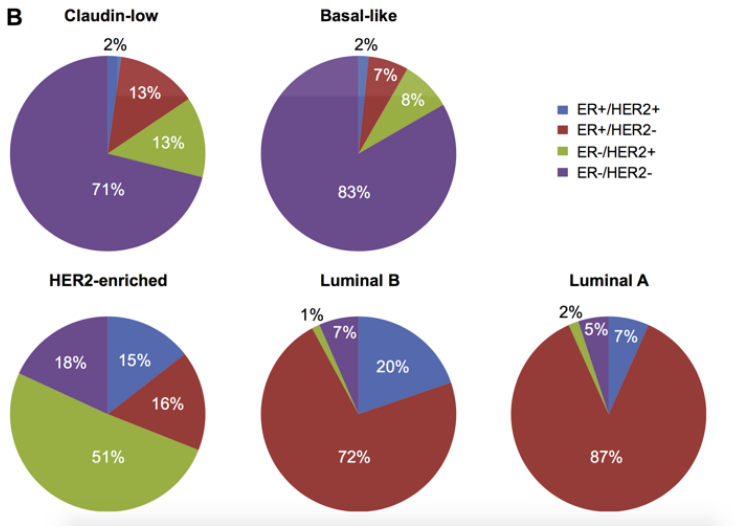

Figure 7. Discrepancies between PAM50 vs IHC Classifications.

Adapted from [28].

One possibility is the false positivity or false negativity of the IHC-based assays that has been challenged for hormone-receptors as well as HER2 status determination, showing the interlaboratory and inter-method discordance rates ~20% [35]. Another possibility could be the intratumour heterogeneity, and regional differences among samples. However, while the IHC-based assay measures the three individual pathology-based biomarkers, the multigene expression use tens to hundreds of genes that might likely better capture the true biological profile of sample [34]. Thus, despite the great knowledge gathered so far, the

discrepancies between intrinsic subtypes based of gene expression profiling and IHC-defined subtypes limit the translatability of the subtypes into every-day clinical practice. Moreover, these observations also demonstrate the fact that the final molecular taxonomy of breast cancers is likely to be even more complex and will most likely evolve further [24].

I.2 TNBC

TNBC represents 10 to 30% of all breast cancer cases and is termed negative due to the absence of ER, PR and HER2 overexpression [36]. TNBC tumours are generally highly proliferative, more biologically aggressive, larger in size with higher histologic grade, poorly differentiated and have usually lymph node involvement at the time of diagnosis [37]. While the majority of TNBC tumours are invasive ductal carcinomas, several other high-grade subtypes of breast cancer have been characterized, including medullary carcinoma, metaplastic carcinoma, adenoid cystic carcinoma and apocrine/histiocytoid carcinoma [38].

Despite the significant advances over the past 5 years that enabled some targeted approaches for TNBC, TNBC is still considered an unmet medical need that is dependent on chemotherapeutic agents [39,40]**.** Even though TNBC tumours are normally chemotherapy-sensitive and respond well to neoadjuvant (presurgical) treatment comparatively to hormone receptor-positive breast cancers, the TNBC patients have higher rate of distant recurrences and consequently poorer overall prognosis. Furthermore, the absence of biomarkers for prediction of response to the treatment as well as great heterogeneity of TNBC tumours difficult its treatment [41]. Less than 30% of women with metastatic TNBC survive 5 years, and almost all die due to disease despite the adjuvant (postsurgical) chemotherapy [4].

I.2.1 TNBC Subtypes

Over the years, the basal-like breast cancer has become the synonym for TNBC as the TNBC tends to have basal-like breast cancer pathology. However, as previously demonstrated, not all TNBC fall into basal-like intrinsic subtype, and not all basal-like cancers are automatically TNBC, having 20-30% discordance between the two definitions [34]. Therefore, significant heterogeneity exists among the patients diagnosed with TNBC. Indeed, based on PAM50, the majority of TNBC fall into basal-like (50-75%) [27] and claudin-low (25 to 39%) subtypes, while all the other non-basal subtypes include HER2-enriched (7 to 14%), luminal B (4 to 7%), luminal A (4 to 5%) and normal breast-like (1%), depending on the population [42,43]. Interestingly, the non-basal-like TNBC (i.e., HER2-enriched and luminal A/B) showed global gene expression patterns neatly similar to those

from non-TNBC tumours despite lacking the expression of hormone receptors or HER2. Accordingly, the non-triple-negative basal-like tumours have shown very similar genomic features and age-associations as basal-like tumours from TNBC [34].

Another approach to TNBC heterogeneity has been proposed by Lehmann and colleagues (2011), identifying 7 distinct molecular subtypes of TNBC: Basal-like (BL1) and Basal-like (BL2), Immunomodulatory (IM), Mesenchymal (M), Mesenchymal Stem-like (MSL), Luminal Androgen Receptor (LAR) subtype and Normal-like [41]. The BL1, heavily enriched in cell cycle and cell division components suggested the potential response to anti-mitotic agents such as taxanes (paclitaxel or docetaxel) of tumours belonging to this subtype. The BL2 showed the unique gene ontologies involving growth factor signalling and has features suggestive of basal/myoepithelial origin. The IM subtype is enriched for genes involved in immune cell processes. The M subtype displays a variety of unique gene ontologies that are heavily enriched in cell motility, extracellular matrix receptor interactions, and cell differentiation pathways. The MSL subtype shares genes for similar biological processes with the M subtype, however, also containing genes involved in growth factor signalling and low expression of claudin 3, 4, 7 (similarity to claudin-low subtype). The LAR subtype is ER negative but displays luminal gene expression patterns [23].

Prat and collaborators (2013) used the list of the 2 188 genes used for the identification of six molecular subtypes (IM, BL1, BL2, M, MSL and LAR) and they have reported a large overlap with the PAM50 and claudin-low subtypes. Within PAM50, the HER2-enriched and luminal tumours were highly expressing the LAR cluster and true normal and normal-like tumours highly expressing the stromal/fibroblast cluster. The basal-like tumours have been split into three groups based on the expression of the immune-related genes, stromal-related genes and the basal genes. Claudin-low tumours have been scattered within the basal-like group expressing the immune and/or stromal gene clusters [34]. Despite a close proximity to basal-like breast cancer subtype features, the claudin-low tumours do not consistently express basal cytokeratins [25]. Furthermore, it has been also demonstrated that the IM and IMSL subtypes are defined by the expressions of genes likely coming from the tumour microenvironment and not from the actual tumour cells, namely stromal/fibroblast and immune gene signatures [34].

DNA repair mechanism maintains the integrity and stability of the genome. Defects in BRCA1 and BRCA2 genes result in impaired DNA double-strand break repair system and subsequent genomic instability. It has been estimated that the BRCA1 and BRCA2 germ-line mutations result in breast cancer by the age of 80 in 72% and 69% of respective carriers [44]. Furthermore, 75% of BRCA1 carries develop TNBC. Despite the BRCA mutation is

mostly hereditary, the sporadic somatic mutations in BRCA genes have also been recognized, known as “BRCAness” [38].

I.2.2 Current Treatments for TNBC and Limitations

Currently, the treatment of patients (**Table 3**) with TNBC remains the biggest challenge without generally accepted guidelines on therapeutic regiment for the neoadjuvant, adjuvant and metastatic settings [6,45]. The chemotherapy remains a backbone for a systemic therapy of TNBC and anthracyclines, taxanes and Pt-based agents are commonly used [38,39]. Moreover, several approved drugs that target programmed cell death protein-1 and programmed death ligand-1, poly ADP-ribose polymerase (PARP), and/or antibody drug conjugates have emerged as promising targeted drugs to improve clinical outcomes in subsets of TNBC patients [46].

Anthracyclines are considered the most effective anticancer drugs ever developed, preventing the DNA replication and transcription. The cardiotoxicity is the main concern for anthracycline-based therapy, including the firstly isolated doxorubicin and daunorubicin as well as the second-generation analogues with improved therapeutic index (epirubicin, idarubicin and mitoxantrone)[47]. Taxanes (docetaxel, paclitaxel) are diterpenes that inhibit cell division by stabilization of microtubules and preventing their depolymerization, thus blocking cells in the G2/M phase of the cell cycle and inducing apoptosis [48]. Pt agents (cisplatin, carboplatin and oxaliplatin) are non-cell-cycle specific metal-based drugs targeting the DNA to form intrastrand crosslinks that affect DNA replication and induce apoptosis. The use of Pt agents is particularly favourable in the treatment of TNBC tumours with BRCA1 mutation [38].

In the early stages, the use of neoadjuvant systemic chemotherapy is the standard therapeutic approach in TNBCs. Despite the overall pathological complete response rates (pCR) are higher among TNBC patients (22% pCR) relative to non-TNBC (11% pCR), the 3-year progression-free survival rates are greatly reduced especially among the patients with the residual disease after neoadjuvant systemic chemotherapy [49]. Currently used sequential anthracycline-taxane-based chemotherapy has pCR between 28-36% [50]. To increase the pCR, other chemotherapy strategies with addition of Pt-based agents have been studied. The GeparSixto study has reported the increase in pCR after addition of carboplatin to anthracycline or taxane-based therapy from pCR 36.9% to 53.2% [51].

Table 3. Overview of Treatment Options for TNBC

Therapeutic classification	Pharmacological group	Example (drug)	via	Mode of action (main)
Chemotherapy (cytotoxics)	**Platinum agents**	cisplatin, carboplatin, oxaliplatin	i.v.	Inhibition of DNA synthesis and repair
	Alkylating agents	cyclophosphamide	i.v./ p.o.	Alkylation of DNA
	Antimetabolites	fluorouracil, capecitabine, gemcitabine, methotrexate	i.v. p.o. i.v. i.v.	Inhibition of metabolic pathways
	Tubulin destabilizers	vinorelbine, vinblastine, eribulin	i.v.	Inhibition of microtubule assembly/polymerization
	Tubulin stabilizers	paclitaxel, docetaxel	i.v.	Inhibition of microtubule depolymerization
	Anthracyclines	doxorubicin, epirubicin, mitoxantrone	i.v.	Inhibition of DNA and RNA synthesis. Inhibition of topoisomerase II.
Targeted therapy	**PARP inhibitors**	olaparib, talazoparib	p.o.	Inhibition of poly ADP-ribose polymerase, a protein involved in DNA repair
	EGFR inhibitors	lapatinib, afatinib	p.o.	Block of target the epidermal growth factor receptor (EGFR) and block downstream signalling pathways that promote cell proliferation,
	Immune checkpoint inhibitors	atezolizumab, pembrolizumab	i.v.	block PD-L1 and PD-1 proteins that inhibit immune cell activity against cancer cells
	CDK 4/6 inhibitors	palbociclib, ribociclib	p.o.	Inhibition of cyclin-dependent kinases 4 and 6, that are involved in cell cycle progression

i.v. – intravenous administration; p.o. – per os administration. EGFR - epidermal growth factor receptor; CDK4/6 - Cyclin-dependent kinase 4/6. Source: Self-made.

Adjuvant therapy for TNBC seeks to extend the disease-free survival and overall survival. The data on impact of adjuvant chemotherapy in TNBC are limited and retrospective in nature. Current evidence shows that patients with TNBC benefit from

adjuvant chemotherapy, however there is no universally accepted standard chemotherapy regimen. The use of CMF (cyclophosphamide, methotrexate and 5-fluorouracil), and anthracycline and taxane-containing regimens have been shown to be beneficial in the terms of the overall survival [52].

In metastatic settings for TNBC, the therapeutic approach has rather palliative intent, focused on improving the quality of live by reduction/stabilization of tumour cancer-related burden, prolonging the progression-free survival and overall survival [6]. The TNBC present a distinct pattern of relapse, with higher risk of developing distant metastasis and death compared to other breast cancer subtypes. The TNBC metastasis are more commonly found in lung and brain comparatively to luminal breast cancers favouring the bone and skin [38]. Currently, there is not standardization for the first-line therapy for advanced TNBC. Several studies have evaluated the effectivity of different chemotherapy regimens containing taxanes, anthracyclines, gemcitabine and/or Pt agents as first-line therapy for metastatic TNBC. In general, the taxanes, Pt or capecitabine mono-chemotherapies in patients with metastatic TNBC has been associated with an objective response rate of 25–35%, a modest progression-free survival (median less than 6 months) and median overall survival of up to 12 months. Even though the combination of cisplatin with gemcitabine or paclitaxel with gemcitabine improved the objective response rate and progression-free survival rates, the overall survival remained poor [43]. Pt-based chemotherapy regimens in monotherapy (cisplatin or carboplatin) are also commonly used for TNBC and present challenges regarding its tolerability and development of the resistance by TNBC cells that hinder their clinical use. Additionally, immune checkpoint inhibitors targeting programmed death receptor-1 (PD-1) and programmed death ligand-1 (PD-L1) have shown some promise in treating advanced and metastatic TNBC in combination with standard chemotherapy [46].

I.2.2.1 Pt(II) Coordination Compounds

The accidental discovery of cisplatin by Barnett Rosenberg in the 1960s and its cytotoxic effects towards cancer cells gained great attention for the application of metal-based drugs in oncology [53]. Since then, Pt-based drugs have become a chemotherapy backbone of cancer therapy. Pt-based drugs constitute 50 to 70% of all chemotherapy schemes administered to oncology patients **(Figure 8**)[54]. Pt complexes such as cisplatin, carboplatin and oxaliplatin are non-cell-cycle specific agents affecting DNA replication and subsequently inducing apoptosis, particularly effective in TNBC with BRCA1/2 mutation. Indeed, the addition of Pt compounds to neoadjuvant and metastatic settings have already

been shown to be beneficial for TNBC patients [55,56]. While in neoadjuvant trials the clinical benefit of carboplatin's addition to treatment regime was independent of germline BRCA status, in metastatic settings the patients with BRCA1/2 mutations presented better clinical outcomes than non-BRCA mutation carriers. Despite the ubiquity of Pt drugs in cancer treatment regimens, several associated disadvantages exist. For example, no single agent is equally effective against all cancer types and some cancer types are inherently resistant to treatment with any of the currently approved Pt agents. Moreover, cancer cells can acquire resistance over time of treatment by a process of somatic evolution. Finally, the dose-limiting toxicity is another concern regarding the treatment with Pt agents [57,58]. These limitations of Pt-based compounds have stimulated the research in the field of metal-based drugs to develop new metal-based drugs with superior efficacy and selectivity towards breast cancer cells [38].

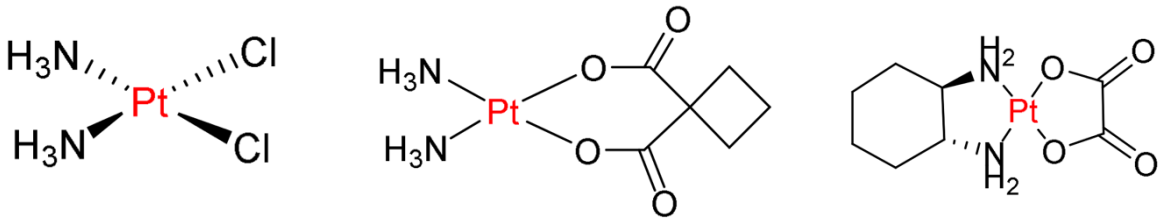

Cisplatin *Carboplatin* *Oxaliplatin*

Figure 8. Chemical structure of Pt-based anticancer agents cisplatin, carboplatin and oxaliplatin.

I.2.2.1.1 Cisplatin

Once cisplatin *cis*-$Pt(NH_3)_2Cl_2$ is transported through the passive diffusion or active transport (e.g., copper transporter 1, CTR1) into cytoplasm with low chloride concentration, the Cl^- ligands are displaced by water molecules, yielding a positively charged unstable and highly reactive *aqua* species. The resulting *monoaqua* $[Pt(NH_3)_2Cl(H_2O)]^+$ and *diaqua* $[Pt(NH_3)_2(H_2O)_2]^{2+}$ complexes form covalent bonds on nucleophilic sites of DNA, especially on the N-7 atom of purine bases (mainly guanine), yielding short-range intrastrand 1,2- and 1,3-crosslinks and interstrand adducts. The Pt-DNA adducts interfere with both DNA transcription and replication and trigger cell cycle arrest and apoptosis. However, severe nephrotoxicity and ototoxicity are the major drawbacks, limiting its clinical use [59].

I.2.2.1.2 Carboplatin

Carboplatin is a second-generation of Pt(II) drugs. While yielding the same type of DNA adducts, carboplatin is clinically approximately 4-times less potent compared to cisplatin due to slower kinetics, leading to lower toxicity but at the same time showing sharing the cross-resistance with cisplatin that hinder its use in resistant cancers. Its molecule comprises a bidentate dicarboxylate ligand as a leaving group, instead of the more labile cisplatin's chlorides. Carboplatin is activated when one arm of the carboxylate ligand is free, a process accelerated by nucleophiles, like sulphur-containing species, chloride, carbonates in blood serum or in the cytoplasm [57]. Carboplatin has longer retention half-life of 30h, as compared to 1.5-3.6h for cisplatin. Moreover, it presents reduced nephrotoxicity relative to cisplatin [59].

I.2.2.1.3 Oxaliplatin

Oxaliplatin is a third generation of Pt agent developed to yield better tolerability, less toxic and high activity owing to the inclusion of diaminocyclohexane moiety [59]. Oxaliplatin exerts its cytotoxic effect mostly through DNA lesions, arrest of DNA synthesis, inhibition of RNA synthesis, and triggering of immunologic reactions. The main concern during therapy with oxaliplatin is dose-limiting neurotoxicity, particularly the development of peripheral sensory neuropathy [60]. Oxaliplatin can bind tightly to DNA >10 times faster than cisplatin and exhibits considerably more potent cytotoxicity and broad-spectrum antitumor activity. While oxaliplatin does not share complete cross-resistance with cisplatin or carboplatin, its activity is also decreased once the resistance is acquired by TNBC cells [61].

I.2.2.2 Advances in TNBC Targeted Therapies

The profound understanding of molecular differences in biology of TNBC and non-TNBC is the fundamental factor for successful targetable therapy. At the present, numerous molecular-oriented studies have appointed different putative targets specific to TNBC, providing a strong rationale for the design and development of targeted therapeutic approaches. Emerged discoveries of molecular alterations (pathways activations, mutations or receptor enrichments) in TNBC tumours have sparked the interest of targeting the p53 and BRCA1/2 mutations, PARP enzymes, epidermal growth factor receptor, androgen receptor, PI3K/AKT/mTOR pathway and vascular endothelial growth factor with already-approved drugs, rather than new molecules in clinical trials.

I.2.2.2.1 PARP Inhibitors

Poly(adenosine diphosphate-ribose) polymerase (PARP) enzymes play a major role in DNA repair mechanisms. Particularly, the most abundant PARP1 isoform play a key role in the single-strand DNA breaks. Inhibition of PARP activity leads to the accumulation of single-strand DNA breaks, which are normally repaired by double-strand homologous recombination pathways that include tumour-suppressor proteins BRCA1 and BRCA2. Thus, TNBC with BRCA1/2 germ-line mutation as well as BRCAness phenotype are particularly vulnerable for targeting the PARP-mediated DNA repair mechanism [62]. Olaparib, one of the PARP inhibitors used for ovarian cancer, has been already approved for the treatment of BRCA-mutated HER2-negative breast cancer. Furthermore, other PARP inhibitors including veliparib, iniparib, niraparib have been developed and studied in clinical trials [62].

I.2.2.2.2 Antibody-Drug Conjugates

A strategy based on antibody-drug conjugates (ADC) have recently provided promising evidence of therapeutic benefits as later-line treatment options for TNBC. ADCs are a type of targeted cancer therapy that combines the specificity of monoclonal antibodies with the cytotoxicity of chemotherapy drugs. The antibodies are designed to recognize and bind to specific proteins on the surface of cancer cells, delivering the attached chemotherapy drug directly to the cancer cell, sparing healthy cells from unnecessary toxicity. This targeted approach has shown great promise in clinical trials for the treatment of TNBC. For example, sacituzumab govitecan is targeting trophoblast cell surface antigen-2 (Trop-2) with payload of SN-38, a topoisomerase-1 inhibitor which is an active metabolite of irinotecan with superior effects than single-arm chemotherapy [63]. Similarly, another ADC trastuzumab deruxtecan showed meaningful overall survival advantage in patients with low expression of HER2 [64], extending a therapeutic landscape of TNBC. Another example is ladiratuzumab vedotin, which targets the LIV-1 protein on cancer cells and delivers the chemotherapy drug monomethyl auristatin E (MMAE) [65]. While ADCs present great promise in the treatment of TNBC, there are still some challenges to overcome including development of drug resistance by cancer cells leading to therapy failure [66].

I.2.2.2.3 Immunotherapy

TNBC has higher portion of tumour infiltrating lymphocytes, especially T cells, that express PD-1 while 5-20% of TNBC express PD-L1. When PD-L1 binds to PD-1, it produces an inhibitory signal that results in T-cell suppression, making immunotherapy a promising option against TNBC [46]. This mechanism has encouraged the development of more

immunotherapy drugs to treat TNBC patients and the addition of immune checkpoint inhibitors atezolizumab/pembrolizumab to chemotherapy improves survival outcomes in TNBC patients [67].

I.2.2.2.4 Inhibition of Vascular Endothelial Growth Factor and its Receptor

Vascular Endothelial Growth Factor (VEGF) is overexpressed in more than 30% of TNBC and has critical role in proliferation, invasion and metastasis due to its key role in promoting angiogenesis (formation of new blood vessels). This supported the clinical trials for incorporating the antiangiogenic treatment in TNBC patients. In metastatic settings, the use of bevacizumab improved the progression-free survival, but overall survival remained unchanged. Additionally, the inhibition of VEGF receptors with tyrosine kinase inhibitors (sunitinib, sorafenib) was also studied in clinical trials with inconclusive data on progression-free survival and appearance of adverse events [38,62].

I.2.2.2.5 Inhibition of Epidermal Growth Factor Receptor

The overexpression of epidermal growth factor receptor is reported in 50% of TNBC patients, providing rationale for its targeting with monoclonal antibodies (cetuximab). Some clinical trials reported encouraging increase of progression-free survival, even though these trials enrolled small number of patients. However, it is important to determine the subpopulation of TNBC patients that would benefit from EGFR inhibition [38].

I.2.2.2.6 Targeting p53 Mutation

The majority of TNBC tumours (80% of basal TNBC tumours) carry the mutation in TP53 gene, encoding the tumour-suppressor protein p53 required for G1 checkpoint regulation in the presence of genotoxic stress [68]. Thus, targeting p53 has attracted great attention supported with encouraging pre-clinical *in vitro* data [68,69]. However, up to date the clinical trials in TNBC did not establish the efficacy of targeting p53 in clinic.

I.2.2.2.7 PI3K/AKT/mTOR Pathway Inhibition

The PI3K/AKT pathway is hyperactivated in approximately 10% of TNBC patients, providing a rationale for its targeting. The serine-threonine kinase mammalian target of rapamycin (mTOR) promotes protein translation, angiogenesis, proliferation, migration and metabolism. The mTOR inhibitor (everolimus) has already proved its clinical benefits for the treatment of postmenopausal women with advanced hormone receptor positive, HER2-negative breast cancer. However, its use in TNBC patients is still being studied in clinical trials to establish suitable combination regimes [45,62].

I.2.2.2.8 Androgen Receptor Inhibition

Approximately 10% of TNBC has been classified as LAR subtype, overexpressing the androgen receptor. The antiandrogen nonsteroidal inhibitor (bicalutamide), used for the treatment of advanced prostate cancer is being tested in several TNBC clinical trials, awaiting for the conclusive results and establishment of the treatment regimens [38].

I.2.2.2.9 Other Emerging Targets for TNBC Therapy

Bromodomain and extra-terminal inhibitors is recently developed novel class of agents with demonstrated *in vitro* and *in vivo* effects to inhibit growth of several tumours, including TNBC. These inhibitors displace bromodomain and extra-terminal proteins such as BRD4 from chromatin by competing with their acetyllysine recognition modules, leading to inhibition of oncogenic transcriptional programs [70,71].

Another emerging approach is targeting overexpressed ERK5 and its upstream activator MEK5 pathway in TNBC. ERK5 belongs to the MAP kinase family of signal transducers, and its deregulation has been linked to the breast cancer. Targeting MEK5/ERK5 with specific inhibitors has already showed *in vitro* and *in vivo* very promising results of inducing apoptotic cell death in TNBC [72,73].

I.2.2.3 TNBC Drug Resistance

Tumour resistance is a severe limiting factor for a successful therapeutic outcome since 90% of all cancer deaths are ascribed to resistance and therapy failure [74]. Resistance to anticancer drugs is a phenomenon that have eluded scientists already for more than 50 years and occurs in drug-naïve patients (intrinsic cancer cell resistance) as well as in patients already undergoing several treatment courses (acquired/developed cancer cell resistance, which is revealed after initially positive outcomes). Drug resistance in TNBC cells is complex and still to be fully understood, but several mechanisms of drug resistance have already been ascribed to decreased intracellular drug concentrations (due to changes in drug efflux and influx, or to parallel reactions), modifications of drug targets, drug inactivation and metabolization, increased DNA repair capacity, inhibition of cell death, activation of signalling cascades and genetic factors (gene mutations, amplifications, and epigenetic alterations) [74–76]. To overcome drug resistance/therapy failure, substantial focus has been given to combinations of existing therapies, as well as to the development of novel drug entities with improved antineoplastic properties and novel mechanisms of action.

Pt-based drugs can induce acquired resistance through mechanisms such as increased DNA repair, activation of survival pathways, and alteration of drug targets. For instance, resistance to Pt-based chemotherapy in TNBC has been associated with upregulation of drug efflux transporters such as P-glycoprotein, which reduces intracellular drug accumulation and prevents drug-induced cell death. Moreover, increased activity of DNA repair enzymes such as poly(ADP-ribose) polymerase (PARP) and Fanconi anaemia (FA) proteins has been implicated in the development of Pt resistance in TNBC cells. In addition to alterations in drug transporters and DNA repair pathways, resistance to chemotherapy in TNBC can also result from activation of survival signalling pathways [77,78].

For instance, PI3K/Akt/mTOR, ERK 1/2 and NFκB signalling pathways have been shown to promote cell survival and are known to be involved in acquired resistance to cisplatin in breast cancer cells [79,80]. Similarly, increased expression and activity of epidermal growth factor receptor (EGFR) and its downstream signalling pathways have also been associated with resistance to chemotherapy in TNBC [81].

It is worth noting that the development of resistance to chemotherapy is not limited to TNBC, but it is a common phenomenon in the treatment of various cancers. Therefore, there is a need to develop strategies that can overcome drug resistance and improve the effectiveness of chemotherapy in TNBC. One promising approach is the development of targeted therapies that can selectively target cancer cells while sparing normal cells, thereby reducing toxicity and improving treatment outcomes. Additionally, combination therapy approaches that target multiple pathways involved in drug resistance may also be effective in overcoming resistance to chemotherapy in TNBC.

I.3 Pd-Based Complexes as Potential Agents Against TNBC

Coordination complexes with transition metals are particularly appealing for medicinal chemistry due to the ion´s variable oxidation states, coordination numbers and ability to bind to a variety of ligands (O, S, N, P, C and halides). A key feature for the design of these transition metal-based complexes is to find the optimal combination of *in vivo* thermodynamic and kinetic stabilities, strongly dependent on the nature of both the ligand(s) and the leaving group(s) [59]. Presently, several metal-based compounds are under study, displaying promising antiproliferative and cytotoxic effects towards a wide range of human tumours. These include palladium(II) [82], gallium(III), ruthenium(II) [83] and ruthenium(III) [84], gold(I) and gold(III), bismuth(III), copper(II), molybdenum(II) [85] and tin(IV) complexes [86–88].

The development of Pd coordination compounds is particularly challenging due to their high lability and *ca.* 10^5 faster ligand exchange rate than Pt analogues. Furthermore, relatively low solubility of the Pd-based complexes is another hurdle that limits their further course towards clinical trials. Notwithstanding these challenges, more than 800 anticancer Pd(II) complexes have already been discovered since 1980s [89] and, in 2017, padeliporfin (TOOKAD®) was the first Pd(II) compound approved for clinical use. This Pd(II)-substituted bacteriochlorophyll derivative, used in photodynamic therapy in patients with prostate cancer [90], demonstrates high potential of Pd agents for clinical applications, especially against chemotherapy-resistant cancers.

We have reviewed studies performed between 1992 and 2018 that report on a total 121 Pd complexes (**Table 4**) and their activity against TNBC. The complexes were divided into eight groups according to structural similarities of their main ligands, including ethyl diamine, biogenic polyamines, benzyl amines/imines, pyridine/pyrazole/imidazole/pyrrol/triazole, chloroquine/clotrimazole, phosphine, thiourea, and thiosemicarbazones. The inhibitory concentration 50% (IC_{50}), TNBC cell line tested, and cancer selectivity (when present) were also reviewed, along with the target/mode(s) of action whenever known. Additionally, since 2018 when the review was conducted, 33 additional Pd-based compounds with promising anti-TNBC activities were reported. These complexes provide a similar outlook regarding antiproliferative TNBC activity and promising cancer selectivity (in some cases). In summary there are: 3 new compounds containing iminophosphine ligands [91]; 3 chiral oxazolinyl palladium complexes [92]; 14 complexes derived from halogen-substituted Schiff bases and 2-picolylamine [93]; 2 complex containing bisdemethoxycurcumin (with TNBC selectivity) [94]; 3 binuclear benzylidene palladacycles with varying phosphine bridging ligands having (with TNBC selectivity) [95]; 2 Pd compounds with tamoxifen vectors able to trigger ROS in TNBC cells [96]; 3 chelates with chromone-based thiosemicarbazone ligands (with TNBC selectivity) [97], 2 complexes with thiosemicarbazone [98] and one Pd complex with 1,2-bis(diphenylphosphino)ethane able to trigger autophagy as a mechanism of its TNBC actions [99] were reported.

Table 4. Overview of Pd-based complexes tested against TNBC.

Group	Complex No.	Complex designation[a]	Cell line	IC_{50}	Target / mode of action	Selectivity towards TNBC	Year Ref.
Derivatives of ethyl diamine	1	1a *cis*-[Pd(H_2dasa)Cl_2 1b *cis*-[Pd(Et_2dasa)Cl_2]	MDA-MB-468	72 hours: 1a 4.61 µM 1b 4.72 µM Ref. drug: Cisplatin 2.67 µM	Modification of secondary structure in isolated DNA.	NA	1994 [100]
	2	2a dichlorido-(O,O′-diethyl-(S,S)-ethylenediamine-N,N′-di-(2,2′-di(4-hydroxy-benzyl))-acetate)-palladium(II) 2b dichlorido-(O,O′-dipropyl-(S,S)-ethylenediamine-N,N′-di-(2,2′-di(4-hydroxy–benzyl))-acetate)-palladium(II) 2c ichlorido-(O,O′-dibutyl-(S,S)-ethylenediamine-N,N′-di-(2,2′-di(4-hydroxy-benzyl))-acetate)-palladium(II) 2d dichlorido-(O,O′-dipentyl-(S,S)-ethylenediamine-N,N′-di-(2,2′-di(4-hydroxy-benzyl))-acetate)-palladium(II)	MDA-MB-231	48 hours: 2a 135 µM 2b 72 µM 2c 36 µM 2d 18 µM	NA	NA	2014 [101]
	3	3a dichlorido[O,O'-diethyl-(S,S)-ethylenediamine-N,N'-di-2-(4-methyl)pentaneate]palladium(II) 3b dichlorido[O,O'-di-n-propyl-(S,S)-ethylenediamine-N,N'-di-2-(4-methyl)pentaneate]palladium(II)	MDA-MB-453	72 hours: 3a >200 µM 3b 93.04 µM 3c 35.31 µM 3d 48.43 µM	DNA fragmentation, induction of apoptosis and sub-G1 cell cycle arrest.	NA	2014 [102]

Group	Complex No.	Complex designation[a]	Cell line	IC_{50}	Target / mode of action	Selectivity towards TNBC	Year Ref.
		3c dichlorido[O,O'-di-n-butyl-(S,S)-ethylenediamine-N,N'-di-2-(4-methyl)pentaneate]palladium(II) 3d dichlorido[O,O'-di-n-pentyl-(S,S)-ethylenediamine-N,N'-di-2-(4-methyl)pentaneate]palladium(II)		Ref. drug: Cisplatin 3.75 µM			
Derivatives of biogenic polyamines	4	4a $Pd_3Spd_2Cl_{12}$ 4b $Pd_3Spd_2Cl_8$ 4c $Pd_3Spd_2Cl_6$	MDA-MB-468	24 hours: 4a 9 µM 4b 1.25 µM 4c 0.9 µM Ref. drug: Cisplatin 2.5 µM	Modification of secondary structure in isolated DNA	NA	1992 [103]
	5	5a $PdPutCl_4$ 5b $Pd_2Put_2Cl_4$ 5c $PdPutCl_2$ + $Pd_2Put_2Cl_4$ 5d Pd_3SpmCl_6 5e Pd_2SpmCl_4	MDA-MB-468	5a 1.60 µM 5b 0.70 µM 5c 0.53 µM 5d 11.51 µM 5e 8.44 µM Ref. drug: Cisplatin 2.50 µM	Modification of secondary structure in isolated DNA	NA	1993 [104]
	5e	Pd_2SpmCl_4	MDA-MB-231	72h hours: 2.8 µM Ref. drug: Cisplatin 3.2 µM	Induction of double-stranded DNA breaks (stronger effect than for cisplatin). Interference with microtubules. Synergism with cisplatin.	Tested vs normal human fibroblasts (BJ)	2011 [105]

Group	Complex No.	Complex designation[a]	Cell line	IC_{50}	Target / mode of action	Selectivity towards TNBC	Year Ref.
	6	Pd_2BENSpm	L56Br-C1	72 hours: 0.4 µM	DNA damage. Reduction of GSH and polyamine levels.	Tested vs normal breast epithelial cells (MCF-10A)	2013 [106]
	7	Pd_3NSpd_2	L56Br-C1	Exposure to 100 µM for 72h significantly reduced cell number.	Reduction of ornithine decarboxylase activity. Prolongation of S phase length.	Tested vs normal breast epithelial cells (MCF-10A)	2013 [107]
Derivatives of benzyl amine/imine	8	8a [Pd(4-$ClC_6H_4N=C(COC_6H_5)C_6H_4)OAc]_2$ 8b [Pd(4-$ClC_6H_4N=C(COC_6H_5)C_6H_4)Cl]_2$	MDA-MB-468	8a 6.75 µM 8b 8.95 µM Ref. drug: Cisplatin 2.67 µM	NA	NA	1996 [108]
	9	9a [Pd(C,N)-$C_6H_4CH_2NH(Et)Cl(Py)$] 9b [Pd(C,N)-$C_6H_4CH_2NH(t\text{-}Bu)Cl(PPh_3)$] 9c [$Pd_2(C,N\text{-}dmba)_2(\mu\text{-}dppe)(Cl)_2$]	MDA-MB-468	72 hours: 9a 2.4 µM 9b 3.3 µM 9c 2.3 µM Ref. drug: Cisplatin 4.8 µM	NA	NA	2012 [109]
	10	10a [Pd {$C_6H_4CPh=NH$}$(\mu\text{-}OAc)]_2$ 10b [Pd{$C_6H_4CPh=NH$}$(\mu\text{-}Cl)]_2$ 10c *trans-N,P*-[Pd{$C_6H_4CPh=NH$}$(OAc)(PPh_3)$] 10d *trans-N,P*-[Pd{$C_6H_4CPh=NH$}$(Cl)(PPh_3)$]	MDA-MB-231	72 hours: 10a 15 µM 10b 13 µM 10c 1.1 µM 10d 1.1 µM	Modification of secondary structure in isolated DNA.	NA	2013 [110]

Group	Complex No.	Complex designation[a]	Cell line	IC_{50}	Target / mode of action	Selectivity towards TNBC	Year Ref.
				Ref. drug: Cisplatin 6.5 μM			
	11	Includes twelve complexes 11a-l whose structures are given in supplementary data S1	MDA-MB-231	72 hours: 11a ~100 μM 11b ~100 μM 11c 4.6 μM 11d 13 μM 11e 40 μM 11f 32 μM 11g 5.2 μM 11h 2.7 μM 11i 25 μM 11j 17 μM 11k 1.4 μM 11l 1.0 μM Ref. drug: Cisplatin 6.5 μM	Modification of secondary structure in isolated DNA.	NA	2014 [111]
	12	12a Pd{C_6H_4(Ph)C=N-phenyl}]$_2$(μ-OAc)$_2$ 12b Pd{C_6H_4(Ph)C=N-1-naphtyl}]$_2$(μ-OAc)$_2$ 12c Pd{C_6H_4(Ph)C=N-benzyl}]$_2$(μ-OAc)$_2$ 12d Pd{C_6H_4(Ph)C=N-α-methylbenzyl}]$_2$(μ-OAc)$_2$ 12e Pd{C_6H_4(Ph)C=NH}]$_2$(μ-OAc)$_2$ 12f Pd{C_6H_4(Ph)C=N-phenyl}]$_2$(μ-Cl)$_2$	MDA-MB-231	72 hours: 12a >100 μM 12b >100 μM 12c >100 μM 12d >100 μM 12e 15 μM 12f 40 μM 12g >100 μM 12h 20 μM	Inhibition of cathepsin B. Modification of secondary structure in isolated DNA.	Tested vs human umbilical vein endothelial cells (HUVEC)	2014 [112]

Group	Complex No.	Complex designation[a]	Cell line	IC_{50}	Target / mode of action	Selectivity towards TNBC	Year Ref.
		12g Pd{C_6H_4(Ph)C=N-1-naphtyl}]$_2$(μ-Cl)$_2$ 12h Pd{C_6H_4(Ph)C=N-benzyl}]$_2$(μ-Cl)$_2$ 12i Pd{C_6H_4(Ph)C=N-α-methylbenzyl}]$_2$(μ-Cl)$_2$ 12j Pd{C_6H_4(Ph)C=NH}]$_2$(μ-Cl)$_2$ 12k *trans-N,P*-[Pd{C_6H_4(Ph)C=N-phenyl}OAc(PPh_3)] 12l trans-N,P-[Pd{C_6H_4(Ph)C=N-1-naphtyl}OAc(PPh_3)] 12m trans-*N,P*-[Pd{C_6H_4(Ph)C=N-benzyl}OAc(PPh_3)] 12n *trans-N,P-[*Pd{C_6H_4(Ph)C=N-α-methylbenzyl}OAc(PPh_3)] 12o trans-*N,P*-[Pd{C_6H_4(Ph)C=NH}OAc(PPh_3)] 12p *trans-N,P-[*Pd{C_6H_4(Ph)C=N-phenyl}Cl(PPh_3)] 12q trans-N,P-[Pd{C_6H_4(Ph)C=N-1-naphtyl}Cl(PPh_3)] 12r *trans-N,P*-[Pd{C_6H_4(Ph)C=N-benzyl}Cl(PPh_3)] 12s *trans-N,P*-[Pd{C_6H_4(Ph)C=N- α-methylbenzyl}Cl(PPh_3)] 12t *trans-N,P*-[Pd{C_6H_4(Ph)C=NH}Cl(PPh_3)]		12i 16 μM 12j 13 μM 12k 12 μM 12l >100 μM 12m >100 μM 12n >100 μM 12o 1.1 μM 12p >100 μM 12q >100 μM 12r 91 μM 12s >100 μM 12t 1.1 μM Ref. drug: Cisplatin 5 μM			
	13	[{ClPd(C_6H_4)CH=N(2,6-di-iPr-C_6H_3)}$_2$(m-$Ph_2P(CH_2)_2PPh_2$)]	MDA-MB-231	48h hours: 0.193 μM	DNA damage. Intrinsic induction	NA	2015

Group	Complex No.	Complex designation[a]	Cell line	IC_{50}	Target / mode of action	Selectivity towards TNBC	Year Ref.
					of apoptosis via release of cytochrome c, upregulation of PUMA, Bax and downregulation of Bcl-2. Extrinsic induction of apoptosis via activation of caspase 8. Induction of autophagy and G1 cell cycle arrest. Putative anti-cancer stem cell activity.		[113]
Derivatives of pyridine/pyrazole/ imidazole/pyrrol/ triazole and their combinations	14	Pd_2Hmtpo	BT-20	Exposure of 2.81 µM for 48h reduced <50% cell number	DNA fragmentation.	NA	2002 [114]
	15	([PdCl(terpy)](sac)·$2H_2O$)	MDA-MB-231 Ehrlich Ascites carcinoma (*in vivo*)	48 hours: 46.50 µM *In vivo:* complex 70% reduction, cisplatin 47% reduction, paclitaxel 59% reduction	Increase of cleaved PARP, caspase 3 activity and pyknotic nuclei	NA	2014 [115]
			MDA-MB-231 MDA-MB-435	72 hours: MDA-MB-231: 2.8 µM	Induction of double-stranded breaks and DNA fragmentation.	Tested vs primary human aortic smooth muscle	2013 [116]

Group	Complex No.	Complex designation[a]	Cell line	IC_{50}	Target / mode of action	Selectivity towards TNBC	Year Ref.
				MDA-MB-435: 11.8 µM	Induction of apoptosis via activation of caspases 3/7. Modification of secondary structure in isolated DNA.	cells (HASMC-1 and HASMC-2)	2017 [117]
	16	[Pd(sac)(terpy)](sac)·4H2O	MDA-MB-231 Ehrlich Ascites carcinoma (*in vivo*)	72 hours: 0.09 µM *In vivo:* complex 68% reduction, cisplatin 33% reduction, paclitaxel 69% reduction	Disruption of tubules. Apoptosis *via* DR4 and DR5.	NA	2011 [118]
			MDA-MB-231		Induction of ROS and DNA damage.	NA	2014 [119]
			MDA-MB-231 MDA-MB-435	72h hours: MDA-MB-231: 20.57 µM MDA-MB-435: 18.30 µM	Induction of apoptosis.	Tested vs primary human aortic smooth muscle cells (HASMC-1 and HASMC-2)	2017 [120]
	17	17a *cis*-[Pd{κ²-N,N′-[1-$(CH_2)_2NMe_2$]pzol}Cl_2] 17b *cis*-[Pd{κ²-N,N′-[1-$(CH_2)_2NMe_2$]-3,5-Me_2-pzol}Cl_2] 17c [Pd{κ²-C,N,N′-{[1-$(CH_2)_2NMe_2$}-3-(C_5H_4)-5-Ph-pzol])}Cl_2]	MDA-MB-231	72 hours: 17a >100 µM 17b >100 µM 17c 16.2 µM Ref. drug: Cisplatin 6.5 µM	Modification of secondary structure in isolated DNA.	NA	2011 [121]

Group	Complex No.	Complex designation[a]	Cell line	IC_{50}	Target / mode of action	Selectivity towards TNBC	Year Ref.
	18	18a 5-Deoxy-1,2- O -isopropylidene-5-(4-(2-pyridyl)- 1H-1,2,3-triazole-1-yl)-α-D-xylofuranose palladium(II) chloride 18b 3-O-Benzyl-5-deoxy-1,2-O-isopropylidene-5-(4- (2-pyridyl)-1H-1,2,3-triazol-1-yl)-α-D-xylofuranose palladium(II) chloride 18c Methyl-5-deoxy-2,3-O-isopropylidene-5-(4-(2- pyridyl)-1H-1,2,3-triazol-1-yl)-β -D-ribofuranose palladium(II) chloride 18d 6-Deoxy-1,2:3,4-di-O-isopropylidene-6-(4-(2- pyridyl)-1H-1,2,3-triazol-1-yl)-α-D-galactopyranose palladium(II) chloride	MDA-MB-231	48 hours: 18a 9.9 µM 18b 7.9 µM 18c NA 18d 12.1 µM Ref. drugs: Doxorubicin <1 µM Cisplatin <1 µM	NA	NA	2012 [122]
	19	19a ([Pd(bpma)(sac)](sac)·2H_2O) 19b ([Pd(bpma)Cl](sac)·2H_2O)	MDA-MB-231	72 hours: 19a 9.3 µM 19b 4.2 µM	Induction of apoptosis via Fas death receptor. Increase of cleaved PARP and caspase 3 activity.	NA	2013 [123]
	20	20a [Pd(bpy)(hmbt)]Cl 20b [Pd(phen)(hmbt)]Cl	MDA-MB-231	120 hours: 20a 45.96 µM 20b 4.85 µM Ref. drug: Cisplatin 32.0 µM	NA	NA	2014 [124]

Group	Complex No.	Complex designation[a]	Cell line	IC_{50}	Target / mode of action	Selectivity towards TNBC	Year Ref.
	21	21a 3-O-Acetyl-5-deoxy-1,2-O-isopropylidene-5-(4-(2-pyridyl)-1H-1,2,3-triazole-1-yl)-a-D-xylofuranose palladium(II) complex 21b 3-O-Benzoyl-5-deoxy-1,2-O-isopropylidene-5-(4-(2-pyridyl)-1H-1,2,3-triazole-1-yl)-a-D-xylofuranose palladium(II) complex 21c [5-Deoxy-3-O-ferrocenoyl-1,2-O-isopropylidene-5-(4-(2-pyridyl)-1H-1,2,3-triazole-1-yl)-a-D-xylofuranose palladium(II) complex	MDA-MB-231	48 hours: 21a >100 µM 21b >100 µM 21c >100 µM Ref. drugs: Doxorubicin 0.91 µM Cisplatin 0.25 µM	NA	NA	2014 [125]
	22	22a *trans*-[Pd{[1-{MeO-$(CH_2)_2$-}-3,5-Ph_2-(C_3HN_2)]$_2Cl_2$] 22b [Pd{k^2,C,N)[1-{MeO-$(CH_2)_2$}-3-(C_6H_4),5-Ph-(C_3HN_2)]}$(\mu$-OAc)]$_2$ 22c [Pd{k^2,C,N)[1-{MeO-$(CH_2)_2$}-3-(C_6H_4),5-Ph-(C_3HN_2)]}$(\mu$-Cl)]$_2$ 22d [Pd{k^2,C,N)[1-{MeO-$(CH_2)_2$-}-3-(C_6H_4),5-Ph-(C_3HN_2)]}(OAc)(PPh_3)] 22e [Pd{k^2,C,N)[1-{MeO-$(CH_2)_2$-}-3-(C_6H_4),5-Ph-(C_3HN_2)]}(Cl)(PPh_3)]	MDA-MB-231	72 hours: 22a 75 µM 22b 9.5 µM 22c 14.4 µM 22d 9.1 µM 22e 13 µM Ref. drug: Cisplatin 6.5 µM	NA	NA	2014 [126]
	23	23a $PdCl_2$(1,2-O-Isopropylidene-α-D-xylofuranose-3,5-(3′-amino)phenyl boronate) 23b $PdCl_2$(1,2-O-Cyclohexylidene-α-D-xylofuranose-3,5-(3′-amino)phenyl boronate)	MDA-MB-231	48h hours: 23a 8.58 µM 23b 8.57 µM 23c 34.76 µM 23d 30.37 µM 23e 15.00 µM 23f >100 µM	Intercalation between strands of isolated DNA.	Tested vs normal human embryonic kidney cells (HEK-293T)	2015 [127]

Group	Complex No.	Complex designation[a]	Cell line	IC_{50}	Target / mode of action	Selectivity towards TNBC	Year Ref.
		23c PdCl2(1-O-Benzyl-2,3-O-isopropylidene-α-L-sorbofuranose-4,6-(3′-amino)phenyl boronate) 23d $PdCl_2$(1,2:5,6-Di-O-isopropylidene-D-mannitol-3,4-(3′-amino)phenyl boronate) 23e $PdCl_2$(1,2:5,6-Di-O-cyclohexylidene-D-mannitol-3,4-(3′-amino)- phenyl boronate) 23f structure given in supplementary data S2 23g structure given in supplementary data S2		23g 47.62 µM Ref. drugs: Cisplatin 7.21 µM Doxorubicin 1 µM			
	24	24a $[Pd_2(tripy)_4](BF_4)_4$ 24b $[Pd_2(bntrz)_4](BF_4)_4$ 24c $[Pd_2(hextrz)_4](BF_4)_4$ 24d $[Pd_2(pegtrz)_4](BF_4)_4$	MDA-MB-231	24 hours: 24a 56.7 µM 24b 18.1 µM 24c 6 µM 24d not determined Ref. drug: Cisplatin 41.2 µM	Induction of late apoptosis and disruption of cell membrane.	Tested vs normal breast epithelial cells (MCF-10A)	2015 [128]
	25	*trans*-bis-(*cis*-7a-ethyl-5-methyl-5-phenylselanylmethyl-tetrahydro-pyrrolo[1,2-c]imidazole-1,3-dionato) palladium(II) chloride	MDA-MB-231	72 hours: 81.7 µM	Induction of iNOS protein expression and superoxide anion radical production. Decrease of cell´s migratory potential.	NA	2017 [129]

Group	Complex No.	Complex designation[a]	Cell line	IC_{50}	Target / mode of action	Selectivity towards TNBC	Year Ref.
	26	Includes two complexes 26a,b whose structures are given in supplementary data S3	MDA-MB-231	48 hours: 26a 2.8 μM 26b 1.5 μM	Induction of apoptosis. Photodynamic therapy.	NA	2017 [130]
	27	27a [{Pd(2,2′-bipy)Cl}$_2$(μ-pz)](ClO$_4$)$_2$ 27b [{Pd(dach)Cl}$_2$(μ-pz)](ClO$_4$)$_2$ 27c [{Pd(en)Cl}$_2$(μ-pz)](ClO$_4$)$_2$ 27d [{Pd(2,2′-bipy)Cl}$_2$(μ-4,4′-bipy)](ClO$_4$)$_2$ 27e [{Pd(dach)Cl}$_2$(μ-4,4′-bipy)](ClO$_4$)$_2$ 27f [{Pd(en)Cl}$_2$(μ-4,4′-bipy)](ClO$_4$)$_2$	MDA-MB-231	48h hours: 27a 17 μM 27b 26 μM 27c 25 μM 27d 70 μM 27e >100 μM 27f >100 μM Ref. drug: Cisplatin 55 μM	Induction of apoptosis and necrosis. G1/S cell cycle arrest.	Tested vs normal human fibroblast (MRC-5)	2017 [131]
Derivatives of thiourea	28	28a [PdCl(PPh$_3$)$_2$(N,N-dimethyl-N′-benzoylthioureato-k^{2}O,S)] 28b cis-[Pd(PPh$_3$)$_2$(N,N-diethyl-N′-benzoylthioureato-k^{2}O,S)]PF$_6$ 28c cis-[Pd(PPh$_3$)$_2$(N,N-diphenyl-N′-benzoylthioureato-k^{2}O,S)]PF$_6$ 28d cis-[Pd(PPh$_3$)$_2$(N,N-dibencyl-N′-benzoylthioureato-k^{2}O,S)]PF$_6$ 28e cis-[Pd(PPh$_3$)$_2$(N,N-diethyl-N′-furoylthioureato-k^{2}O,S)]PF$_6$ 28f cis-[Pd(PPh$_3$)$_2$(N,N-diphenyl-N′-furoylthioureato-k^{2}O,S)]PF$_6$ 28g cis-[Pd(PPh$_3$)$_2$(N,N-dibenzyl-N′-furoylthioureato-k^{2}O,S)]PF$_6$	MDA-MB-231	48 hours: 28a 2.15 μM 28b 1.12 μM 28e <0.8 μM 28c,28d,28f,28g >200 μM Ref. drug: Cisplatin 2.43 μM	NA	NA	2014 [132]

Group	Complex No.	Complex designation[a]	Cell line	IC_{50}	Target / mode of action	Selectivity towards TNBC	Year Ref.
Derivatives of chloroquine/ clotrimazole	29	29a *trans*-$PdCQ_2Cl_2$ 29b *trans*-$Pd(CTZ)_2Cl_2$*2/3CH_2Cl_2	MDA-MB-231	24 hours: 29a 49 µM, 29b 159 µM	NA	NA	2005 [133]
Phosphine derivatives and others	30	30a [$Pd(ca_2$-o-phen$)Cl_2$] 30b [Pd(dmba)(dppp)Cl]	MDA-MB-435	Complexes (0.1-5 µM) inhibited 90-95% of cell growth relative to cisplatin (5 µM).	NA	NA	2012 [134]
	31	31a *trans*-[$PdCl_2${$P(C_2H_4COOH)_3$}$_2$] 31b *trans*-[Pd_2Cl_4{$P(C_2H_4COOH)_3$}$_2$]	MDA-MB-231	24 hours: 31a 8.1 µM 31b 30.5 µM Ref. drug: Cisplatin 63 µM	NA	NA	2016 [135]
Derivatives of thiosemicarbazones	32	chloro, mono(phenanthrenequinone thiosemicarbazonato) pal- ladium(II) dimethyl formamide solvate	MDA-MB-231 BT-20	Exposure to 3 µg/ml for 72h reduced cell viability to 15% (MDA-MB-231),and 36% (BT-20).	NA	Tested vs 21 NT (mortal mammary epithelial cells (21NT) and normal breast epithelial cells (MCF-10A)	2005 [136]
	33	2-acetyl pyridine 4N-Ethyl Thiosemicarbazone Palladium(II) complex	MDA (type not further specified)	96 hours: ~0.7 µM Ref. drug: Cisplatin:~2.5 µM	NA	NA	2007 [137]

Group	Complex No.	Complex designation[a]	Cell line	IC_{50}	Target / mode of action	Selectivity towards TNBC	Year Ref.
	34	3,4-difluoroacetophenone-thiosemicarbazone palladium(II) complex	MDA-MB-231	Exposure to 10 µg/ml for 48h reduced cell viability to 50%.	NA	NA	2013 [138]

[a]Complex designation given by the original authors. 2,2′-bipy = 2,2′-bipyridyl; 4,4′-bipy = 4,4′-bipyridyl; BENSpm = N^1,N^{11}-bis(ethyl)norspermine; bpma = bis(2-pyridylmethyl)amine; bpy = 2,2-bipyridine; ca_2-o-phen = bis(cinnamaldehyde)-o-phenylenediimine); CQ = chloroquine; CTZ = clotrimazole; dach = *trans*-(±)-1,2-diaminocyclohexane; dmba = dimethylbenzylamine; dppe = 1,2-bis(diphenylphosphino)ethane); dppp = (diphenylphosphine)propane); en = ethylenediamine; Et = ethyl; Et_2dasa = diaminosuccinate diethyl ester dihydrochloride; H_2dasa = diaminosuccinic acid; hmbt = 2-(2‘-hydroxy-5‘-methylphenyl)-benzotriazole; Hmtpo = 5,7-dihydro-7-oxo-5- methyl[1,2,4]triazolopyrimidine; iPr = isopropyl; Me = methyl; MeO = methoxy; NSpd = norspermidine; OAc = Acetyl-oxy; pegtrz = (1,3-bis(1-(2-(2-methoxyethoxy)ethyl)-1H-1,2,3-triazol-4-yl)benzene) ligand; Ph = Phenyl; Phen = phenanthroline; PPh3 = Triphenylphosphine; Put = putrescine; Py = pyridine; pz = pyrazine; sac = saccharinate; Spd = spermidine; Spm = spermine; t-bu = tert-butyl; TCEP = tris(2-carboxyethyl)phosphine; terpy = 2,2‘:6‘,2‘‘terpyridine; tripy = 2,6-bis(pyridin-3-ylethynyl)pyridine).’

The wide range of distinct Pd-based compounds reported to this date as potential anticancer agents against TNBC, as well as the great variability in the cytotoxicity evaluation studies, hinder the establishment of accurate Structure-Activity Relationships. Nevertheless, some conclusions can be drawn specifically regarding their biological effects and potency (**Table 4**):

i. The complexes comprising amine ligands (linear alkylamines including biogenic polyamines and benzyl-amines/imines (**C1-C13**) were shown to be predominantly DNA damaging agents through covalent binding of the metal ion to the nucleophilic nitrogen atoms of the DNA bases (mainly the purines); for some complexes with modified biogenic polyamines (**C6**), binding to glutathione was also evidenced.
ii. For some of the benzyl-amine/imine complexes (**C13**), the induction of apoptosis was reported.
iii. The derivatives of pyridine/pyrazole/imidazole/pyrrol/triazole (**C14-C27**) were shown to be responsible for the induction of both apoptosis and necrosis. In turn, for a quite large number of investigated Pd-complexes displaying promising antineoplastic properties (*e.g.,* S-containing complexes of thiourea (**C28a-g**) or thiosemicarbazones (**C32-C34**), the mode of action, at the molecular level, is still unknown.
iv. Regarding the choice of ligands for the Pd(II)-complexes with activity against TNBC, they are either N-containing polydentate molecules and/or sulphur-moieties (Pd(II) having a higher affinity for sulphur *vs* nitrogen), in order to compensate for the high lability of these compounds, thus ensuring intracellular stability and avoiding drug inactivation.
v. Considering the *in vitro* potency towards TNBC cell lines, almost one third of the studied compounds exhibit IC_{50} between 0.1 and 5 μM, thus having an activity comparable or superior to the reference Pt(II) drug cisplatin. In particular, compounds with ligands such as biogenic polyamines (**C4b,c**; **C5a-c**; **C5e**; **C6**), thiourea (**C28a,b,e**) and thiosemicarbazones (**C33**), as well as some complexes with either ethyl diamine (**C1a,b**), benzyl amine/imine (**C9a-c**; **C10c,d**; **C11c,g,h,k,l**; **C12o,t**; **C13**) and pyridine/pyrazole/imidazole/pyrrol/triazole (**C14**; **C15**; **C16**; **C19b**; **C20b**; **C26a,b**) deserve further attention to verify and study their antitumour properties.
vi. In addition, even though there have already been reported syntheses of Pd(IV) complexes [139] that could be theoretically suitable for oral administration, up to this date only Pd(II) complexes have been screened as to their activity against TNBC cell lines.

vii. The moderate hydrophilicity of Pd(II) complexes points to an intravenous administration for the compounds developed so far. With a view to increase water solubility, aiming at a most desired oral administration, highly advantageous for patient compliance, several combinations of ligands have been tried, going from just one type of molecule within the first coordination sphere of the metal(s) to more than one kind of binding atoms and bridging moieties between them. These structural features are also aimed at tailoring the overall flexibility and stereochemistry of the compound, which are expected to facilitate its transport and enhance its interaction with the target(s). Furthermore, the nature of the leaving ligands – usually chlorides or acetoxy groups ($H_3C(C=O)O–$) – and their number and position in the molecule (*cis* or *trans*) are relevant features, since they regulate the drug activation mechanism inside the cell, that occurs through chloride hydrolysis (in the low [Cl^-] intracellular medium) followed by aquation, to yield an active drug prone to bind to its target(s) (*e.g.* DNA).

viii. Interestingly, a variety of Pd(II) complexes investigated so far (**C5e; C6; C7; C12o; C15; C16; C23; C24; C27; C32**) have already exhibited cancer selectivity towards TNBC, coupled to less deleterious effects towards non-cancerous cells.

I.3.1.1 Chemotherapeutic Mechanisms of Pd(II) Complexes against TNBC

TNBC is a breast cancer subtype that resists both conventional chemotherapy and surgical strategies, yielding unsatisfying clinical results and compelling the need for the search/development of mechanism-based approaches. The profound knowledge of signalling transduction pathways involved in the regulation of cell proliferation/survival are particularly important since most of the alterations occur in effector(s) of these signalling pathways during carcinogenesis. Such effectors are protein kinases, transcription factors and receptors known to maintain homeostasis. Thus, any abnormal activation or silencing of these effectors as well as their downstream signalization may contribute to uncontrolled cell growth leading to cell malignant transformation. This section briefly summarizes possible mechanisms of Pd complexes and their chemotherapeutic properties in TNBC (**Figure 9**).

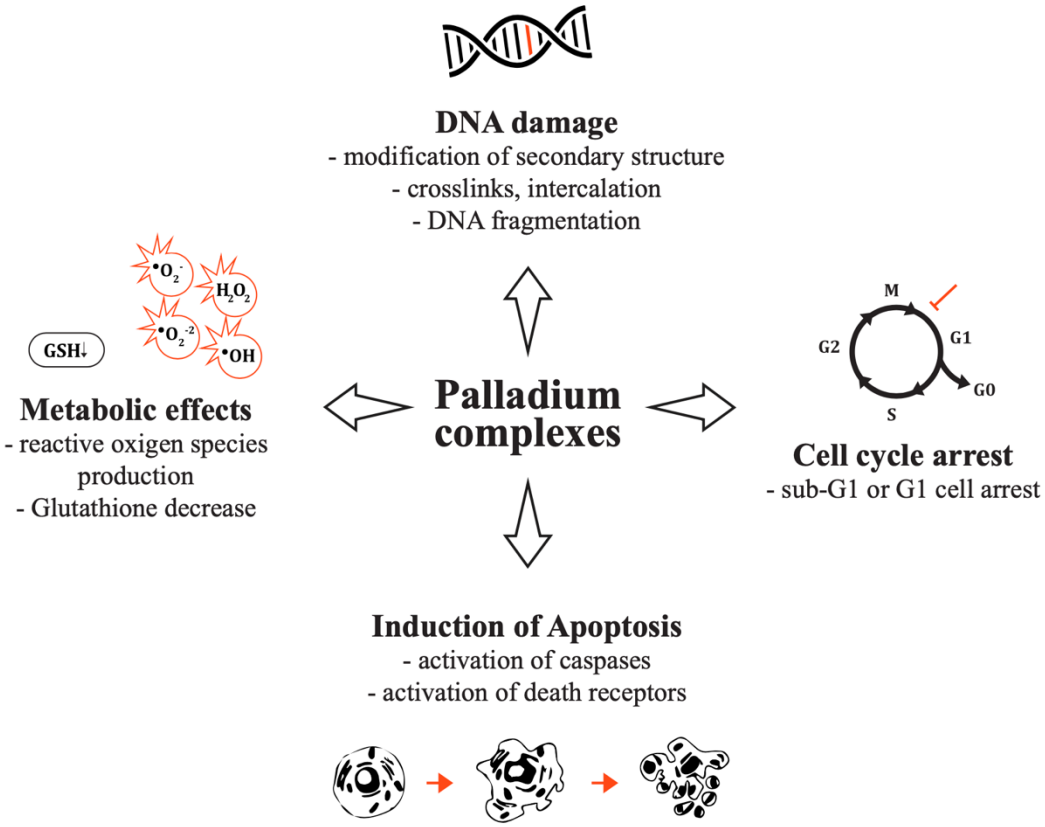

Figure 9. Mechanisms of action of Pd-based compounds.

I.3.1.1.1 DNA damage

Pd complexes may act as a novel class of metal-based agents that bind covalently to DNA´s nitrogen bases, resulting in DNA fragmentation by hindering an adequate DNA synthesis and RNA transcription from the affected DNA areas. DNA damage occurs through formation of cross-links, preventing DNA strands from being separated for synthesis or transcription, and inducing mispaired nucleotides which can lead to mutations [140]. Several Pd complexes, namely **C5e, C6, C13**-**C16** and **C19** have been identified to cause DNA conformational changes or fragmentation. The damaged DNA induces the DNA repair mechanisms, which in turn may lead to apoptosis when DNA repair is impeded.

I.3.1.1.2 Induction of Apoptosis

Several Pd complexes have been associated with pro-apoptotic events in TNBC, namely **C13, C15, C16, C19, C24, C26** and **C27**. Apoptosis occurs via activation of two major complex/energy-dependent pathways, the extrinsic (via death receptor) and the intrinsic (via mitochondria) pathways [141]. Some Pd complexes have been linked to the alterations in key proteins involved in the extrinsic pathway, such as caspase 3 (**C15, C19**),

caspase 8 (**C13**) and Fas death receptor or TNF-related apoptosis-inducing ligand (Trail) receptors 1 (DR4) and 2 (DR5) as reported for **C16**. Influence of Pd complexes on the intrinsic pathway such as cytochrome c release and upregulation of Bax and PUMA (p53 upregulated modulator of apoptosis) genes have also been demonstrated for **C13**.

I.3.1.1.3 Cell Cycle Arrest

It is well accepted that carcinogenesis is associated with cell cycle deregulation and/or overexpression of growth kinases [142]. Pd complexes (**C3, C13** and **C27**) arrest cell cycle of TNBC cells in G1 or G1/S phase and these effects may be either direct or indirect. The appearance of the sub-G1 peak that generally represents dead cells has been also reported for **C3** and **C13**. Indeed, DNA damage can lead to cell cycle arrest by triggering the p53 pathway, which, in turn, may lead to initiation of DNA repair or apoptosis.

I.3.1.1.4 Increase in Reactive Oxygen Species Levels

Reactive oxygen/nitrogen species (ROS/RNS) are formed by metabolic reactions and can interact with biomolecules resulting in oxidation of amino acyl residues in proteins, mutations in DNA, and lipid peroxidation producing more free radicals that increase the risk of mutations [143]. The ROS production was reported for **C16** and **C25**. Notwithstanding ROS–induced damage, this can be restored by internal surveillance and repair systems. However, high levels of ROS overwhelm cellular detoxifying systems, and cell division is stalled, and after prolonged arrest, cells may die from apoptosis. The decrease in glutathione levels, indicating an increase in the intracellular redox status, was reported for **C6**.

I.3.1.1.5 Necroptosis and Autophagy

Recently, the view on the triggers and mechanisms that lead to the process of cell death have been updated [144]. In addition to programmed cell death type such as apoptosis, recent studies have shown that some compounds may induce necroptosis and autophagy in cancer cells, leading to cell death [99,145–148]. Necroptosis is a form of programmed cell death occurring in cells exposed to stress factors, such as oxidative stress or DNA damage. Autophagy is a catabolic process that degrades cellular components and organelles, assuring cell survival in in nutrient-deprived conditions under usual circumstance. However, depending on the context and stimuli, excessive or prolonged autophagy can lead to autophagic cell death [149]. During autophagic cell death, autophagosomes engulf and degrade the cytoplasmic contents, leading to the breakdown of cellular components and ultimately resulting in cell death. Autophagic cell death is

characterized by the accumulation of autophagic vacuoles or autophagosomes in the cytoplasm and is often associated with the activation of caspase-independent cell death pathways such as necroptosis. Despite being reported as possible mechanisms to evade cancer drug resistance, the impact of Pd-based compounds on necroptosis and autophagy in TNBC still largely unknown and yet to be explored [150].

I.3.2 Pd(II)-Polyamine Complexes

The biogenic polyamines putrescine (Put), spermine (Spm) and spermidine (Spd) are low molecular weight organic polycations that are biosynthesized intracellularly (**Figure 10**) from arginine and methionine, as well as obtained exogenously through the diet [151]. These biogenic polyamines are essential for eukaryotic cell proliferation and differentiation [152]. Thus, it is not surprising that highly proliferating cancer cells have increased polyamine concentrations, as well as enhanced uptake and biosynthetic mechanisms. Therefore, depletion of the intracellular polyamine pool, through specific polyamine analogues or inhibitors of the polyamine biosynthetic enzymes, is an antineoplastic strategy that has been the object of research for the last 30-40 years. It has been demonstrated that after inhibition of polyamine biosynthesis with difluoromethylornithine (DFMO), cells quickly adapt to new condition by increase of extracellular polyamine uptake mediated by polyamine transport system. Thus, simultaneous inhibition of polyamine biosynthesis as well as inhibition of polyamine transport system with specific inhibitors such as “Trimer PTI” or “AMXT 1501” is required for successful depletion of intracellular polyamines [153]. This double-inhibition strategy is currently studied in clinical trials to demonstrate its efficacy. Nevertheless, these approaches have not yet delivered effective anticancer treatment to be implemented in a clinical practice, they have proved the importance and targetability of polyamines and their pathway as an anticancer strategy. Additionally, the polyamine transport system (for Put, Spd and Spm) is deemed capable of transporting polyamine-based molecules [154], such as Pd-polyamine complexes (**C4-7**). Therefore, the selectivity of Pd(II)-polyamine complexes towards cancer cells (namely TNBC) could be partially explained by this transport mechanism. Additionally, polynuclear complexes (comprising 2 or 3 metal centres) with linear aliphatic amines are particularly promising drugs, since they display a very high conformational freedom and variable length ligands (different bridging chains separating the metal ions within the chelate) [155,156]. This provides stable Pd(II)-agents able to interact with the DNA double helix in a very efficient way – *via* binding to more than one site, leading to the formation of long-range interstrands responsible for a more severe damage to DNA (as compared to the mononuclear clinically used drugs,

cisplatin, carboplatin and oxaliplatin), and therefore inducing cell death to a larger extent [157]. However, more detailed processes may be involved and need further elucidation.

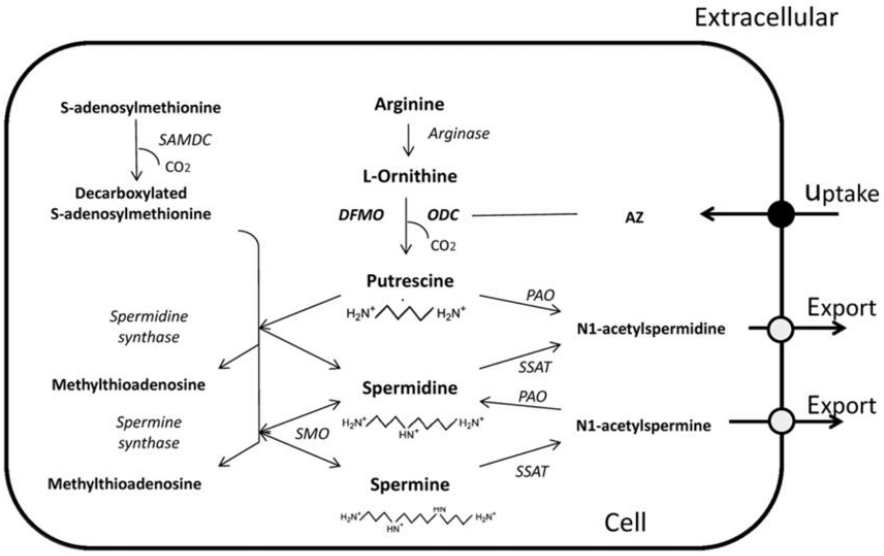

Figure 10. The Polyamine Metabolic Pathway.

ODC, ornithine decarboxylase; SAM-DC, S-adenosylmethionine decarboxylase; SSAT, spermidine-spermine-N1-acetyl transferase; PAO, polyamine oxidase; AZ, antizyme; DFMO, difluoromethylornithine; SMO, spermine oxidase. Adapted from [158].

I.3.2.1 Pd_2Spm and Pd_3Spd_2

Both Pd_2Spm (**C5e**) and Pd_3Spd_2 (**C4c**) are linear polyamine complexes with spermine and spermidine ligands, respectively, yielding stable chelates (**Figure 11**). Pd_2Spm comprises two Pd(II) centres coordinated to one polydentate spermine ligand (containing four N coordinating atoms). Pd_3Spd_2 comprises three Pd(II) centres coordinated to two polydentate spermidine ligands (each of them containing three N coordinating atoms). Pd_2Spm and Pd_3Spd_2 can bind with high affinity to the nitrogen atoms of the DNA bases, mainly to the purines (the adduct with guanine being favoured by intramolecular H-bonds). Their chemical features are responsible for an amphiphilic character and a high flexibility that enable an effective interaction with the DNA's double helix at distinct sites, both intra- and interstrand. Additionally, the hydrophobic moiety of the complexes (carbon aliphatic chains) allows quite a strong interplay with the DNA's backbone (pre-association), which favours the Pd–N- or Pt-N-binding process. Despite the advances achieved so far,

little is known regarding their mechanism of action, *in vivo* TNBC activity, selectivity and ability to overcome TNBC resistance to Pt drug.

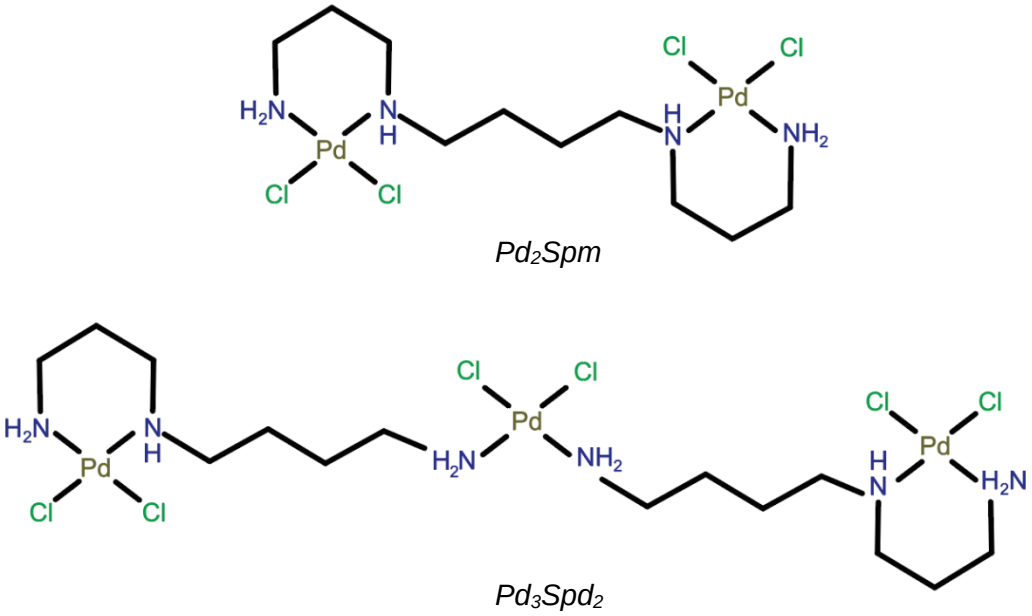

Figure 11. Chemical structure of Pd-based agents Pd_2Spm and Pd_3Spd_2

CHAPTER II: GENERAL SCOPE AND AIMS OF THE WORK

CHAPTER II – GENERAL SCOPE AND AIMS OF THE WORK

STUDY BASIS

- TNBC is an aggressive subtype of breast cancer subtype that lacks hormone receptors and HER2 expression, hindering the use of targeted therapies available for other breast cancer subtypes. Thus, therapy options for TNBC are limited, resulting in urgent medical need to be addressed.
- Cisplatin is a commonly used chemotherapy drug for the treatment of TNBC but presents significant side effects and becomes less effective or completely ineffective over the time-course of the treatment due to development of resistance by cancer cells.
- Pd(II)-based compounds with polyamines seem to present an appealing alternative to cisplatin due to their similarity in coordination chemistry and potentially having lower toxicity.
- The study involves di-nuclear (Pd_2Spm) and tri-nuclear (Pd_3Spd_2) Pd(II)-based compounds with biogenic polyamines previously synthesized and characterized by our partners at the Molecular-Physical Chemistry R&D Group, Department of Chemistry, University of Coimbra (Portugal).

STUDY HYPOTHESIS

- The hypothesis of this study is that selected Pd(II)-based compound(s) present comparable or superior therapeutic potential than cisplatin, in regard to its (i) efficacy to inhibit TNBC growth, both *in vitro* and *in vivo*; (ii) ability to circumvent cisplatin's resistance; (iii) having good pharmacokinetic properties and biodistribution; (iv) and presenting lower toxicity than cisplatin.

STUDY GOALS

1. Develop and characterize cisplatin-resistant model of TNBC cells via continuous exposure of MDA-MB-231 to cisplatin.
2. Compare the antiproliferative activity, potency, selectivity and ability to circumvent resistance of Pd(II)-based compounds (Pd_2Spm and Pd_3Spd_2) with that of cisplatin in breast cancer MDA-MB-231, MDA-MB-231/R and non-neoplastic breast cells MCF-12A. Select the most promising compound from this screening to be used in further experiments.

3. Develop and validate an ICP-MS method for a quantitative analysis of Pd and Pt in animal biologic samples due to inexistence of a suitable method validated for different biological fluids and samples.
4. Compare the pharmacokinetics and the biodistribution of the selected Pd(II)-based compound and cisplatin in mice.
5. Assess the *in vivo* efficacy of selected Pd(II)-based compound against TNBC in mouse xenograft models, measuring tumour growth inhibition and toxicity.
6. Investigate the mechanisms of action of selected Pd(II)-based compound and its putative targets.

CHAPTER III: MATERIAL AND METHODS

III.1 Reagents, Materials, Equipment and Software

The reagents, materials, equipment and software used in this work are listed in **Appendix A** in **Table A1** (Reagents), **Table A2** (Materials) and **Table A3** (Equipment and Software).

III.2 Pd_2Spm and Pd_3Spd_2 Syntheses

The Pd_2Spm complex was synthesized according to published procedures [159] that were further optimized [156]: 2 mmol of K_2PdCl_4 was dissolved in a minimal amount of water and 1 mmol of spermine aqueous solution was added dropwise under continuous stirring. After 24 h, the resulting orange powder was filtered and washed with acetone, and the yellow-orange needle-shaped crystals were recrystallized from water. The composition and purity of the synthesized compound were fully obtained by elemental analysis and vibrational spectroscopy (FTIR, Raman and inelastic neutron scattering), which were compared with the previously calculated vibrational profiles (by ab initio methods) [156,160]. Yield: 68%. Elemental analysis ($Pd_2(C_{10}N_4H_{26})Cl_4$): Found—C: 21.2%; H: 4.7%; N: 9.6%, Cl: 25.9%.

The Pd_3Spd_2 complex was synthesized according to published procedures [103,161] that were further optimized: 3 mmol of K_2PdCl_4 was dissolved in a minimal amount of water, and 1.98 mmol of spermidine trihydrochloride aqueous solution was added dropwise under continuous stirring. After 15 min, the resulting orange precipitate was isolated by filtration and washed with water, ethanol and acetone and air-dried.

III.3 *In Vitro* Cell-Based Methodologies

III.3.1 Drug Formulations

A Pd_2Spm stock solution (400 µM) and Pd_3Spd_2 stock solution (400 µM) were freshly prepared by dissolving an appropriate quantity of drug in phosphate-buffered saline (PBS) (H_2PO_4 1.5 mM, Na_2HPO_4 4.3 mM, KCl 2.7 mM, NaCl 150 mM, pH 7.4) containing 3% of DMSO, and sterile-filtered. A stock solution of cisplatin (500 µM) was prepared in PBS and sterile-filtered. A stock solutions of oxaliplatin (5 mM) and carboplatin (5 mM) was prepared in ultrapure water and sterile-filtered.

III.3.2 Cell Cultures

The human TNBC MDA-MB-231 cell line (ATCC HTB-26) and the non-cancerous breast cell line MCF-12A (ATCC CRL-10782) were purchased from ATCC (Manassas, VA, USA). DMEM-HG cell growth medium supplemented with 10% (v/v) FBS was used to culture breast cancer cells. To establish a cisplatin-resistant cell strain, MDA-MB-231 cells were continuously treated with increasing concentrations of cisplatin (up to 2 µM) during a period of 6 months. When a consistent cell growth rate in the presence of cisplatin was achieved, these cells were named MDA-MB-231/R and stocked to assure the consistency of the phenotype for future use and experiments. All posterior experiments were performed within 10 passages to maintain the resistance while routinely growing the MDA-MB-231/R cell line in a cell culture medium without the addition of cisplatin. MCF-12A cells were cultured in DMEM/F12 medium supplemented with 100 ng/mL cholera toxin, 0.01 mg/mL bovine insulin, 20 ng/mL hEGF, 500 ng/mL hydrocortisone and 5% (v/v) horse serum. Cells were grown in monolayers in a sterile environment at 37 °C with a 5% CO_2 humidified atmosphere. Under these conditions, the population doubling time was 25.5 ± 0.9 h and 30.6 ± 1.1 h for MDA-MB-231 and MDA-MB-231/R cells, respectively, and 20.6 ± 3.1 h for MCF-12A cells. The cell cultures were routinely screened for mycoplasma contamination, yielding negative results.

III.3.3 Cell Proliferation Assay

Cells were seeded in 96-well microplates at the cell density 1.5×10^4 cells/cm^2 (final volume 200 µL/well) and left 24 h to attach. Afterwards, the growth medium was replaced with the growth medium containing cisplatin (0.1–200 µM), carboplatin (0.3–200 µM), oxaliplatin (0.3–200 µM), Pd_3Spd_2 (0.3–200 µM),or Pd_2Spm (1–160 µM).

Cell proliferation was monitored with the direct image acquisition of cells on microplates at 0, 24, 48 and 72 h post-addition of the tested compounds using a LionheartFX automated microscope (BioTek, Winooski, VT, USA). Label-free kinetic 4× images were acquired and processed using Gen 5 Image Analysis software (BioTek, Winooski, VT, USA). Individual cells per image were identified and counted, and normalized cell growth (%) was calculated using the following formula:

$$\mathrm{C(t)} = \left[\frac{(\text{Number of Treated Cells(t)} - \text{Number of Treated Cells(0)})}{(\text{Number of Untreated Cells(t)} - \text{Number of Untreated Cells(0)})}\right] \times 100$$

where C(t) is the percent of net cell growth over time, Number of Treated Cells(t) is the count of cells treated with drug at each time point, Number of Treated Cells(0) is the

count cells treated with drug at time 0 h, Number of Untreated Cells(t) is the count of untreated (control) cells at each time point and Number of Untreated Cells(0) is the count of untreated (control) cells at time 0 h.

III.3.4 Cell Migration – Wound Healing Assay

The effect of compounds on cell migration was studied using wound healing assay (or scratch assay). Triple-negative breast cancer MDA-MB-231 cells were seeded in 24-well microplate at the cell density 12.5 × 10^4 cells/cm^2 (1 mL final volume) and left 24 h to attach and create a confluent monolayer. The cell monolayer was scratched with 200 µL pipette tip, producing a vertical straight wound in the middle of the well; growth medium was removed and wells were washed twice with growth medium to remove all detached cells. Growth medium containing Pd_2Spm (12.5–200 µM) or cisplatin (6.25–200 µM) was added to the wells, and microplates were imaged using LionheartFX automated microscope at 0, 3, 18, 20, 24 and 48 h. Wound closure was analysed as a confluence of the initial cell-free area covered by migrating cells at the indicated time points measured with *G*en 5 Image Analysis software. Confluence was calculated using the following formula:

$$\mathrm{C(t)} = \left[\frac{(\text{Object Sum Area(t)} — \text{Object Sum Area(0)})}{(\mathrm{I(A)} — \text{Object Sum Area(0)})}\right] \times 100$$

where C(t) is the percent wound confluence over time, Object Sum Area(t) is the area covered by cells at each time point, Object Sum $\text{Area}_{(0)}$ is the area covered by cells at time 0 h and $I_{(A)}$ is the total area of the 4X image. The area under the curve (AUC) of kinetic time–confluence profiles obtained within 0–18 h for each concentration was calculated ($AUC_{0\text{-}18h}$), plotted against the drug concentration and analysed with nonlinear regression to obtain the half maximal effective concentration (EC_{50}) for Pd_2Spm and cisplatin.

III.3.5 Quantitative Analysis of Vascular Endothelial Growth Factor (VEGF) Production

MDA-MB-231 cells were seeded in 96-well microplates at the cell density 1.5 × 10^4 cells/cm^2 (final volume 200 µL/well) and left 24 h to attach. The growth medium was replaced with growth medium containing Pd_2Spm (5–20 µM) or cisplatin (5–20 µM), and cells were incubated for 12 h. VEGF concentration in cell culture medium was determined in undiluted samples in duplicate using the Human VEGF Quantikine ELISA Kit (R&D Systems Inc., Minneapolis, MN, USA) according to the manufacturer's protocol. In brief, 200 µL of conditioned media was added to a 96-well microplate pre-coated with monoclonal

antibody for human VEGF and the plate was incubated for 2 h. After washing with wash buffer, enzyme-linked polyclonal antibody specific for human VEGF was added, followed by incubation for 2 h. The plate was washed to remove unbound antibody-enzyme reagent, substrate solution was added and incubated for 30 min and the reaction was terminated by the addition of the stop solution, producing a yellow solution. The optical density at 450 nm with wavelength correction at 540 nm was measured using a Synergy HT microplate reader (BioTek, Winooski, VT, USA). The concentration of VEGF was interpolated from the standard curve (15.6–1000 pg/mL) prepared in parallel.

III.3.6 Intracellular Accumulation of Pd2Spm or Cisplatin in Breast Cancer Cells

The intracellular Pt and Pd accumulation in MDA-MB-231 and MCF-12A cells was analysed using ICP-MS. First, $3 \times 10^4/cm^2$ cells were seeded in T75 culture flasks and allowed to attach for 24 h. Cells were subsequently treated for 24 h with 2, 4 or 8 μM of either Pd_2Spm or cisplatin in four independent experiments (n = 4). The cells were trypsinised, washed twice with ice-cold 0.9% saline solution, and 10^6 cells were pelleted and freeze-dried. The lyophilized cell pellets were digested and analysed using the same analytical procedure described for the pharmacokinetic study (*please see the section III.4.3.4*). The quantity of accumulated Pd and Pt in cells was converted in the correspondent concentration of Pd_2Spm and Cisplatin in pmoles per 1 mg of protein. The protein concentration used for the data normalization was determined from identical samples that were prepared in parallel and quantified with the Bradford protein assay, following the manufacturer's instructions.

III.3.7 Western-blot analysis

Cells were seeded in T25 cm^2 flask (1.5×10^4 cells/cm^2) and left for 24 h to attach. Afterwards, cells were exposed to 10 μM of Pd_2Spm or Cisplatin for 48 h, washed with PBS and lysed with RIPA buffer supplemented with protease inhibitors cocktail (Abcam, UK). Protein concentration in lysates was determined using the Bradford assay. Samples (20 μg of proteins in 6X Laemmli sample loading buffer) were separated by SDS–PAGE using 12% TGX Stain-free gels (Bio-Rad, Lisbon, Portugal) and blotted onto PVDF membrane. Membranes were blocked with 5% BSA, during 1 h at room temperature (RT) and probed with rabbit anti-cleaved caspase-3 (1:500), and rabbit anti-LC3B (1:2000) antibodies overnight at 4 °C. Blots were washed with TBST, incubated with goat anti-rabbit horseradish peroxidase (HRP) conjugated secondary antibody (1:5000) during 1 h, at RT, washed with

TBST and the immunocomplexes were detected using the Novex ECL Chemiluminescent kit (Invitrogen, Life Technologies, Madrid, Spain) and ChemiDoc MP Imaging System (Bio-Rad, Lisbon, Portugal). Chemiluminescent signal was quantified using ChemiDoc™ Imaging Systems with Image Lab™ Software Instrument (Bio-Rad, Lisbon, Portugal). The stain-free signal of total protein per lane was also captured and used for the normalization of immunolabeled protein bands relative to the total proteins in the respective lane.

III.3.8 Detection of autophagic vesicles – MDC staining

Autophagy was detected with monodansylcadaverine (MDC), a fluorescent compound that is incorporated into autophagic vacuoles by both an ion trapping mechanism and the interaction with membrane lipids in cultured cells. First, cells were treated with Pd_2Spm or cisplatin for 48 h and then growth medium was replaced with 100 μM of MDC in HBSS for 15 min at 37 °C. Cells were washed and fresh HBSS medium was added to cells. LionheartFX automated microscope with direct image acquisition of cells in microplates was used to acquire images, which were further processed using Gen 5 Image Analysis software.

III.3.9 Apoptosis monitoring – externalization of phosphatidylserine residues

Externalization of phosphatidylserine in living cells was performed using polarity-sensitive indicator of viability and apoptosis (pSIVA)-IANBD, a polarity-sensitive probe. Briefly, MDA-MB-231 and MDA-MB-231/R cells were 96-well ½ area black microplates at the cell density 1.5 × 10^4 cells/cm^2 (final volume 100 μL/well) and left 24 h to attach. Afterwards, the growth medium was replaced with the growth medium containing Pd_2Spm or cisplatin together with pSIVA probe. LionheartFX automated microscope was used to acquire 4X cell images in microplates at 48 h post-addition of the tested compounds. Images were processed and analysed using Gen 5 Image Analysis software allowing identification and counting of individual cells per image.

III.3.10 ERK1/2 Phosphorylation Assay

Changes in phosphorylated ERK1/2 (pERK) were detected using the AlphaScreen SureFire pERK1/2 Kit. Briefly, 10 μL of total protein lysate (prepared for WesternBlot) was transferred into 384-well ProxiPlates and mixture of acceptor beads and donor beads were added manufacturer's instructions. Alpha fluorescent signal was normalized to total protein content determined in parallel, and data were expressed as fraction of control.

III.3.11 NF-κB Phosphorylation Assay

Changes in phosphorylated NF-κB (p-NF-κB) were detected using the AlphaScreen SureFire p-NF-κB Kit. Briefly, 10 µL of total protein lysate (prepared for WesternBlot) was transferred into 384-well ProxiPlates and mixture of acceptor beads and donor beads were added manufacturer's instructions. Alpha fluorescent signal was normalized to total protein content determined in parallel, and data were expressed as fraction of control.

III.4 *In Vivo* Animal-Based Methodologies

III.4.1 Ethical Considerations

The European Directive 2010/63/EU on the protection of laboratory animals used for scientific purposes (European Parliament, Council of the European Union, 2010) and the Portuguese law on animal welfare (Decreto-Lei 113/2013) were followed for designing and conducting all research procedures. The study protocol was approved by the Ethics Committee of the Faculty of Pharmacy of the University of Porto, Porto, Portugal (Permit Number: 25-10-2015), and by the Ethics Committee and the Organ Responsible for the Welfare of Animals of ICBAS-UP, Porto, Portugal (Permit number 134/2015).

III.4.2 ICP-MS Analytical Method Development and Validation

III.4.2.1 Animals and Housing & Husbandry

Adult, 18-week-old, male Wistar Han rats (5 animals in total) with a mean weight of 466 ± 51 g were used (Charles River Laboratories, Barcelona, Spain). Animals were housed under the standard conditions (controlled light/dark cycles of 12 h, 20–22 °C and unlimited access to water and standard pellet food).

III.4.2.2 Preparation of In-House Material and Animal Procedures

Due to the inexistence of certified reference materials (animal tissues containing Pd and Pt), an in-house material was prepared for each tissue and biofluid under study. To obtain a sample matrix representing the true complexity of biologic tissues with intracellular incorporation and metabolism of Pd and Pt compounds, a standard solution containing 200 µg/mL of Pd and Pt (in Phosphate-Buffered Solution, pH 5.5) was administrated *via* intraperitoneal injection (1 mL/administration) twice in each animal within 16 h. Animals were euthanized by decapitation and white adipose tissue from peritoneal cavity (visceral

depots), abdominal muscle, liver, kidney, spleen, testis, heart, lungs and brain were collected, weighed and stored at –80 °C. Blood was also collected at the same time into tubes with sodium heparin to obtain whole blood samples. Tubes without anticoagulant were used for blood serum separation after leaving the blood to coagulate for 30 min at room temperature and centrifuging at 500 x g and 4 °C for 15 min.

III.4.2.3 Sample Preparation

Solid tissues were freeze-dried (0.016 mBar, –80.8 °C, 48 h; Telstar®, model Cryodos Barcelona, Spain) and pulverized with mortar and pestle or using a Precellys® Evolution tissue homogenizer (Bertin-Instruments, Montigny-le-Bretonneux, France) in case of hard tissues such as lungs, heart and muscle (2.8 mm stainless steel beads, ten cycles of 60 s at 7500 rpm speed). Freeze-dried solid tissues, serum and blood (50 mg or 50 µL) were accurately weighed into 10 mL polypropylene tubes and 0.9 mL of HNO_3 (≥ 69.0% w/w) plus 0.3 mL of HCl (37% w/w) were added to the tubes. The tubes were closed and placed in a water bath at 90 °C for 1 h. Then, sample digests were cooled to room temperature, 1 mL of the 100 µg/L internal standard (IS) solution was added, and the final volume was adjusted to 6 mL with ultrapure water. Prior to ICP-MS analysis, samples were further diluted 5-fold with a diluent solution (2% HNO_3 + 3% HCl + 16.66 µg/L IS).

Microwave-assisted acid digestion was performed as reference digestion procedure using an MLS 1200 Mega high-performance microwave digestion unit (Milestone, Sorisole, Italy) equipped with an HPR-1000/10 S rotor. Samples (50 mg) were accurately weighed into previously decontaminated microwave oven PTFE vessels and 0.9 mL of HNO_3 (≥ 69.0% w/w) plus 0.9 mL of HCl (37% w/w) were added. Afterward, vessels were closed, placed in the microwave oven and heated using the manufacturer's recommended program: 250 W for 1 min, 0 W for 2 min, 250 W for 5 min, 400 W for 5 min, and 600 W for 5 min. After cooling, 1 mL of the IS solution was added and the final volume was adjusted to 6 mL with ultrapure water.

III.4.2.4 ICP-MS Instrument and Conditions

An iCAP™ Q (Thermo Fisher Scientific, Bremen, Germany) ICP-MS was used for the determination of Pd and Pt. Calibration standards ranging from 0.025 to 10 µg/L were prepared from the 100 mg/L multi-element commercial TraceCERT®, ICH Q3D oral, Standard 2 solution. The IS solution was prepared at 100 µg/L by appropriate dilution of the ICP-MS-200.8-IS-1 solution. The IS solution was added to the samples resulting in a final

concentration of 16.66 µg/L. The elemental isotopes (*m/z* ratios) monitored were ^{108}Pd and ^{195}Pt. The elemental isotopes ^{89}Y, ^{115}In, ^{159}Tb and ^{209}Bi were used as internal standards.

III.4.2.5 Method Optimization

Several experiments were conducted to optimize the acid digestion procedure in closed tubes with screw cap for the quantitative analysis of Pd and Pt. The liver tissue was used during the method optimization due to its higher availability compared to the other tissues. Two types of experimental designs were used: 1) a two-level (2^k) full factorial design that was aimed to screen the main variables affecting the acid digestion procedure; 2) a central composite design (CCD) that was used to optimize the significant variables selected from the previous experimental design. The response was the sum of Pd and Pt concentration in the in-house material. One full factorial design was created at low (−1) and high (+1) levels four factors, accounting 21 experiments (five central points were included). This full factorial design was created to evaluate the significance of the variables HNO_3 volume (0.3–0.9 mL), HCl volume (0.3–0.9 mL), reaction time (10–60 min), reaction temperature (60–90 ºC).

The four variables were selected for the CCD because all of them were considered significant in the two-level factorial design. Thus, a CCD consisting of a complete 30-factorial design with six centre points and two axial points on the axis of each design variable at a distance of α = 1.682 from the design centre was performed. Experiments were carried out as follows: HNO_3 volume (0.3–0.9 mL), HCl volume (0.3–0.9 mL), reaction time (30–60 min), reaction temperature (60–90 ºC). The complete experimental design was performed using the Design Expert Trial Version 10 (Stat-Ease, Inc., MN, USA) software. The appropriate fitting model for the response was selected based on the comparison of various statistical parameters such as R^2, Q^2, lack of fit and adequate precision. After the fitting of the mathematical model, the desirability function was studied for the optimization of independent variables for desirable responses.

III.4.2.6 Method Validation

The limits of detection (LOD) and limits of quantitation (LOQ) of the developed procedure were calculated from the standard deviation of digested blank samples ("procedural blanks") using the formulae: $LOD = 3 \times \sigma$ and $LOQ = 10 \times \sigma$, where σ is the standard deviation of digested blank samples. The repeatability of the developed procedure was evaluated for the 11 matrices under study: adipose tissue, abdominal muscle, liver,

kidney, spleen, testis, heart, lungs, brain, blood, and serum. Samples were digested in duplicate (using optimal digestion conditions identified by CCD optimization) and the digests were analysed also in duplicate (at the beginning and end of the ICP-MS analytical run). The results were expressed as coefficient of variation (%CV). The overall %CV was calculated considering the %CV obtained for each type of analysed matrix. The between-run precision (intermediate precision) was evaluated by analysing the samples digests in three non-consecutive days (three ICP-MS runs). The results were also expressed as %CV. Accuracy was also studied for all the tissues and biofluids by comparing the Pd/Pt contents obtained in the proposed method with those obtained with microwave-assisted sample digestion, which is considered the "reference method"[162–164]. Accuracy was calculated from the mean Pd and Pt contents using the following formula:

$$Accuracy\ (\%) = \frac{metal\ content\ obtained\ by\ developed\ method}{metal\ content\ obtained\ by\ reference\ method} \times 100$$

The matrix effect was evaluated using sample digests spiked at 1 µg/L of Pd/Pt. The recovery was calculated using the following formula:

$$Recovery\ (\%) = \frac{(spiked\ sample\ concentration\ -\ original\ sample\ concentration)}{spiked\ sample\ concentration} \times 100$$

The agreement between the newly developed method and reference method (microwave-assisted digestion) was analysed using the Bland–Altman plot [165].

III.4.3 Pharmacokinetics of Pd_2Spm

III.4.3.1 Animals and Housing & Husbandry

Six-week old, Specific-Pathogen-Free (SPF), female BALB/cByJ mice (60 animals in total) were purchased from Charles River Laboratories (L'Arbresle, France) and acclimatized at ICBAS-UP Rodent Animal House Facility (Porto, Portugal) for one week. Animals were randomly distributed into groups of five per individually ventilated cage and were housed under controlled SPF environmental conditions (temperature 22.5 ± 1.5 °C; relative humidity 50 ± 10%; 12 h light/dark cycle) with ad libitum access to water and standard pellet food (4RF21, Mucedola, Italy). Environmental enrichment included corncob bedding, paper roll tube and one large sheet of tissue paper for nesting. Animals were monitored daily for health status, and no adverse events were observed during the study.

III.4.3.2 Drug Formulations

Pd_2Spm 0.3 mg/mL solution for *in vivo* administration was freshly prepared by dissolving an appropriate quantity of drug in Phosphate-Buffered Saline (PBS) (H_2PO_4 1.5 mM, Na_2HPO_4 4.3 mM, KCl 2.7 mM, NaCl 150 mM, pH 7.4) containing 1% of DMSO and sterile-filtered. The solution of cisplatin 0.35 mg/mL was prepared in PBS and sterile-filtered.

III.4.3.3 Study Design and Animal Procedures

Animals were randomly allocated into two study groups (30 animals/group): Pd_2Spm and cisplatin. No control group was used since Pt and Pd metals were inexistent in drug-naïve rodents. On the day of the experiments, animals were weighed (mean ± SD: 20.4 ± 1.7 g), and a single dose of Pd_2Spm 3 mg/kg BW (corresponds to 1.15 mg/kg BW of Pd) or cisplatin 3.5 mg/kg BW (corresponds to 2.28 mg/kg BW of Pt) was administered via intraperitoneal bolus injection (200 µL/injection) in Pd_2Spm and cisplatin groups, respectively. After drug administration, five animals from each group were euthanized at selected time-points (0.5, 1, 6, 12, 24 and 48 h) with pentobarbital intraperitoneal injection (120 mg/kg) followed by cardiac puncture for blood collection. Blood serum was separated after leaving the blood to coagulate for 30 min at room temperature and centrifugation (at 500× *g*, and 4 °C for 15 min). The serum was separated, and a small aliquot was filtered using Amicon Ultra-0.5mL Centrifugal Filters (14,000× *g*, 20 °C, 30 min) with 30K NMWL (Merck KGaA, Darmstadt, Germany) to obtain serum ultrafiltrate for the study of drug binding to plasma proteins. Both blood serum and serum ultrafiltrate were aliquoted (50 µL) and stored at −80 °C until ICP-MS analysis. Right brain hemisphere, liver, lungs, heart, right kidney, ovaries, abdominal white adipose tissue and abdominal mammary glands were excised at the same time, washed in cold PBS, blotted dry on filter paper and weighed. Solid tissues were freeze-dried (0.016 mBar, −80.8 °C, 48 h; Telstar®, model Cryodos Barcelona, Spain) and stored hermetically sealed at −80 °C until ICP-MS analysis.

III.4.3.4 Sample Preparation and ICP-MS Analysis

Quantification of Pd and Pt in the biologic samples collected from *in vivo* pharmacokinetic studies was achieved using a validated method as specificized in the section *III.4.2 ICP-MS Analytical Method Development and Validation.* Briefly, 50 µL of blood serum, 50 µL of serum ultrafiltrate and weighed entire freeze-dried organs/tissues (up to 50 mg) were placed into 10 mL polypropylene conical tubes. In the case of liver, for which the weight surpassed 50 mg, the tissue was first pulverized with a Precellys® Evolution

tissue homogenizer (Bertin-Instruments, Montigny-le-Bretonneux, France) using 2.8 mm stainless steel beads (two cycles of 10 s at 6000 rpm speed) and accurately weighed (50 mg) in tubes. Samples were digested directly in tubes with 0.9 mL of HNO_3 (≥69.0% *w*/*w*) plus 0.3 mL of HCl (37% *w*/*w*) in a water bath at 90 °C for 1 h. Sample digests were cooled to room temperature, 0.5 mL of a 100 µg/L internal standards (IS) solution was added and the final volume was adjusted to 5 mL with ultrapure water (final concentration of IS = 10 µg/L). Prior to ICP-MS analysis, samples were further diluted 5-fold with a diluent solution (2% HNO_3 + 3% HCl + 10 µg/L IS). An iCAP™ Q (Thermo Fisher Scientific, Bremen, Germany) ICP-MS was used for the determination of Pd and Pt in the obtained solutions. Calibration standards ranging from 0.025 to 100 µg/L were prepared from the 100 mg/L multi-element commercial TraceCERT®, ICH Q3D oral, Standard 2 solution. The IS solution was prepared at 100 µg/L by appropriate dilution of the ICP-MS-200.8-IS-1 solution. The elemental isotopes (*m/z* ratios) ^{108}Pd and ^{195}Pt were used for analytical determination. ^{89}Y, ^{115}In, ^{159}Tb and ^{209}Bi were used as internal standards.

III.4.3.5 Pharmacokinetic Analysis

Pharmacokinetic parameters for Pd_2Spm and cisplatin were estimated using Phoenix WinNonlin v8.3.1.5014 (Certara USA Inc., Princeton, NJ, USA). The data were expressed as nanograms of Pd (from Pd_2Spm) or Pt (from cisplatin) measured by ICP-MS per gram of wet tissue weight or per mL of serum/serum ultrafiltrate. Considering the molecular weights of each compound and the molar ratios of respective atoms, the molar ratio of Pd atom in Pd_2Spm molecule is 2:1 with mass Pd (%) = 38.21%, [MW(Pd_2Spm) = 557 g/mol]; and the molar ratio of Pt atom in cisplatin molecule is 1:1 with mass Pt (%) = 65.02%, [MW(cisplatin) = 300.01 g/mol]. Accordingly, the administered dose of Pd (from Pd_2Spm 3 mg/kg) was 1.15 mg/kg, and the administered dose of Pt (from cisplatin 3.5 mg/kg) was 2.28 mg/kg. The mean concentrations of Pd or Pt in serum and serum ultrafiltrate were plotted logarithmically versus time. Non-compartmental analysis was performed on sparse data with $1/Y^2$ weighting, which was selected based on the highest correlation coefficients and agreement between observed versus predicted pharmacokinetic parameters. The highest drug concentration observed following administration (C_{max}) and the time at which it was observed (t_{max}) were established from the temporal evolution of respective Pd/Pt concentrations in serum and serum ultrafiltrate. The area under the curve (AUC) from time zero to the last time with quantified concentration ($AUC_{0\text{-}48h}$) was calculated by a linear log trapezoidal (linear up log down) method. The AUC from time zero to infinity ($AUC_{0-\infty}$) was extrapolated as $AUC_{0-48\ h} + C_{48h}/\lambda z$, where C_{48h} is

the last measured concentration, and λz is the elimination constant rate calculated using linear regression of the terminal portion of the log–linear serum concentration–time curve. The drug half-life ($t_{1/2}$) was calculated as ln2/λz. The rate of total clearance (CL/F) of the compound was calculated as the administered metal dose divided by the $AUC_{0-\infty}$. The distribution volume based on the terminal phase (Vz/F) was calculated as dose/[λz.$AUC_{0-\infty}$].

III.4.4 Efficacy and Safety of Pd_2Spm: *In Vivo* Tumour Xenografts

III.4.4.1 Animals and Housing & Husbandry

Female CBA nude (N:NIH(S)II-nu/nu) mice (6-7 weeks old, 21 animals in total) with combined immunodeficiency [166] were purchased from i3S Animal Facility (Porto, Portugal). Animals were acclimatized at ICBAS-UP Rodent Animal House Facility (Porto, Portugal) at least one week prior to the experiments, were randomly distributed into groups of three per individually ventilated cage and were housed under controlled specific-pathogen-free (SPF) environmental conditions (temperature 22.5 ± 1.5 °C; relative humidity 50 ± 10%; 12 h light/dark cycle) with ad libitum access to water and standard pellet food (4RF21, Mucedola, Italy). Environmental enrichment included corncob bedding, paper roll tube and one large sheet of tissue paper for nesting. Animals were monitored daily for health status and welfare.

III.4.4.2 Drug Formulations

A Pd_2Spm 0.28 mg/mL solution for *in vivo* administration was freshly prepared by dissolving an appropriate quantity of drug in phosphate-buffered saline (PBS) (H_2PO_4 1.5 mM, Na_2HPO_4 4.3 mM, KCl 2.7 mM, NaCl 150 mM, pH 7.4) containing 0.5% of DMSO and sterile-filtered. A solution of cisplatin 0.35 mg/mL was prepared in PBS and sterile-filtered.

III.4.4.3 Study Design and Animal Procedures

Mice were subcutaneously implanted in the left flank with breast cancer MDA-MB-231 cells (25G needle, 5×10^6 cells in 150 µL of PBS). At day 25 post-implantation, when tumours reached a mean volume of ~250 mm^3, mice were randomly allocated into three groups (7 animals per group) using computer-generated randomization sequence followed by random group allocation to the treatment with either A) Pd_2Spm, B) cisplatin or C) vehicle. The Pd_2Spm (5 mg/kg/day), cisplatin (2 mg/kg/day) or vehicle (PBS + 0.5% DMSO) were administered via intraperitoneal injection (500 µL injection volume) during five

consecutive days in the A) Pd_2Spm, B) cisplatin and C) vehicle group, respectively. The animals were monitored daily for physical activity, wellbeing and measurements of body weight. Tumour measurements were performed by two independent researchers using a digital calliper in two perpendicular diameters of the implant. Tumour volumes were calculated using the Carlsson formula [167]: tumour volume (mm^3) = 0.5 × largest diameter (mm) × smallest diameter^2 (mm). Researchers were blinded to treatment allocation while performing outcome measurements. At day 39 post-implantation (end of the study), animals were euthanized with isoflurane followed by cardiac puncture for blood collection. Blood was collected into K3EDTA tubes for haematological and biochemical analyses. Brain, heart, lungs, liver, kidneys, spleen, inguinal lymphatic nodes, and tumour were excised, washed in PBS and weighed. Two animals from the vehicle group developed ulcerated tumours during the treatment period (day 28 post-implantation); thus, these animals were euthanized and excluded from the study.

III.4.4.4 Histological Analysis and Immunohistochemistry

Animal tissues were fixed in 10% buffered formalin, routinely processed and embedded in paraffin wax. Serial sections with 2 µm thickness were cut from each paraffin block; one section was stained with haematoxylin–eosin for histological examination, and the others were used for immunohistochemistry. Histological grading of the mammary carcinomas was performed according to the Nottingham histological grading method [21] based on a semi-quantitative assessment of three histological parameters: tubular formation, nuclear pleomorphism and mitotic figures count. The score of these parameters is used to assign the tumour grade: grade I (well-differentiated tumours), grade II (moderately differentiated tumours) or III (poorly differentiated tumours).

For the immunohistochemical study, tissue sections were dewaxed and rehydrated. Slides were submitted to proteolytic digestion by immersion in 10% retrieval solution (Dako) and kept in a water bath at 100 °C for 20 min. After blocking of non-specific staining, slides were incubated with primary antibody for Ki-67 (1:50 dilution, clone MIB-1, Dako) overnight at 4 °C. Slides were then stained with Novolink Polymer Detection Systems (Leica Biosystems Inc., Buffalo Grove, IL, USA) following manufacturer's instructions, counterstained with hematoxylin and permanently mounted. The nuclear Ki-67 staining was analysed using Fiji's high-throughput automatic quantitation with Andy's Algorithm pipeline, as described elsewhere [168]. The immunoreactivity was evaluated, counting at least 600 nuclei/field from 5 representative fields of the lesion at high magnification, avoiding necrotic

areas. The ratio of Ki-67 positive nuclei per all counted nuclei was expressed as a percentage (Ki-67 proliferation index).

III.4.4.5 Detection of Apoptosis with Labelling of DNA Strand Breaks (TUNEL Assay)

The paraffin-embedded tumour sections were deparaffinized, rehydrated through a graded series of ethanol and double distilled water and then stained with In Situ Cell Death Detection Kit (Roche Diagnostics GmbH, Mannheim, Germany) as per manufacturer's instructions. Apoptosis was quantified at single-cell level by counting the number of cells positive for terminal deoxynucleotidyl transferase (TdT) dUTP nick-end labelling (TUNEL-positive cells). Briefly, tumour sections were incubated with 20 µg/mL proteinase K solution (in 10 mM Tris/HCl, pH 7.4–8) for 30 min at 37 °C. Slides were washed and stained with TUNEL reaction mixture (mixture of terminal deoxynucleotidyl transferase with labelled nucleotides) for 60 min at 37 °C in the dark followed by three washes. Slides were mounted with VECTASHIELD Antifade Mounting Medium with DAPI, and coverslips were sealed. At least twenty nonoverlapping high-power microscope fields of each tumour section were captured while avoiding areas with central necrosis. Fluorescence images were acquired using the LionHeartFX automated microscope at Ex: 520–560 nm and Em: 570–620 nm.

III.4.4.6 Biochemical and Haematological Analyses

Red blood cells (RBC), haemoglobin (Hb), haematocrit (Hct), mean corpuscular volume (MCV) and mean corpuscular haemoglobin (MCH) were analysed in a small aliquot of whole blood using ABX Micros 60 automated analyser (Horiba ABX SAS, Montpellier, France). The remaining blood was centrifuged at 900 × g for 15 min, and plasma was separated into aliquots and frozen at −80 °C for biochemical assays. Plasma parameters were analysed using commercial kits for aspartate aminotransferase—AST (AST CP, A11A01629), alanine transaminase—ALT (ALT CP, A11A01627), cholesterol (CHOL CP, A11A01634), creatinine (Creatinine 120 CP, A11A01868), glucose (Glucose PAP CP, A11A01668), total protein (Total protein CP, A11A01669), triglycerides (Triglycerides CP, A11A01640) and urea (Urea CP, A11A01641). All parameters were determined with an automated analyser Pentra 400 (ABX Horiba diagnostics, Montpellier, France).

III.4.5 *In Ovo* Chorioallantoic Membrane (CAM) Assay

The chicken embryo chorioallantoic membrane (CAM) assay was used to study the effect of tested drugs on neovascularization *in ovo*, as described elsewhere [169]. Briefly, fertilized chicken eggs were incubated at 37.5 °C in a humidified atmosphere with agitation. After 3 days of incubation, 2.5 mL of albumen was removed to detach developing CAM from the shell. A window in the eggshell was cut off to expose the embryo, and then, the eggshell was sealed with paraffin. Incubation of fertilized eggs continued until day 9, when the windows were unsealed and four paper disks previously sterilized and pre-treated with hydrocortisone (a cyclooxygenase inhibitor to avoid inflammatory responses) were placed in direct contact with CAM in each egg (3 PBS-soaked disks and 1 VEGF-soaked (10 ng/mL) disk), and windows were re-sealed with paraffin. On day 11, two of the PBS-soaked disks were treated with Pd_2Spm (2 to 8 µM) or cisplatin (2 to 8 µM). The remaining two disks were used as negative/vehicle (treated with PBS) and positive (treated with VEGF) controls. The eggs were further incubated two more days, and at day 13, the disks bound to the CAM were removed, placed in PBS and imaged using a contrast-phase microscope (Motic® AE200 inverted microscope, Spectra Services, VWR International) (with a 4X magnification) coupled to a Moticam 5 digital camera. Images were analysed using the Angiogenesis Analyzer for Fiji [170].

III.5 Statistical Data Analysis

Data are expressed as the mean ± standard error of the mean (SEM) or medians with corresponding quartiles. Statistical analysis was performed using two-tailed Student's *t*-test or one-way ANOVA followed by Dunnett's multiple comparisons for analysis of means. Changes over the time were analysed with two-way ANOVA followed by Tukey's multiple comparisons test. Medians were compared with nonparametric Kruskal–Wallis test followed by Dunn's multiple comparisons test. The half-maximal inhibitory concentration values (IC_{50}) were calculated by interpolation from the nonlinear regression curves obtained from cell proliferation/cytotoxicity data using "log(inhibitor) versus the normalized response–variable slope equation". GraphPad Prism 7 Software (San Diego, CA, USA) was used. A p-value < 0.05 was considered statistically significant.

CHAPTER IV: RESULTS AND DISCUSSION

Parts of this chapter are available in the following publications:

Vojtek M, Pinto E, Gonçalves-Monteiro S, Almeida A, Marques MPM, Mota-Filipe H, Ferreira IMPLVO, Diniz C. Fast and reliable ICP-MS quantification of palladium and platinum-based drugs in animal pharmacokinetic and biodistribution studies. Analytical Methods. 2020;12(39):4806–4812.

Vojtek M, Gonçalves-Monteiro S, Pinto E, Kalivodová S, Almeida A, Marques MPM, Batista de Carvalho ALM, Martins CB, Mota-Filipe H, Ferreira IMPLVO, Diniz C. Preclinical Pharmacokinetics and Biodistribution of Anticancer Dinuclear Palladium(II)-Spermine Complex (Pd_2Spm) in Mice. Pharmaceuticals. 2021;14(2):173.

Vojtek M, Gonçalves-Monteiro S, Šeminská P, Valová K, Bellón L, Dias-Pereira P, Marques F, Marques MPM, Carvalho ALMB de, Mota-Filipe H, Ferreira IMPLVO, Diniz C. Pd_2Spermine Complex Shows Cancer Selectivity and Efficacy to Inhibit Growth of Triple-Negative Breast Tumors in Mice. Biomedicines. 2022;10(2):210.

Vojtek M, Martins CB, Ramos R, Duarte SG, Ferreira IMPLVO, Batista de Carvalho ALMB, Marques MPM, Diniz C. Pd(II) and Pt(II) Trinuclear Chelates with Spermidine: Selective Anticancer Activity towards TNBC-Sensitive and -Resistant to Cisplatin. Pharmaceutics. 2023;15(4):1205.

IV.1 Screening of Antiproliferative Effects and Selectivity Elicited by Selected Pt(II) Agents—Cisplatin, Carboplatin and Oxaliplatin—in MDA-MB-231, MDA-MB-231/R and MCF-12A cells

To establish the reference *in vitro* potency of metal-based drug currently used in the clinical practice, antiproliferative effects of cisplatin has been investigated in breast cancer MDA-MB-231 cells and non-neoplastic breast MCF-12A cells. We have also used MDA-MB-231/R cells that were developed in-house as an *in vitro* cell model of acquired resistance to cisplatin by continuously exposing breast cancer MDA-MB-231 cells to increasing concentrations of cisplatin over the course of 6 months. Effects of carboplatin and oxaliplatin have also been investigated in MDA-MB-231, MDA-MB-231/R and MCF-12A cells to provide a broader context on the activity of the Pt(II)-based drugs used in the clinical practice and to understand if MDA-MB-231/R cells present cross-resistance to carboplatin and oxaliplatin, known as Pt(II)-resistance.

The effects of cisplatin, carboplatin and oxaliplatin on the proliferation of MDA-MB-231, MDA-MB-231/R and MCF-12A cells at 24, 48 and 72 h are shown in **Figure 12** as dose–response curves within a concentration range of 0.1–200 µM for cisplatin and 0.3–200 µM for carboplatin and oxaliplatin. The full cell growth inhibition was achieved with the concentration of 100 µM of cisplatin in MDA-MB-231 and MCF-12A cells at all incubation times tested. In MDA-MB-231/R cells, full growth inhibition was achieved with concentration of 200 µM at 48 and 72 h. A clear separation of dose–response curves obtained for MDA-MB-231 and MDA-MB-231/R cells as well as between MDA-MB-231/R and MCF-12A cells was observed for cisplatin at all incubation periods indicating a lower activity of cisplatin in MDA-MB-231/R cells. When comparing dose-response curves obtained in MDA-MB-231 and MCF-12A cells, an apparent overlap was observed indicating similar potency of cisplatin for both breast cancer cells and non-neoplastic breast cells. For carboplatin and oxaliplatin, the highest concentration tested (200 µM) did yield maximum cell growth inhibition only in cells treated with oxaliplatin while carboplatin was not able to achieve full cell proliferation suppression, indicating different potencies.

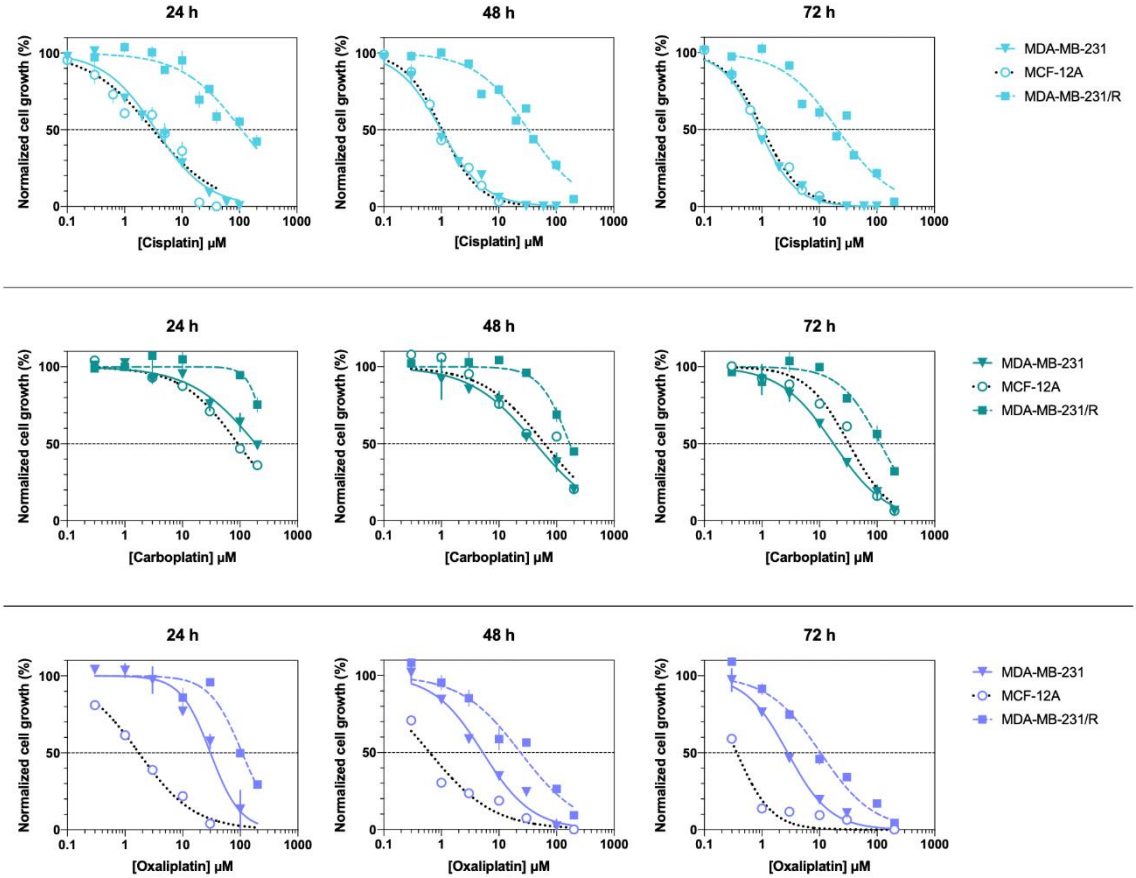

Figure 12. Dose–response curves of cisplatin (blue), carboplatin (green) and oxaliplatin (violet) in MDA-MB-231 (solid line), MDA-MB-231/R (dashed line) and MCF-12A (dotted line) cells.

Values are expressed as mean ± SEM, n = 4 (in triplicates), analysed with non-linear regression. Data points with no visible error bars have errors smaller than the size of the symbol.

Nonlinear regression analysis of dose–response curves was used to compute the half maximal inhibitory concentration (IC_{50}) for cisplatin, carboplatin and oxaliplatin **Table 5**. For cisplatin, the IC_{50} values ranged 0.9–3.5 µM, 20.9–109.3 µM and 1–3.1 µM for MDA-MB-231, MDA-MB-231/R and MCF-12A cells, respectively. Carboplatin has shown IC_{50} values ranging 17.5–187.7 µM, 114.7–292.5 µM and 32.4–92.3 µM in MDA-MB-231, MDA-MB-231/R and MCF-12A cells, respectively. Oxaliplatin's IC_{50} values ranged IC_{50} 2.8–30.3 µM, 10.4–107.7 µM and 0.4–1.7 µM in MDA-MB-231, MDA-MB-231/R and MCF-12A cells, respectively.

Table 5. The half maximal inhibitory concentration (IC_{50}) of cisplatin, carboplatin and oxaliplatin and in triple-negative human breast cancer (MDA-MB-231 and MDA-MB-231/R) and non-cancer breast (MCF-12A) cells at 24, 48 and 72 h of incubation.

Drug	Time (h)	MDA-MB-231		MDA-MB-231/R		MCF-12A		p-value (MDA-MB-231 vs MCF-12A)	p-value (MDA-MB-231 vs MDA-MB-231/R)
		IC_{50}	$logIC_{50}$ ± SEM	IC_{50}	$logIC_{50}$ ± SEM	IC_{50}	$logIC_{50}$ ± SEM		
Cisplatin	24	3.5	–5.457 ± 0.034	109.3	–3.961 ± 0.08	3.1	–5.51 ± 0.062	0.4819	<0.0001
	48	1.0	–6.005 ± 0.027	32.4	–4.489 ± 0.038	1.0	–5.988 ± 0.029	0.6829	<0.0001
	72	0.9	–6.043 ± 0.02	20.9	–4.68 ± 0.046	1.0	–5.981 ± 0.026	0.1076	<0.0001
Carboplatin	24	187.7	–3.727 ± 0.073	292.5	–3.534 ± 0.17	92.3	–4.035 ± 0.078	0.0279	0.3371
	48	43.2	–4.365 ± 0.071	168.4	–3.774 ± 0.048	62.0	–4.208 ± 0.132	0.3352	0.0005
	72	17.5	–4.757 ± 0.052	114.7	–3.941 ± 0.054	32.4	–4.49 ± 0.067	0.0199	<0.0001
Oxaliplatin	24	30.3	–4.518 ± 0.078	107.7	–3.968 ± 0.106	1.7	–5.762 ± 0.066	<0.0001	0.0058
	48	5.2	–5.281 ± 0.075	23.6	–4.627 ± 0.104	0.6	–6.204 ± 0.11	0.0004	0.0022
	72	2.8	–5.553 ± 0.044	10.4	–4.983 ± 0.073	0.4	–6.435 ± 0.07	<0.0001	0.0005

IC_{50} values are expressed in μM, and as a mean $logIC_{50}$ ± SEM, n = 4; Student's t-test comparison of $logIC_{50}$ means between the two cell lines at a specified time.

Significantly higher IC_{50} values observed for MDA-MB-231/R cells compared to MDA-MB-231 cells suggest a lower sensitivity of MDA-MB-231 cells to cisplatin that is also evidenced by high resistance index >23.06 **Table 6**, which indicates that at least 23.06-fold higher concentration of cisplatin is required to be applied to MDA-MB-231/R cells to obtain equipotent effects observed in MDA-MB-231 cells. High resistance indexes for carboplatin (1.56–6.55) and oxaliplatin (3.55–4.51) evidenced that MDA-MB-231/R also developed resistance to these agents, however to lesser extent than for cisplatin **Table 6**.

Table 6. Selectivity and resistance indexes of cisplatin, carboplatin and oxaliplatin.

Drug	Time (h)	Selectivity index for MDA-MB-231	Selectivity index for MDA-MB-231/R	Resistance index
Cisplatin	24	0.89	0.03	31.33
	48	1.04	0.03	32.79
	72	1.15	0.05	23.06
Carboplatin	24	0.49	0.32	1.56
	48	1.43	0.37	3.90
	72	1.85	0.28	6.55
Oxaliplatin	24	0.06	0.02	3.55
	48	0.12	0.03	4.51
	72	0.13	0.04	3.72

Assessing selectivity of Pt(II)-based agents, cisplatin has shown selectivity indexes of 0.89–1.15 (MCF-12A vs MDA-MB-231) and 0.03–0.05 (MCF-12A vs MDA-MB-231/R); carboplatin's selectivity indexes ranged 0.49–1.85 (MCF-12A vs MDA-MB-231) and 0.28–0.37 (MCF-12A vs MDA-MB-231); and oxaliplatin has shown selectivity indexes of 0.06–0.13 (MCF-12A vs MDA-MB-231) and 0.02–0.04 (MCF-12A vs MDA-MB-231/R). The selectivity index <1 is a strong indication of a drug having higher effects in non-neoplastic cells compared to cancer cells, which may be understood as indiscriminatory effects affecting both target cancer cells as well as non-neoplastic cells and, thus, resulting into the development of adverse drug events. All three Pt(II)-based agents have shown low selectivity indexes at least for some of the tested incubation time, which is evidence that these drugs may likely cause off-target toxicities as also observed in the clinical practice.

When comparing the *in vitro* potency of studied Pt(II)-based compounds, we have ordered cisplatin, carboplatin and oxaliplatin from the most potent (i.e. the lowest IC_{50}) to least potent (i.e. the highest IC_{50}) as follows: in MDA-MB-231 cells cisplatin > oxaliplatin >>

carboplatin, in MCF-12A cells oxaliplatin > cisplatin >> carboplatin and in MDA-MB-231/R as oxaliplatin > cisplatin >> carboplatin.

Contrast phase images evidenced that the usual spindle-shaped phenotype of control (untreated cells) MDA-MB-231 or MDA-MB-231/R cells differs from drug-treated cells as presented in **Figure 13**. In MDA-MB-231 and MDA-MB-231/R cells, treatment with 10 or 20 µM of cisplatin or carboplatin has induced rounded cell morphology, indicating disruption of cellular homeostasis. These effects were not observed in cells treated with carboplatin. In MCF-12A, treatment with either cisplatin, carboplatin or oxaliplatin induced visible changed in cell morphology compared to untreated cells. This observation allowed visual confirmation of antiproliferative data that indicated stronger impact Pt drugs on non-neoplastic cells compared to TNBC cells.

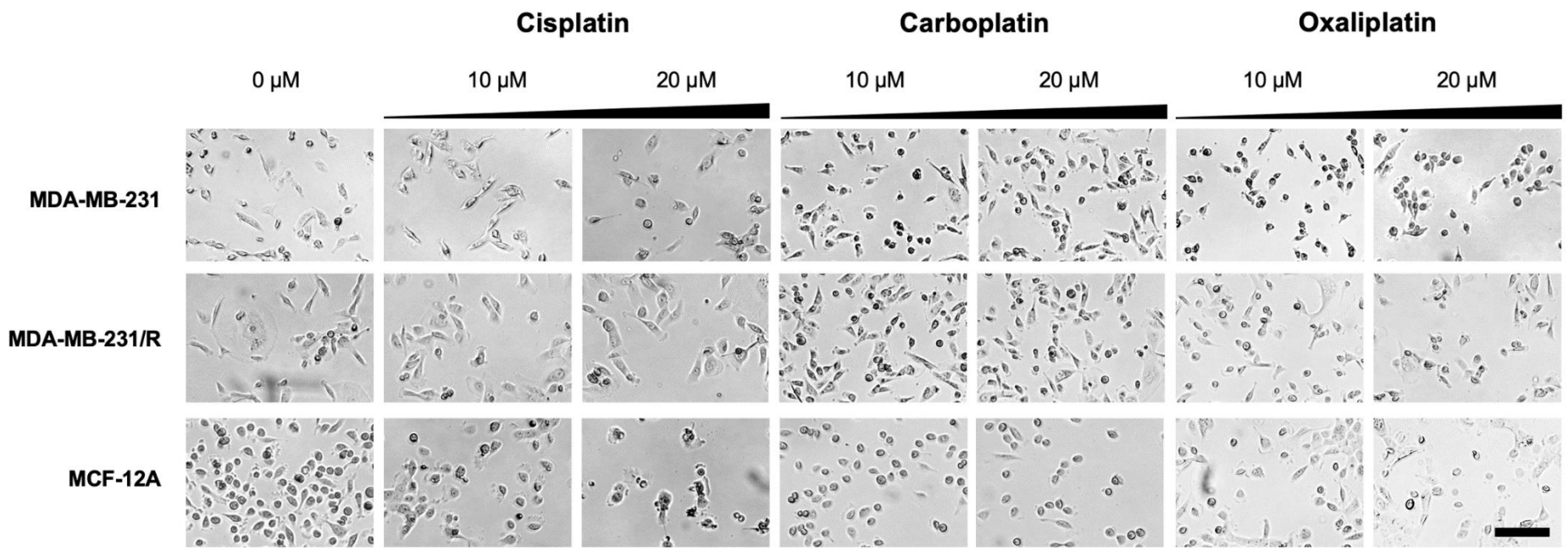

Figure 13. Representative photomicrographs of MDA-MB-231, MDA-MB-231/R and MCF-12A cells exposed to increasing concentrations (0–20μM) cisplatin, carboplatin or oxaliplatin for 24 h.

Images obtained with a phase-contrast objective lens of the LionheartFX microscope. Scale bar = 150 μm.

IV.2 Screening of Antiproliferative Effects and Selectivity Elicited by Selected Pd(II) Agents—Pd_2Spm and Pd_3Spd_2—in MDA-MB-231, MDA-MB-231/R and MCF-12A cells

The effects of Pd_2Spm and Pd_3Spd_2 on the proliferation of MDA-MB-231, MDA-MB-231/R and MCF-12A cells at 24, 48 and 72 h are shown in **Figure 14** as dose–response curves. The full range of antiproliferative activity of Pd_2Spm and Pd_3Spd_2 on net cell growth (0–100%) was achieved with the tested concentrations (1 to 100 µM) in MDA-MB-231 cells. For MCF-12A cells, the highest concentration of Pd_2Spm (100 µM) did not produce a maximum growth inhibition when compared to the same dosage of Pd_3Spd_2. A clear separation of dose–response curves obtained for MDA-MB-231 and MCF-12A cells as well as MDA-MB-231/R and MCF-12A cells was observed for Pd_2Spm and Pd_3Spd_2 at all incubation periods.

Nonlinear regression analysis of dose–response curves was used to compute the half maximal inhibitory concentration (IC_{50}) for Pd_2Spm and Pd_3Spd_2 with results being summarized in **Table 7**. For Pd_2Spm, the IC_{50} values ranged 7.3–8.3 µM, 11.3–12.1 µM and 89.5–228.9 µM for MDA-MB-231, MDA-MB-231/R and MCF-12A cells, respectively. Significantly lower IC_{50} values observed for MDA-MB-231 or MDA-MB-231/R cells compared to MCF-12A cells suggest a lower sensitivity of non-neoplastic breast cells MCF-12A to Pd_2Spm and selectivity towards breast cancer cells. Higher selectivity of Pd_2Spm towards breast cancer cells was also evidenced from selectivity indexes >11.64 (MCF-12A vs MDA-MB-231) and >7.90 (MCF-12A vs MDA-MB-231/R) which indicate that at least 11.64-fold or 7.90-fold higher concentration of Pd_2Spm is required to be applied to MCF-12A cells to obtain equipotent effects observed in MDA-MB-231 and MDA-MB-231/R cells, respectively (**Table 8**). Additionally, when comparing the IC_{50} in MDA-MB-231 and MDA-MB-231/R cells, the resistance indexes varied between 1.45 and 1.54, indicating that only <1.54-fold higher concentration of Pd_2Spm is required in MDA-MB-231/R cells to achieve comparable effects observed in MDA-MB-231 cells (**Table 8**).

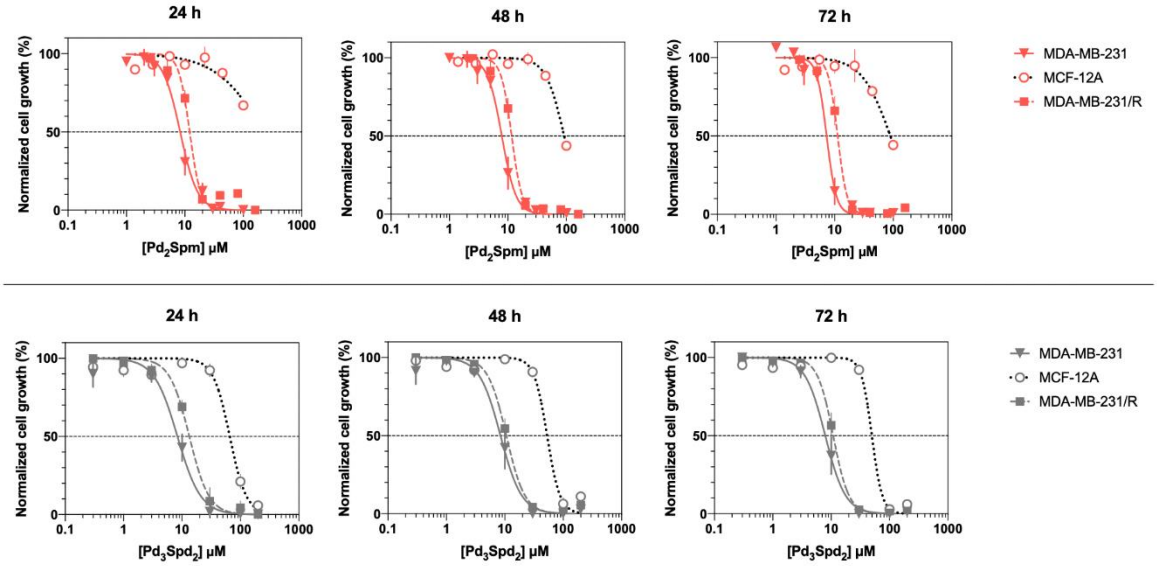

Figure 14. Dose–response curves of Pd_2Spm (red) and Pd_3Spd_2 (grey) in MDA-MB-231 (solid line), MDA-MB-231/R (dashed line) and MCF-12A (dotted line) cells.

Values are expressed as mean ± SEM, n = 4 (in triplicates), analysed with non-linear regression. Data points with no visible error bars have errors smaller than the size of the symbol.

For Pd_3Spd_2, the IC_{50} ranged 7.9–8.4 µM, 10.6–13.3 µM and 49.7–65.7 µM for MDA-MB-231, MDA-MB-231/R and MCF-12A cells, respectively. Significantly lower IC_{50} values observed for MDA-MB-231 or MDA-MB-231/R cells compared to MCF-12A cells suggest a lower sensitivity of non-neoplastic breast cells MCF-12A to Pd_3Spd_2 and selectivity towards breast cancer cells. Higher selectivity of Pd_3Spd_2 towards breast cancer cells was also evidenced from selectivity indexes >6.28 (MCF-12A vs MDA-MB-231) and >4.60 (MCF-12A vs MDA-MB-231/R) which indicate that at least 6.28-fold or 4.60-fold higher concentration of Pd_3Spd_2 is required to be applied to MCF-12A cells to obtain equipotent effects observed in MDA-MB-231 and MDA-MB-231/R cells, respectively (**Table 8**). Additionally, when comparing the IC_{50} in MDA-MB-231 and MDA-MB-231/R cells, the resistance indexes varied between 1.26 and 1.6, indicating that only <1.60-fold higher concentration of Pd_3Spd_2 is required in MDA-MB-231/R cells to achieve comparable effects observed in MDA-MB-231 cells.

Comparing the antiproliferative effects prompted by Pd_2Spm and Pd_3Spd_2 agents, both agents showed similar potency in MDA-MB-231 and MDA-MB-231/R as well as similar ability to circumvent the Pt resistance in MDA-MB-231/R cells. However, in MCF-12A, Pd_2Spm showed superior selectivity towards breast cancer cells, with almost 2-fold lower

impact on non-neoplastic breast cells compared to Pd_3Spd_2. For this reason, further studies presented in this thesis were conducted using only the Pd_2Spm chelate.

Contrast phase images evidence that the normal spindle-shaped phenotype of control (untreated cells) MDA-MB-231 or MDA-MB-231/R cells differs from drug-treated cells as presented in **Figure 15**. In MDA-MB-231 cells, treatment with 10 or 20 µM of Pd_2Spm or Pd_3Spd_2 induced several morphological changes: the cells exposed to Pd_2Spm and Pd_3Spd_2 showed a rounded morphology with one prominent protrusion of the cell membrane or blebbing (white arrows), indicating disruption of cellular homeostasis. These effects were also observed in MDA-MB-231/R cells treated with Pd_2Spm at the same concentrations, the highest one (20 µM) having more marked effects than the lowest one. Additionally, no impact on morphology of MCF-12A cells treated with Pd_2Spm or Pd_3Spd_2 was observed.

Table 7. The half maximal inhibitory concentration (IC_{50}) of Pd_2Spm and Pd_3Spd_2 in triple-negative human breast cancer cells (MDA-MB-231 and MDA-MB-231/R) and non-neoplastic breast cells (MCF-12A).

Drug	Time (h)	MDA-MB-231		MDA-MB-231/R		MCF-12A		p-value (MDA-MB-231 vs MCF-12A)	p-value (MDA-MB-231 vs MDA-MB-231/R)
		IC_{50}	$logIC_{50}$ ± SEM	IC_{50}	$logIC_{50}$ ± SEM	IC_{50}	$logIC_{50}$ ± SEM		
Pd_2Spm	24	8.3	–5.081 ± 0.024	12.1	–4.918 ± 0.02	228.9	–3.64 ± 0.215	0.0006	0.002
	48	7.9	–5.105 ± 0.022	11.6	–4.936 ± 0.017	91.5	–4.039 ± 0.023	<0.0001	0.0009
	72	7.3	–5.137 ± 0.021	11.3	–4.948 ± 0.019	89.5	–4.048 ± 0.068	<0.0001	0.0005
Pd_3Spd_2	24	8.3	–5.079 ± 0.041	13.3	–4.875 ± 0.029	65.7	–4.182 ± 0.039	<0.0001	0.0066
	48	8.4	–5.074 ± 0.04	10.6	–4.974 ± 0.019	53.0	–4.276 ± 0.041	<0.0001	0.0647
	72	7.9	–5.101 ± 0.026	10.8	–4.966 ± 0.018	49.7	–4.303 ± 0.041	<0.0001	0.0053

IC_{50} values are expressed in µM, and as mean $logIC_{50}$ ± SEM, $n = 4$; [a] Student's *t*-test comparison of $logIC_{50}$ means between the two cell lines at a specified time.

Table 8. Selectivity and resistance indexes of Pd_2Spm and Pd_3Spd_2.

Drug	Time (h)	Selectivity index for MDA-MB-231	Selectivity index for MDA-MB-231/R	Resistance index
Pd_2Spm	24	27.56	18.96	1.45
	48	11.64	7.90	1.47
	72	12.25	7.95	1.54
Pd_3Spd_2	24	7.87	4.93	1.60
	48	6.28	4.99	1.26
	72	6.28	4.60	1.37

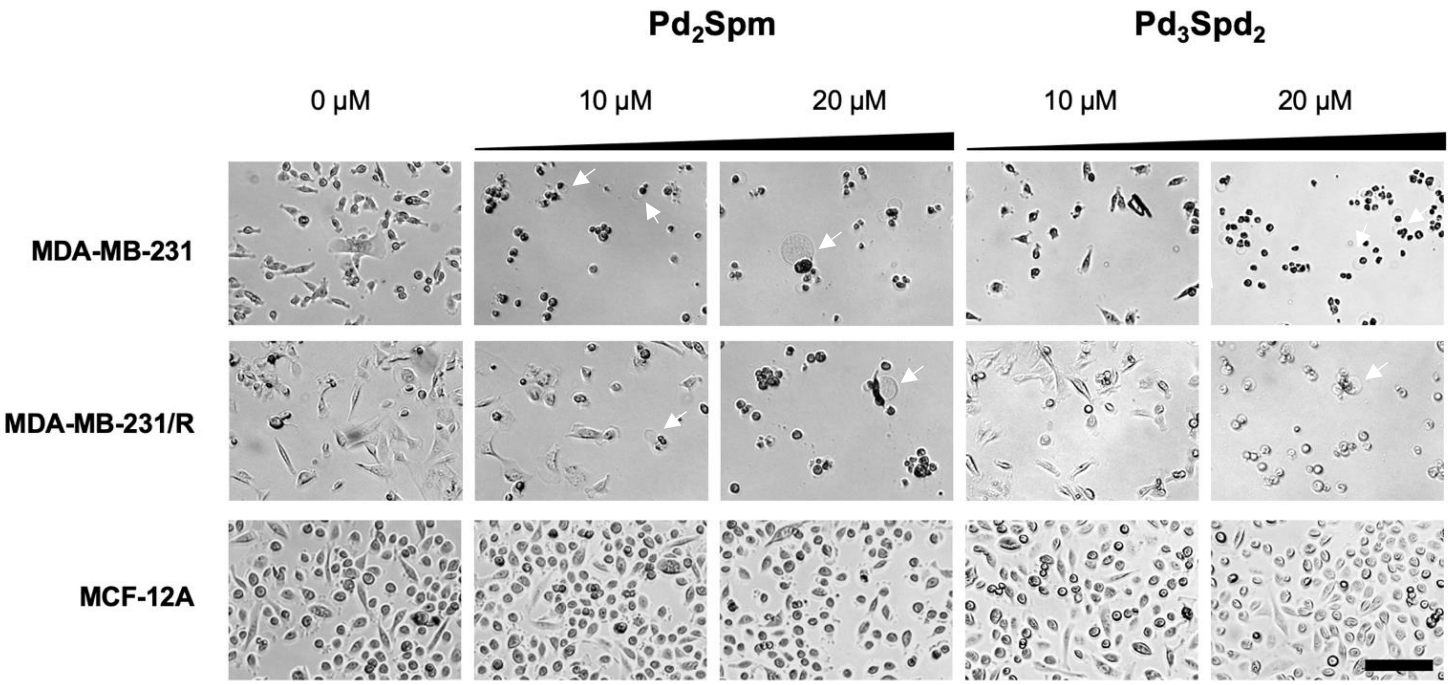

Figure 15. Representative photomicrographs of MDA-MB-231, MDA-MB-231/R and MCF-12A cells exposed to increasing concentrations (0–20µM) Pd_2Spm or Pd_3Spd_2 for 24 h.

Images obtained with a phase-contrast objective lens of the LionheartFX microscope. Scale bar = 150 µm.

IV.3 Putative *In Vitro* Targets of Pd_2Spm

IV.3.1 Cell uptake

Since Pd_2Spm has shown promising *in vitro* anticancer activity against TNBC, the *in vitro* cellular uptake/accumulation of either Pd_2Spm or cisplatin in MDA-MB-231 and MCF-12A cells was evaluated by ICP-MS. The results of Pd_2Spm or cisplatin accumulation in cells treated with equimolar drug concentrations for 24 h (between 2 and 8 µM) are depicted in **Figure 16** and evidenced a lower intracellular Pd_2Spm increase as compared to cisplatin for both MDA-MB-231 and MCF-12A cells. The cellular drug uptake was shown to increase linearly with drug concentration in the cell culture medium, suggesting passive transport as a primary mechanism of cellular uptake for the two compounds. Interestingly, almost 2-fold higher accumulation of Pd_2Spm was observed in MCF-12A cells relative to MDA-MB-231 cells ($p<0.05$), while cisplatin's accumulation between the two cell lines was almost identical ($p>0.05$)

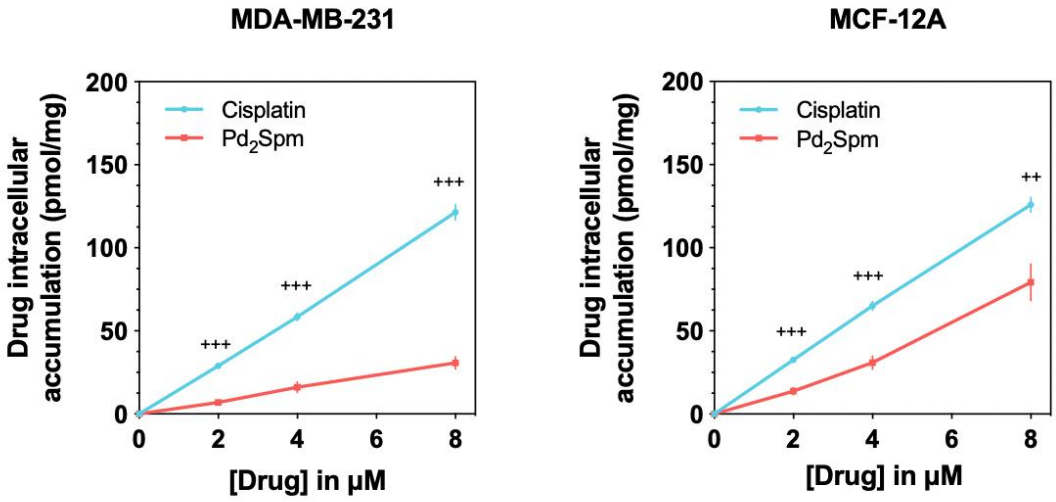

Figure 16. Cellular accumulation of Pd_2Spm and cisplatin in MDA-MB-231 and MCF-12A cells for 24 h.

Values are expressed as mean ± SEM (n = 4, in triplicates). Significant differences of Pd_2Spm vs cisplatin at respective concentration levels compared with Student's t-test: $p < 0.01$ (++), $p < 0.001$ (+++).

IV.3.2 Impact on Polyamine Pathway

Since Pd_2Spm contains a biogenic polyamine spermine in its structure, we have probed the putative involvement of polyamine pathway in its antiproliferative effects in MDA-MB-231 cells. The exogenous addition of putrescine (put), spermidine (spd) and spermine (spm) to MDA-MB-231 cells differentially impacted the cell proliferation as shown in **Figure 17**. While 1 mM of putrescine did not impact the cell proliferation, 1 mM of spermidine and 1 mM of spermine completely inhibited the cell growth. The addition of 1 mM of putrescine to cells treated with 10 µM of Pd_2Spm has resulted in the cell rescue, indicating the putrescine interferes with Pd_2Spm's antiproliferative effects. The addition of spd or spm did not rescue cells exposed to Pd_2Spm as expected, since spd and spm at 1 mM concentration already showed notable antiproliferative effects per se. Interestingly, the addition of putrescine to cells treated with 10 µM of cisplatin did not rescue cells from the cisplatin's effects. Since these results indicated manipulation of biogenic polyamine biosynthesis via exogenous addition of putrescine hampers the effects of Pd_2Spm but not cisplatin, we have also explored the effects of blockage of intracellular polyamine biosynthesis with the addition of DFMO that blocks the intracellular conversion of ornithine to putrescine. The concentration of 20 µM of DFMO did not impact the proliferation of MDA-MB-231 cells, however its addition to cells treated with 10 µM of Pd_2Spm resulted in cell rescue, but to a lower extent that was observed with the addition of putrescine. In cisplatin-treated cells, the addition of DFMO did not impact cell proliferation. These results indicated that differential mechanism is most likely responsible for antiproliferative effects exerted by Pd_2Spm and cisplatin. While Pt drug did not lose its activity in the presence of put or DFMO, Pd compound lost some of its effects. Since both increase of intracellular putrescine via put addition and blockage of intracellular putrescine synthesis decreased the activity of Pd_2Spm, via the mechanism yet to be elucidated, these results demonstrate the involvement of different mechanisms elicited by Pd chelate compared to cisplatin that retained its activity.

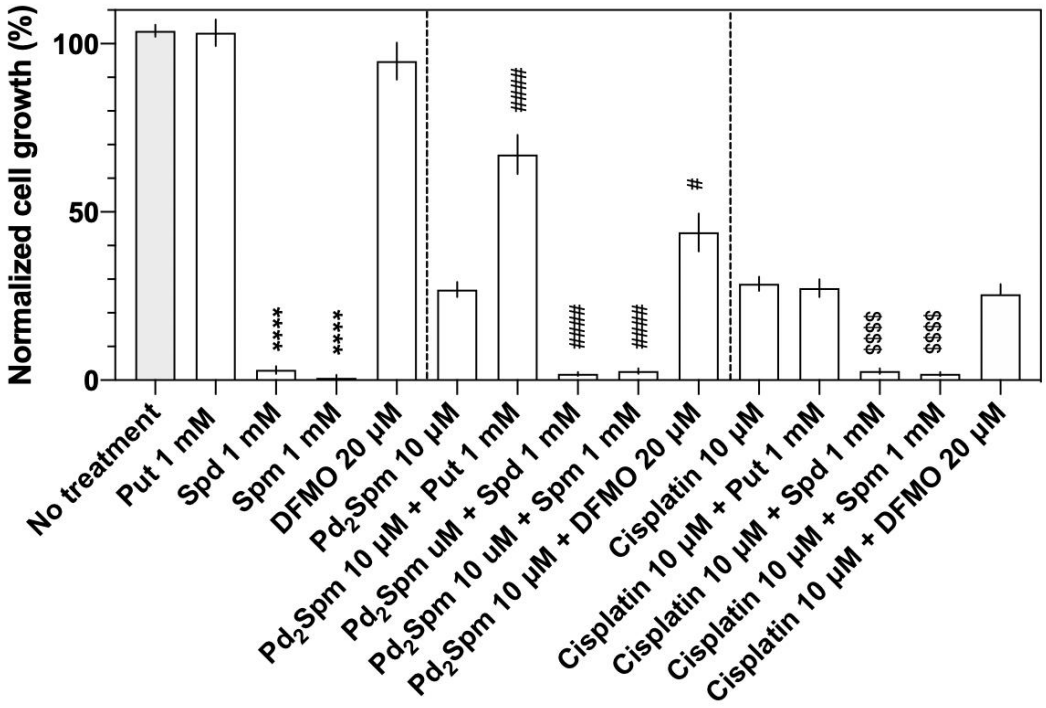

Figure 17. The impact of 24 h co-treatment of Pd_2Spm or cisplatin with exogenous addition of biogenic polyamines or DFMO on proliferation of MDA-MB-231 cells.

Values are expressed as mean ± SEM, n = 4 (in triplicates). Data points with no visible error bars have errors smaller than the size of the symbol. Significant differences from control (untreated cells): $p<0.0001$ (****). Significant differences from treatment with Pd_2Spm alone: $p<0.05$ (#) and $p<0.0001$ (#####); Significant differences from treatment with cisplatin alone: $p<0.0001$ ($$$$).

IV.3.3 Impact on TNBC Invasion

IV.3.3.1 In Vitro Migration of MDA-MB-231 cells

The effects of Pd_2Spm and cisplatin on the migration of MDA-MB-231 cells is depicted in **Figure 18**. The kinetic profiles (between 0 and 48 h) of migrating cells exposed to different concentrations of either Pd_2Spm (**Figure 18a**) or cisplatin (**Figure 18b**) showed similar dose-dependent effects on cancer cell migration, expressed as a percentage of wound confluency. Untreated cells displayed an almost complete wound closure, reaching a maximum ~100% wound confluence between 18 and 24 h after creation of the scratch in the cell monolayer (**Figure 18d**). Thus, the area under the curve for the wound confluence–time plot between 0 and 18 h ($AUC_{0\text{-}18h}$) was analysed (**Figure 18c**) to reliably capture the drugs' effects on cell migration. The half maximal effective concentrations (EC_{50}) of Pd_2Spm

and cisplatin are summarized in **Table 9**, showing no significant difference in the potency of Pd_2Spm versus cisplatin in inhibiting the migration of MDA-MB-231 cells.

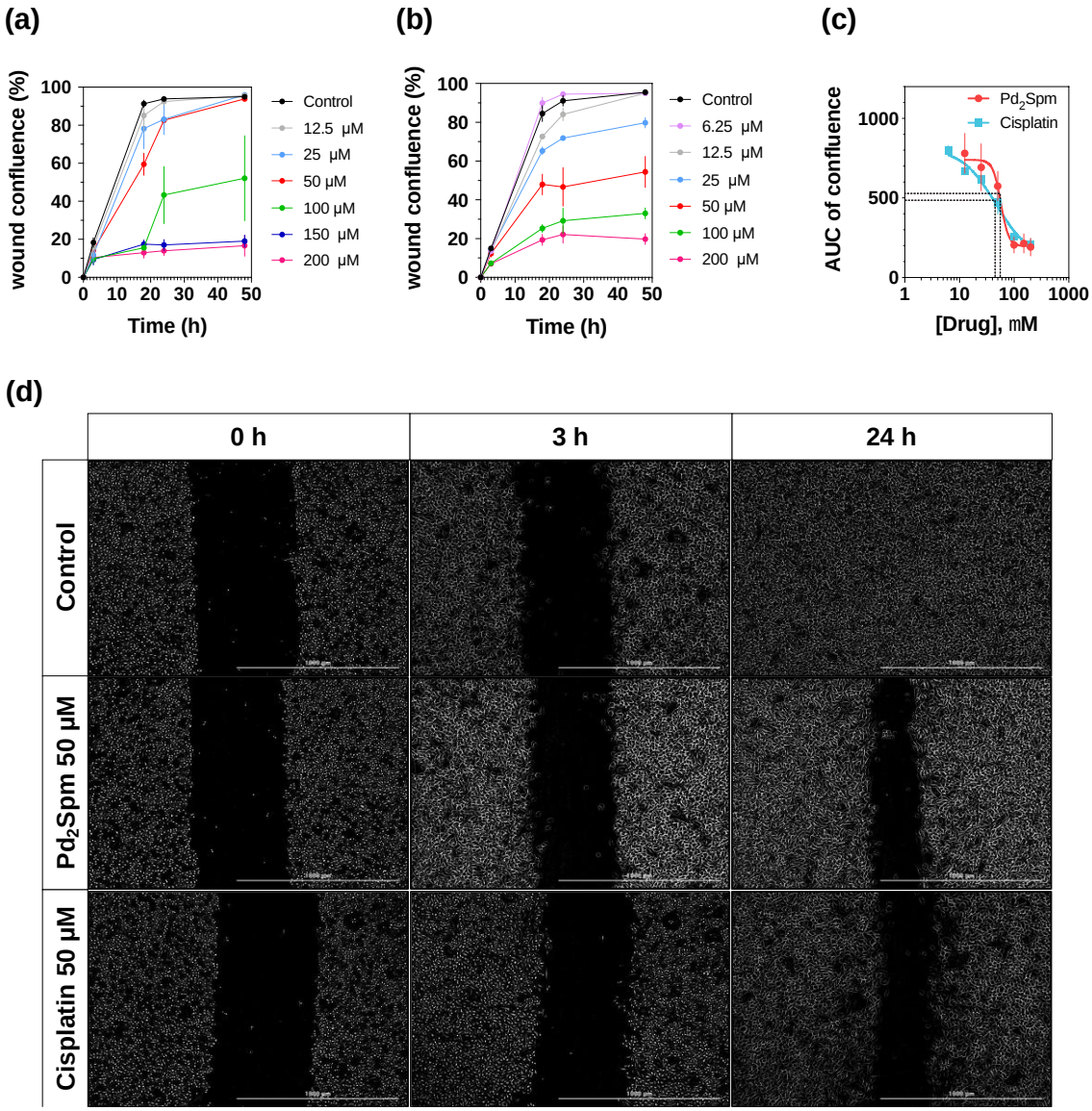

Figure 18. Effects of Pd_2Spm and cisplatin on migration of MDA-MB-231 cells using scratch/wound healing assay.

(**a**) Dose-dependent effect of Pd_2Spm on migration of MDA-MB-231 cells expressed as wound confluence for tested Pd_2Spm concentrations. (**b**) Dose-dependent effect of cisplatin on migration of MDA-MB-231 cells expressed as wound confluence for tested cisplatin concentrations. (**c**) Dose–response curve obtained from measuring the area under confluence curve (AUC) between 0 and 18 h of exposure to Pd_2Spm or cisplatin. (**d**) Representative images from 5 independent experiments showing effects of 0 µM (control) and 50 µM of Pd_2Spm or cisplatin on cell migration at 0, 3 and 24 h. Scale bar = 1000 µm. (**a-c**) Values are expressed as mean ± SEM, *n* = 5. Data points with no visible error bars have errors smaller than the size of the symbol.

Table 9. Migration of MDA-MB-231 cells (logEC50 values of Pd_2Spm and cisplatin).

Drug	logEC50	*p*-Value
Pd_2Spm	−4.243 ± 0.113 (57.2)	0.631
Cisplatin	−4.329 ± 0.130 (46.9)	

Data are expressed as mean $logEC_{50}$ ± SEM (EC_{50} in µM), n = 5.

IV.3.3.2 VEGF Secretion by MDA-MB-231 cells

Since VEGF plays a crucial role in angiogenesis, we have explored the hypothesis that Pd_2Spm may impact the secretion of VEGF by MDA-MB-231 cells. As shown in **Figure 19**, both Pd_2Spm (5–20 µM) and cisplatin (5–20 µM) inhibited VEGF secretion in cell culture medium in a dose-dependent manner. Compared to cisplatin, Pd_2Spm incubation resulted in a similar decrease in VEGF secretion by MDA-MB-231. These results indicated that Pd_2Spm may possess anti-angiogenic potential to be further explored and that this effect can be ascribed, at least in part, to its ability to reduce the secretion of VEGF.

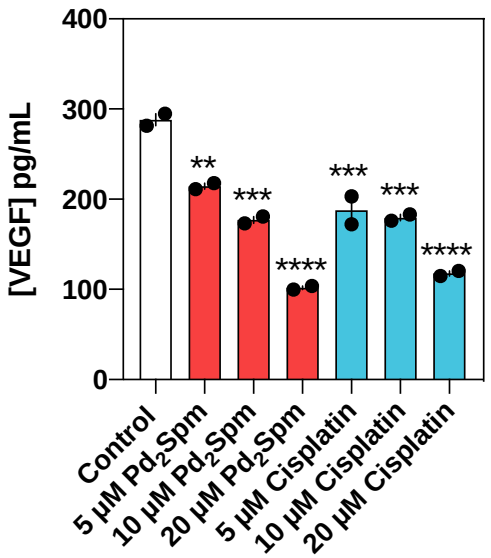

Figure 19. Quantitative results of VEGF secretion by MDA-MB-231 incubated for 12 h with Pd_2Spm (red) or cisplatin (blue).

Data are shown as means ± SEM (n = 2) and analysed with one-way ANOVA followed by Dunnett's multiple comparison test. Significant differences from the control: $^{**}p < 0.01$, $^{***}p < 0.001$, $^{****}p < 0.0001$.

IV.3.3.3 Impact on Angiogenesis in CAM model

As angiogenesis plays an important role in the carcinogenesis of TNBC [171], the antiangiogenic potential of Pd_2Spm was investigated and compared to cisplatin. We determined the effect of Pd_2Spm treatment on the neovascularization steps using the CAM assay. As also previously described [82], increasing concentrations of Pd_2Spm (2 to 8 µM) and of cisplatin (2 to 8 µM) were able to decrease, in a dose-dependent manner, the number of nodes, junctions and segments, which are parameters associated with the early steps of angiogenesis (**Figure 20a**). Similarly, Pd_2Spm and cisplatin, in the concentrations tested, reduced, in a dose-dependent manner, the total length, total branching length and total segment length, which are linked to the expansion of newly formed vessels in later steps of angiogenesis (**Figure 20b**). Thus, these data indicate that both Pd_2Spm and cisplatin have the ability to inhibit angiogenesis, in both the initial and later steps, with a similar potency ($p > 0.05$).

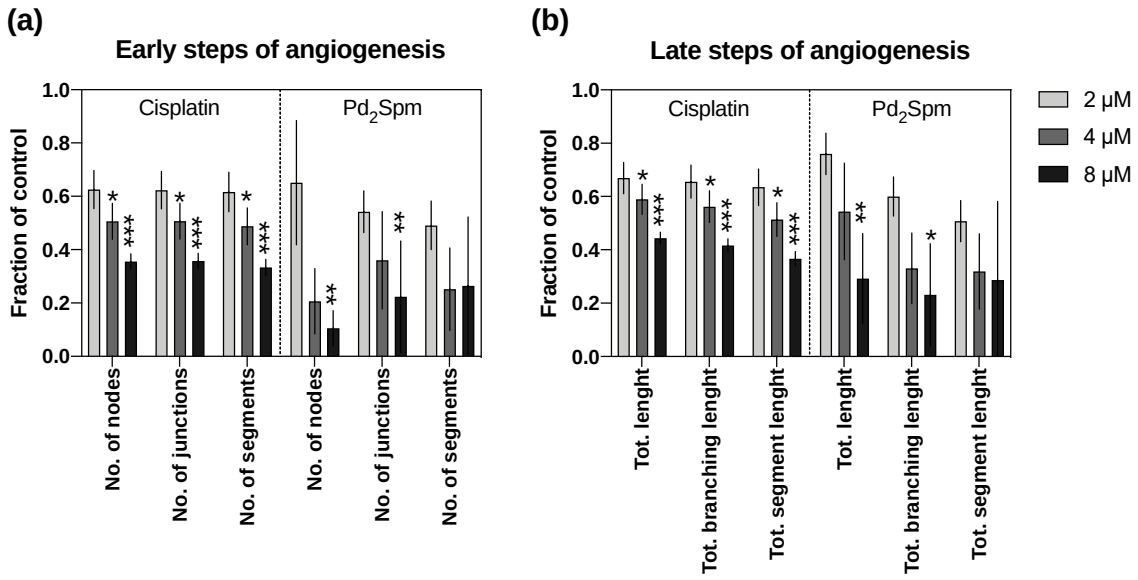

Figure 20. Quantitative results of CAM angiogenesis in the presence of increasing concentrations (2–8 µM) of either cisplatin or Pd_2Spm.

(**a**) Parameters of early steps of angiogenesis: number of nodes, junctions and segments. (**b**) Parameters of later steps of angiogenesis: total length, branching length and segment length of vessels. The results are expressed as means of the fraction of the control ± SEM from 2 independent experiments (n = 2, 8 replicates). Significant differences from the vehicle control: *$p < 0.05$, ** $p < 0.01$, *** $p < 0.001$ (one-way ANOVA followed by Dunnett's multiple comparison test).

Since angiogenesis and cell migration are significant contributors to TNBC pathogenesis, particularly regarding its metastatic potential and aggressive biology, the development of agents able to suppress cancer cell proliferation, migration and angiogenesis are highly desired. In this study, Pd_2Spm-mediated effects against cancer cell invasion yielded promising results since Pd_2Spm: (i) inhibited the migration of MDA-MB-231 cells; (ii) inhibited angiogenesis in CAM; and (iii) suppressed VEGF secretion by MDA-MB-231 cells with similar potency to cisplatin.

IV.3.4 Impact on Apoptosis and Necroptosis

To understand the impact of apoptosis and necroptosis on antiproliferative effects elicited by Pd_2Spm, cell proliferation was measured in cells co-treated with Pd_2Spm (20 mM) and either 50 µM Z-VAD (a cell-permeable, irreversible pan-caspase inhibitor that prevents apoptosis,[172] or 50 µM Nec-1 (an ATP-competitive, allosteric inhibitor of receptor-interacting protein kinase 1 (RIPK1) that prevents necroptosis,[173]). No cell growth rescue was observed in co-treatment of Pd_2Spm+Z-VAD or Pd_2Spm+Nec-1 in MDA-MB-231 and MDA-MB-231/R cells (**Figure 21a**). On the other hand, co-treatment of cisplatin+Z-VAD or cisplatin+Nec-1 in MDA-MB-231 cells was able to rescue the cell growth but such effects were not observed in MDA-MB-231/R cells. An annexin-based polarity-sensitive probe (pSIVA) was also applied to evaluate the putative occurrence of apoptosis' induction by detection of exposed phosphatidylserine (PS) residues at the outer plasma membrane. Treatment of MDA-MB-231 and MDA-MB-231/R cells with 20 µM Pd_2Spm, for 48 h, increased the population of cells with positive staining for PS residues in both cell lines when compared to control (untreated) cells (Control; **Figure 21b,c**). When the effects were compared between the two cell lines, Pd_2Spm exposure resulted in similar effects in both cell lines ($p>0.05$). Simultaneous treatment of Pd_2Spm with Z-VAD or Nec-1 decreased the percentage of MDA-MB-231 cells with positive staining for PS residues compared to treatment with Pd_2Spm alone. Moreover, no decrease in PS residue staining was observed in MDA-MB-231/R cells simultaneously exposed to Pd_2Spm and either Z-VAD or Nec-1. Sole 20 µM cisplatin treatment (48 h) of MDA-MB-231 and MDA-MB-231/R cells resulted in increased PS residues' staining relative to untreated cells (**Figure 21b,c**). When cisplatin's effects towards MDA-MB-231 and MDA-MB-231/R cells were compared, the latter showed a lower response to cisplatin that MDA-MB-231 ($p<0.05$). When cisplatin was combined with Z-VAD, both MDA-MB-231 and MDA-MB-231/R cells showed a reduction of PS residue staining. Co-treatment of Necrostatin-1 with cisplatin also reduced the number of pSIVA staining cells in MDA-MB-231, but had no significant effect in MDA-MB-231/R.

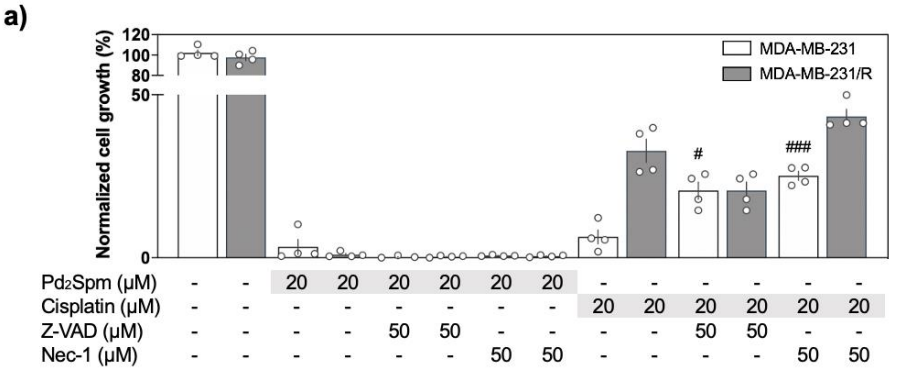
a)
Normalized cell growth (%)
120
100
80
50
0
MDA-MB-231
MDA-MB-231/R
#
###
Pd2Spm (μM) - - 20 20 20 20 20 20 - - - - - -
Cisplatin (μM) - - - - - - - - 20 20 20 20 20 20
Z-VAD (μM) - - - - 50 50 - - - - 50 50 - -
Nec-1 (μM) - - - - - - 50 50 - - - - 50 50

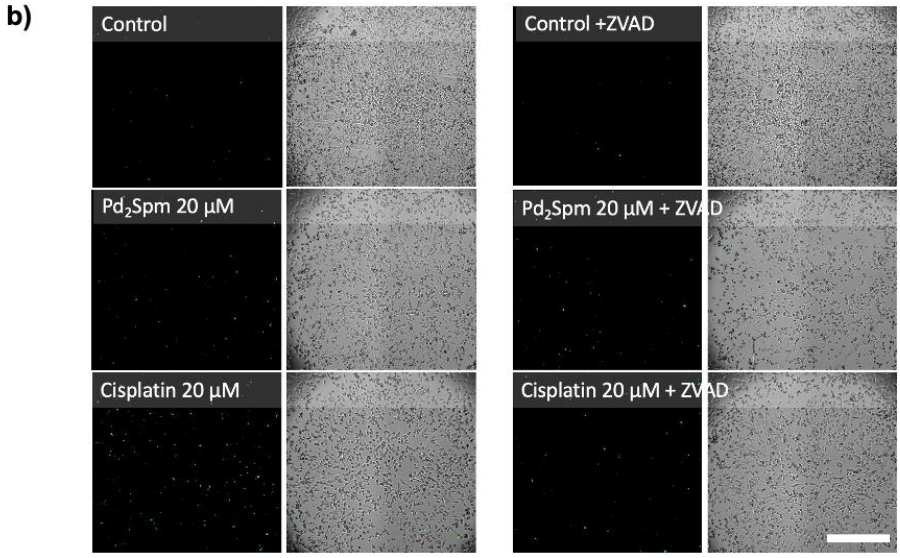
b)
Control
Control +ZVAD
Pd2Spm 20 μM
Pd2Spm 20 μM + ZVAD
Cisplatin 20 μM
Cisplatin 20 μM + ZVAD

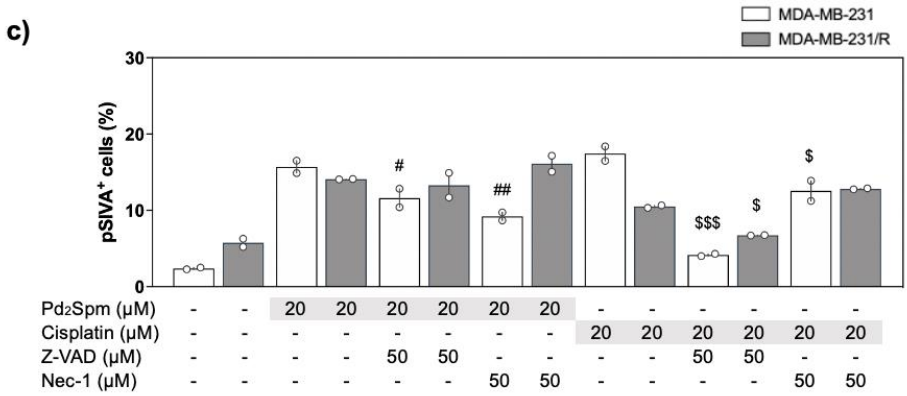
c)
MDA-MB-231
MDA-MB-231/R
pSIVA+ cells (%)
30
20
10
0
#
##
$$$
$
$
Pd2Spm (μM) - - 20 20 20 20 20 20 - - - - - -
Cisplatin (μM) - - - - - - - - 20 20 20 20 20 20
Z-VAD (μM) - - - - 50 50 - - - - 50 50 - -
Nec-1 (μM) - - - - - - 50 50 - - - - 50 50

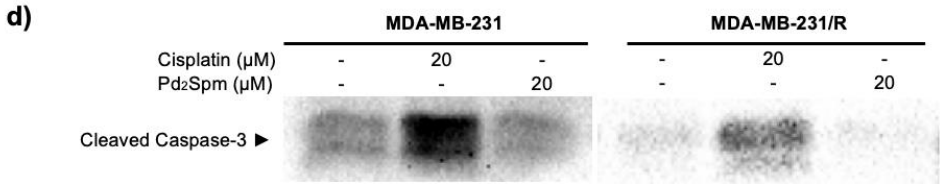
d)
MDA-MB-231
MDA-MB-231/R
Cisplatin (μM) - 20 - - 20 -
Pd2Spm (μM) - - 20 - - 20
Cleaved Caspase-3 ►

Figure 21. Effect of Pd_2Spm or cisplatin on apoptosis or necroptosis.

(a) Effects of Pd_2Spm and cisplatin on the proliferation of MDA-MB-231 (white colour) and MDA-MB-231/R (grey colour) cells, in the presence of the specific apoptosis inhibitor Z-VAD and necroptosis inhibitor Nec-1. Cells were treated with 10 μM of either Pd_2Spm or cisplatin, for 48 h, in the presence or absence of Z-VAD (50 μM) and Nec-1 (50 μM). Values are expressed as mean ± SEM, n = 4 (in triplicates). **(b)** Representative images depicting fluorescent pSIVA signal in MDA-MB-231 cells exposed to 20 μM of either Pd_2Spm or cisplatin for 48 h, in the presence or absence of Z-VAD and Nec-1. Images obtained with a fluorescence and phase-contrast objective lens of the LionheartFX microscope. Scale bar = 1000 μm. **(c)** Quantitative analysis of pSIVA-positive cells upon exposure to Pd_2Spm and cisplatin in the presence of the specific apoptosis inhibitor Z-VAD and the necroptosis inhibitor necrostatin-1 (Nec-1). Cells were treated with 20 μM of either Pd_2Spm or cisplatin, for 48 h, in the presence or absence of Z-VAD (50 μM) and Nec-1 (50 μM). Values are expressed as mean ± SEM, n = 4 (in triplicates). **(d)** Representative blot of expression of cleaved caspase-3 measured by western blot, in MDA-MB-231 and MDA-MB-231/R cells exposed to either cisplatin or Pd_2Spm, for 48 h, n = 3 **(a,c)** Data points with no visible error bars have errors smaller than the size of the symbol. Significant differences from treatment with Pd_2Spm alone: $p<0.05$ (#), $p<0.01$ (##), and $p<0.001$ (###); Significant differences from treatment with cisplatin alone: $p<0.05$ ($), $p<0.01$ ($$), and $p<0.001$ ($$$).

Furthermore, the levels of cleaved caspase-3 (an effector caspase necessary for cell apoptosis) in MDA-MB-231 and MDA-MB-231/R cells treated with 20 μM of either Pd_2Spm or cisplatin, for 48 h, were examined (**Figure 21d**). Cisplatin treatment of MDA-MB-231 cells increased the levels of cleaved caspase 3, while this effect was attenuated in MDA-MB-231/R cells. Pd_2Spm was not found to induce the expression of cleaved caspase-3, in either of the treated cell lines (as compared to untreated cells).

Since co-treatment of Pd_2Spm with an apoptosis inhibitor, Z-VAD-FMK, was unable to rescue the proliferation on Pt-sensitive or -resistant TNBC cells from the Pd_2Spm's effect, is seems that Pd_2Spm activates other forms of cell death different to apoptosis. This conclusion is further supported by the absence of caspase-3 cleavage (in Pd_2Spm-treated cells). Supporting these findings, reports with some metal-based compounds such as cyclopalladated [174] or cyclometalated iminophosphorane Gold(III) and Pt(II) complexes [175], that described to exert their effects via non-apoptotic pathways.

In addition, even though the cell proliferation was not rescued by co-treatment of Pd_2Spm+Z-VAD, this combination of compounds decreased the externalization of phosphatidylserine residues, contrasting with the effects observed in cisplatin-treated cells:

co-treatment with cisplatin+Z-VAD rescued proliferation of Pt-sensitive TNBC cells, decreased externalization of phosphatidylserine residues and resulted in increase of cleaved caspase-3 in both Pt-sensitive and -resistant TNBC cells (to a lower extent in the latter, as expected). Such effects are consistent with the described cisplatin's mode of action to trigger apoptosis in cancer cells [57]. Nonetheless all the above-mentioned data support that other type(s) of cell death apart from apoptosis may be implicated in Pd_2Spm's antineoplastic effects, although an apoptotic pathway may still be involved probably as an initial trigger or as a concomitant event triggering other form(s) of cell death [176]. In this regard, necroptosis was discarded as a mechanism of cell death triggered by Pd_2Spm since Nec-1 was unable to rescue the proliferation of either Pt-sensitive or -resistant cells from the effects of Pd_2Spm. By contrast, in cisplatin-treated cells, addition of Nec-1 rescued proliferation of Pt-sensitive cells but not of Pt-resistant cells, demonstrating that necroptosis could be associated with TNBC sensitivity to Pt-drugs, as previously described for cisplatin's [177], or to some anticancer nickel(II)-based compounds' [178].

IV.3.5 Impact on Autophagy

Putative involvement of autophagy [53] was also examined. 3-MA rescued the proliferation of MDA-MB-231 and MDA-MB-231/R cells treated with Pd_2Spm, thus decreasing its antineoplastic mediated-effects, restoring cell proliferation, surpassing > 90% net cell growth for both cell lines (**Figure 22c).** Morphologically, cells treated with Pd_2Spm showed a rounded shape with plasma membrane blebs that disappeared when 3-MA was added (**Figure 22a,** white arrow). Co-treatment with cisplatin and 3-MA rescued MDA-MB-231/R but had no impact on MDA-MB-231 cells (there were no morphological changes: **Figure 22a).**

To measure autophagic vesicles, monodansylcadaverine (MDC) staining was performed on MDA-MB-231 cells treated with either Pd_2Spm or cisplatin, and increased staining of acidic vesicles in Pd_2Spm-treated cells having been detected, while no differences in the staining of cisplatin-treated cells were observed (**Figure 22b** and **Figure 22d**).

Finally, Western-blot analysis (**Figure 22e** and **Figure 22f**) was performed in order to study the expression of LC3B-II (Microtubule-Associated Protein 1 Light Chain 3B-II, a conjugated form of LC3B-I with phosphotidylethanolamine constituting autophagosomal membranes) and Beclin-1, in MDA-MB-231 and MDA-MB-231/R cells treated with Pd_2Spm or cisplatin for 48 h. Pd_2Spm increased the conversion of LC3B-I/II in MDA-MB-231 and MDA-MB-231/R cells. When cells were co-incubated with Pd_2Spm and 3-MA, a notable

decrease in the LC3B-I/II conversion was observed in both TNBC cell lines. In cisplatin-treated MDA-MB-231 and MDA-MB-231/R cells, increased levels LC3B-II protein were observed, but to a lower magnitude compared to that observed upon Pd_2Spm treatment. The Beclin-1, an essential mediator of autophagy (required for formation of autophagosome) and a tumour suppressing protein) expression was found to decrease in Pd_2Spm- and in cisplatin-treated MDA-MB-231 cells. By opposition, in MDA-MB-231/R cells an increase in the expression of Beclin-1 was observed for both Pd_2Spm- and cisplatin-treated cells.

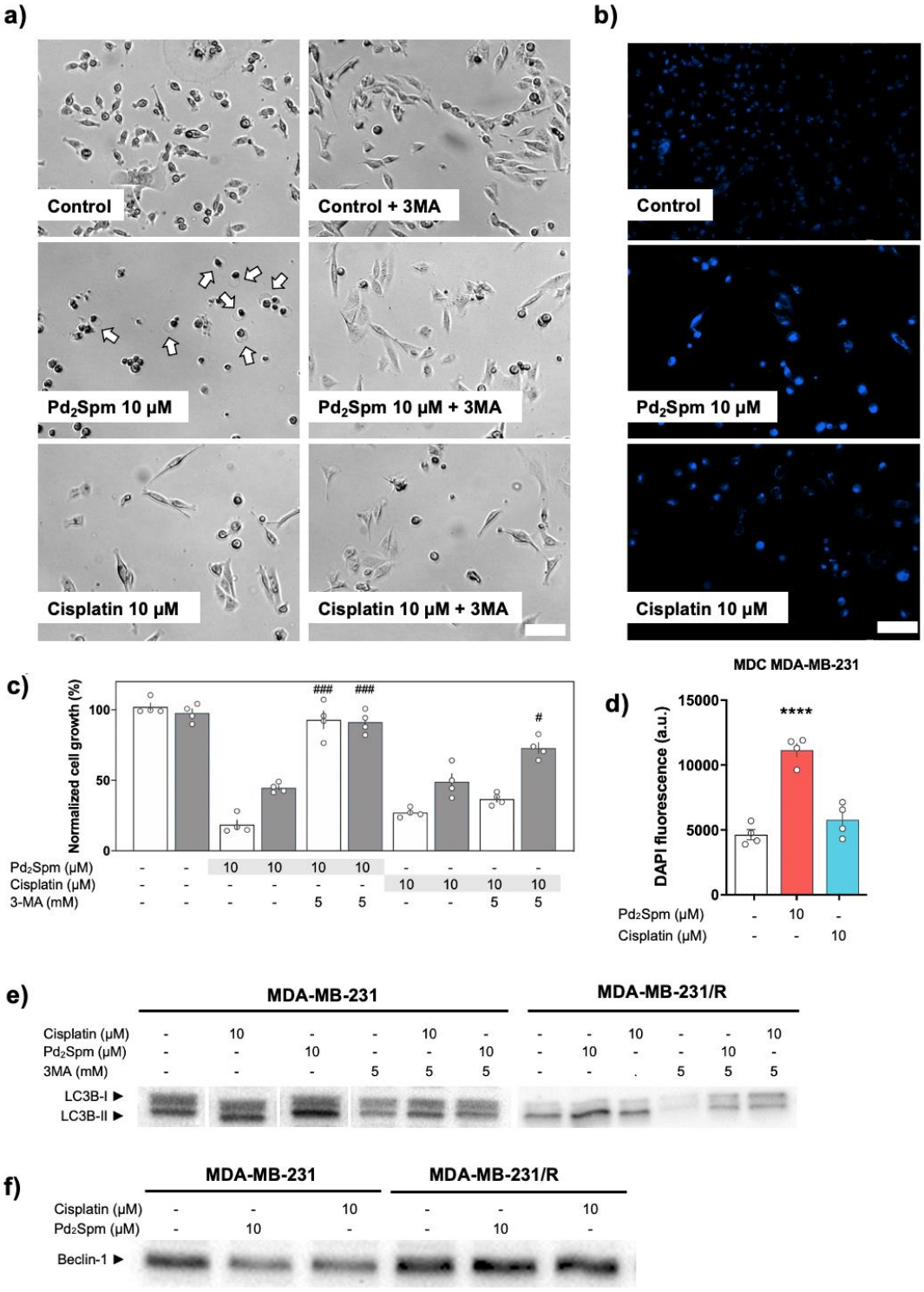

Figure 22. Effect of Pd_2Spm or cisplatin on autophagy.

(a) Representative photomicrographs of MDA-MB-231 cells treated with either Pd2Spm or cisplatin in the absence or presence of 3-MA. Images obtained with a phase-contrast objective lens of the LionheartFX microscope. Scale bar = 100 µM. **(b)** Representative photomicrographs of MDA-MB-231 cells stained with MDC. Images obtained with a fluorescent objective lens of the LionheartFX microscope. Scale bar = 100 µM. **(c)** Effect of Pd_2Spm or cisplatin on the proliferation of MDA-MB-231 (white colour) and MDA-MB-231/R (grey colour), in the presence of the specific autophagy inhibitor 3-methyladenine (3-MA, 5 mM). **(d)** Accumulation of autophagic vesicles in MDA-MB-231 cells treated with 10 µM of either Pd_2Spm or cisplatin, for 48 h, measured with monodansyl cadaverine. **(e)** Protein expression of LC3BI/II **(e)** and **(f)** beclin-1 in cells exposed to either Pd_2Spm or cisplatin. **(c,d)** Values are expressed as mean ± SEM, n = 4 (in triplicates). Significant differences from control: $p<0.0001$ (****); Significant differences from treatment with Pd_2Spm alone: $p<0.001$ (###); Significant differences from treatment with cisplatin alone: $p<0.05$ ($).

As so, the putative occurrence of cell death through autophagy induction by Pd_2Spm treatment was considered since: i) a remarkable rescue of cell proliferation (> 90%) in both Pt-sensitive and -resistant cells was observed for co-incubation of Pd_2Spm+3MA, which had also induced morphological changes visualized as rounded shape cells with prominent blebs in the plasma membrane that were attenuated in the presence of the 3MA; ii) the intensity of vesicles labelled with MDC was increased in Pt-sensitive cells treated with Pd_2Spm compared to control cells or cisplatin-exposed cells, supporting the occurrence of autophagic vesicles which is consistent with putative induction of autophagy [179]; iii) overexpression of LC3B-II was found in Pt-sensitive and -resistant cells treated with Pd_2Spm (for 48h) and were effectively inhibited by co-treatment with 3-MA, being consistent with the induction of autophagy [180] and iv) differential expression of Beclin-1 was found upon Pd_2Spm treatment: decrease in Pt-sensitive cells and increase in Pt-resistant cells. In line with this data, sulphamoylated estrone analogue induced death in breast cancer cells in a process that was suggested to occur through autophagy (using similar research strategies as employed in the present study) and, thus, autophagy was proposed as mechanism of cell death [180]. Similarly, LC3B-II induction as a measurement of autophagy induction was also reported for other metal-based compounds, such as titanocenes [181]. Since Beclin-1 is considered one of the key proteins for autophagy induction, a reduction in its expression (as observed in Pt-sensitive cells) was an unexpected finding, which could, in turn, suggest the putative occurrence of a Beclin 1-independent autophagy induction in these cells as described previously [182]. Since Pd_2Spm induced an autophagic response with higher magnitude than cisplatin this may indicate that autophagy may be associated to Pd_2Spm's mechanism of action in a greater extent than for cisplatin, in TNBC cells. This

suggestion is supported by reports evidencing that cisplatin-induced autophagy could have protective effects rather than triggering a death of breast cancer cells [183]. Altogether, the data herein presented are consistent with the putative induction of autophagy triggered by Pd_2Spm in Pt- sensitive and -resistant TNBC cells. Although, autophagy has also been implicated to enable neoplastic cells to acquire resistance to drugs, persistent and/or excessive activation of autophagy in neoplastic cells may induce autophagic cell death [184], having both positive or a negative role(s) in carcinogenesis depending on the stimuli and context. Such effects were described for other Pd(II)-based compound [PdCl(terpy)](sac)·4 H_2O that induced autophagy and caspase-independent cell death in prostate cancer PC3 cells [145]. Even though the evidence gathered in this study supported an increase of autophagosomes upon Pd_2Spm treatment, further investigation will be required to fully understand if this Pd(II)-agent induces autophagy or disrupts the autophagic flux (fusion or degradation).

IV.3.6 Impact on ERK 1/2 and NF-κB Signalling Pathways

Extracellular-signal-regulated kinase (ERK) 1/2 signalling and NF-κB pathway were also probed since those constitute an essential link with autophagy [147,185], and are also involved in development resistance to cisplatin by breast cancer cells [79,80]. To assess constitutive activation of NFκB and ERK1/2 pathways in MDA-MB-231 *versus* MDA-MB-231/R cells, the basal expression of phosphorylated forms of NF-κB and ERK1/2 among these two cell strains (control, untreated cells) was assessed. Development of drug resistance increased the basal phosphorylation of NF-κB by 17% in MDA-MB-231/R as compared to MDA-MB-231 cells. On the other hand, acquired resistance decreased the basal levels of phosphorylated ERK1/2 by 50% in MDA-MB-231/R relative to MDA-MB-231 cells.

Cells treated with 20 μM of Pd_2Spm showed an increased expression of phosphorylated-ERK1/2 in MDA-MB-231 and MDA-MB-231/R cells (**Figure 23a**) compared to control (untreated) cells. In addition, when comparing the increased phosphorylation of ERK 1/2 upon Pd_2Spm treatment (20 μM), MDA-MB-231/R showed a higher effect than MDA-MB-231. Upon exposure to 20 μM of cisplatin, both MDA-MB-231 and MDA-MB-231/R cells showed increased levels of phosphorylated ERK1/2, but no significant difference was detected between the two cell lines (**Figure 23a**).

Considering the phosphorylation of the NF-κB protein, 20 μM of Pd_2Spm did not induce any increase in either MDA-MB-231 or MDA-MB-231/R cells, compared to control

(untreated) cells. In addition, no differences were detected between the two TNBC cell lines (**Figure 23b**). In turn, for cisplatin-treated MDA-MB-231 and MDA-MB231/R cells, there was an increase in the levels of phosphorylated NF-κB (**Figure 23b)** compared to controls, MDA-MB-231/R showing a slight decrease in p-NF-κB levels (not statistically significant) relative to MDA-MB-231 cells.

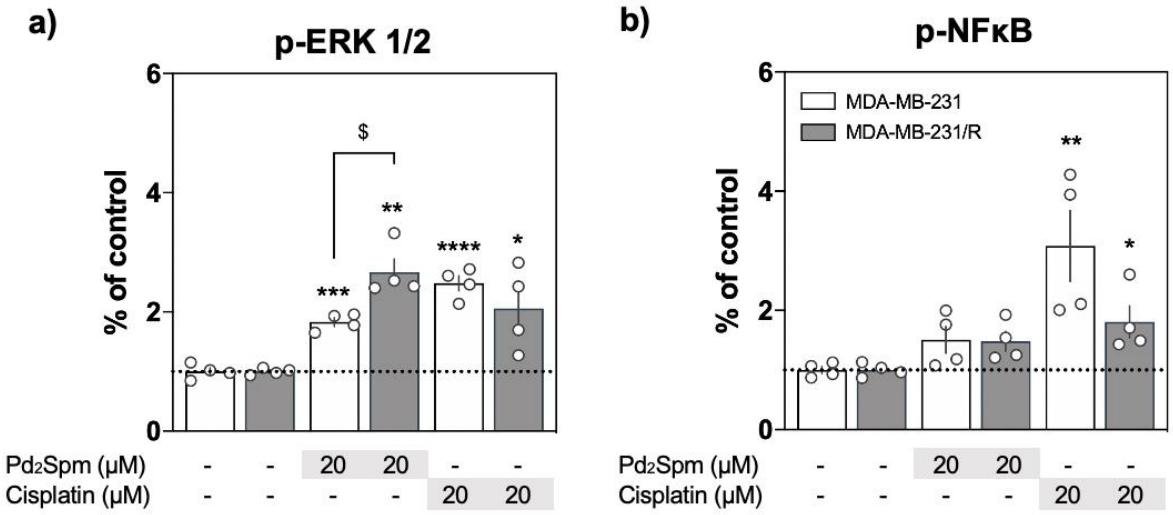

Figure 23. (a) Phosphorylation of ERK1/2 and **(b)** phosphorylation of NF-κB in MDA-MB-231 (white colour) and MDA-MB-231/R cells (grey colour).

(a,b) Cells were treated with 20 μM of either Pd_2Spm or cisplatin, for 48 h, lysed and, then, p-ERK 1/2 or p-NF-κB were detected using AlphaScreen Sure Fire technology. Values are expressed as mean ± SEM, n = 4 (in triplicates). Significant differences from the appropriate untreated control: $p<0.05$ (*), $p<0.01$ (**), $p<0.001$ (***) and $p<0.0001$ (****); Significant differences from MDA-MB-231 cells: $p<0.05$ ($).

Both Pd_2Spm and cisplatin were found to trigger an increased phosphorylation of ERK 1/2 protein (compared to untreated control in Pt-sensitive and -resistant cells). As previously described, activation of ERK 1/2 can mediate cell death in cisplatin-treated cells [64][65]. Interestingly, our data showed that acquiring the Pt-resistance by TNBC MDA-MB-231 cells is associated with lower basal activation of ERK1/2, thus possibly allowing higher survival of the resistant cells. When comparing effects between Pt-sensitive and -resistant cells, Pd_2Spm caused a stronger phosphorylation of ERK 1/2 in Pt-resistant cells compared to Pt-sensitive cells, while cisplatin triggered lower ERK 1/2 phosphorylation in Pt-resistant cells, indicating cisplatin's lower ability to engage this signalling pathway in cells with acquired resistance compared to Pd_2Spm. These effects could be explained by: (i) the putative engagement of different targets that lead to ERK 1/2 activation; (ii) distinctive

intracellular targets engaged by Pd_2Spm and cisplatin or (iii) by the ability of Pd_2Spm to surpass adaptative mechanisms developed by resistant cells to cisplatin.

Pd_2Spm treatment did not change NF-κB p65 protein phosphorylation in Pt-sensitive nor Pt-resistant cells. Cisplatin, on the other hand, increased the levels phosphorylated NF-κB p65 protein in Pt-sensitive and -resistant cells when compared to the untreated controls, with Pt-sensitive cells having more phosphorylated NF-κB p65 than Pt-resistant cells, thus, evidencing a lower activity of cisplatin in Pt-resistant cells. These findings corroborate previous studies that reported cisplatin-triggered phosphorylation of NF-κB *via*, activating the mitogen-activated protein kinase (MEK)/ERK signalling cascade [66]. The lower phosphorylation of NF-κB observed in Pt-resistant cells treated with cisplatin could be explained by stronger basal phosphorylation of NF-κB protein that may not further increase with additional stimuli. Other studies have reported that resistant cells show increased expression of NF-κB, compared to their sensitive parent, implicating NF-κB as a potential mediator of acquired Pt resistance [67]. Also, NF-κB activation has been described as an essential factor for cisplatin's mechanisms of action [66], which could explain both lower activation of effects NF-κB and, consequently, lower effects of cisplatin in Pt-resistant cells.

IV.3.7 Final Remarks

In vitro study revealed that Pd_2Spm triggers different intracellular events than cisplatin in TNBC cells and allowed to draw the following conclusions: (i) Pd_2Spm showed similar antineoplastic activity in both Pt-sensitive and -resistant TNBC cells that contrast with the loss of activity of cisplatin in Pt-resistant cells; (ii) Pd_2Spm showed a clear selectivity towards TNBC cells with minimal effects to healthy non-neoplastic cells, while cisplatin was equally deleterious to healthy non-neoplastic breast cells as to breast cancer cells; (iii) Cells treated with Pd_2Spm did not shows typical features of apoptosis and caspase-3 cleavage which were visible in cisplatin-treated cells and demonstrated a possible involvement of autophagic machinery in its mechanisms of cell death; (iv) Differences between activation of ERK 1/2 and NF-κB have shown that while both Pd_2Spm triggers the phosphorylation of ERK 1/2 pathways, its effects on NF-κB activation are limited. Finally, Pd_2Spm showed attractive chemotherapeutic potential for Pt resistant TNBC and to trigger differential mechanisms of action compared to cisplatin, namely via inducing autophagic cell death pathway and most probably involving ERK activation. Therefore, this Pd (II) chelate could possibly be used for the treatment of cancers with mutated apoptotic signalling and/or in combination with other compounds to hinder the development of the resistance and therapy failure.

IV.4 ICP-MS Method Development and Validation

Quantification of metal-based compounds in animal tissues and biofluids is typically achieved with microwave-assisted sample digestion and ICP-MS (inductively coupled plasma-mass spectrometry) analysis [186]. However, microwave-assisted digestion requires the acquisition of specific equipment and is time-consuming when hundreds of samples need to be analysed—such as during the *in vivo* pharmaco-toxicokinetic and biodistribution animal studies. Additionally, it is noteworthy that the sample amounts available from *in vivo* rodent studies are limited and insufficient for conventional methods that typically require between 0.4 to 1 g of sample, which is difficult to obtain without pooling the samples [162,187,188]; thus, fast and reliable micro methods suitable for the analysis of reduced amounts of animal sample is a relevant topic.

Pt quantification in biologic fluids with no previous sample digestion has been described for plasma [186,189–191], urine [189–191], and peritoneal fluid [190]. Validated ICP-MS methods for Pt quantification that include pre-treatment by heating the samples with nitric acid at 90–100 °C [192], or microwave-assisted acid digestion of plasma [193], urine and liver samples [162] were also reported. However, validated ICP-MS methods for Pd quantification in a variety of biologic matrices such as adipose tissue, muscle, liver, kidney, spleen, testis, heart, lungs, and brain obtained from *in vivo* pharmaco-toxicokinetic studies, or methods that could be readily used for the simultaneous quantification of Pd and Pt content in those animal samples are not described.

The use of a water bath for sample digestion is a possibility that was applied for Pt quantification in rat dorsal root ganglion (10 mg sample) using acid sample digestion (HNO_3), and a 90 °C water bath for 2 h followed by H_2O_2 overnight treatment at 50 °C [194]; and for Pt quantification in rat blood, brain, intestine, prostate and testis (0.4 g sample), using sample acid digestion (HNO_3 + H_2O_2) with heating in a 80 °C water bath for 1 h followed by sample neutralization with NH_4OH [188]. Nevertheless, the applicability, reliability, and performance of these methods for Pd quantification in biologic matrices were not addressed.

The principal limitation for the development of new methods for a Pd/Pt quantitative analysis in biologic matrices, particularly in animal tissues, is the absence of commercially available certified reference material. The present study overcomes this difficulty and provides a simple ICP-MS method for the simultaneous quantification of Pd- and Pt-based drugs in serum, blood, adipose tissue, muscle, liver, kidney, spleen, testis, heart, lungs and brain samples. The novel analytical procedure was developed and validated using in-house

materials (animal tissues and biofluids) with intracellular incorporation of Pd and Pt, prepared *via* intraperitoneal injection of Pd/Pt standard solutions in rodents. Since the incorporation of Pd/Pt is tissue dependent, the Pd/Pt reference concentrations in each type of the prepared tissue and biofluid were first obtained by microwave-assisted acid digestion. This strategy significantly differs from the conventional method developments that use sample spiking with known amounts of analytes (Pd and Pt), since in the latter, Pd/Pt are not tightly bound to the tissue. Therefore, Pd and Pt may be more easily extracted during sample digestion, which may confound the identification of significant variables in method optimization process. Furthermore, the approach applied in present study is closely similar to real samples from pharmaco-toxicokinetic and biodistribution animal studies. The goal of this study was to develop and validate an ICP-MS method for Pd and Pt quantification in a variety of animal tissues and biofluids, requiring a small amount of sample (up to 50 mg), low reagents consumption and allowing simultaneous preparation of hundreds of samples per hour, which are significant improvements for successful application in animal pharmacokinetic and biodistribution studies, comparatively to microwave-assisted sample digestion. Optimal conditions for complete sample digestion were searched by two-level factorial and central composite designs (CCD).

IV.4.1 Variable Identification Using Two-Level Factorial Design

The effect of the four tested variables (HNO_3 volume, HCl volume, reaction time and reaction temperature) is presented in **Figure 24,** in the form of a Pareto chart (the bar height is proportional to the significance of the variable). The sum of Pd and Pt content in the in-house material was used as the response. All tested variables were considered statistically significant ($p < 0.05$), with reaction time, reaction temperature and HNO_3 volume having a positive effect on the response, while the HCl volume had a negative effect. In addition, the interaction between the variables, reaction time and HNO_3 volume as well as between reaction time and HCl volume were considered statistically significant ($p < 0.05$), both with a negative effect on the response. Considering these results, the four variables were selected for further evaluation in the CCD.

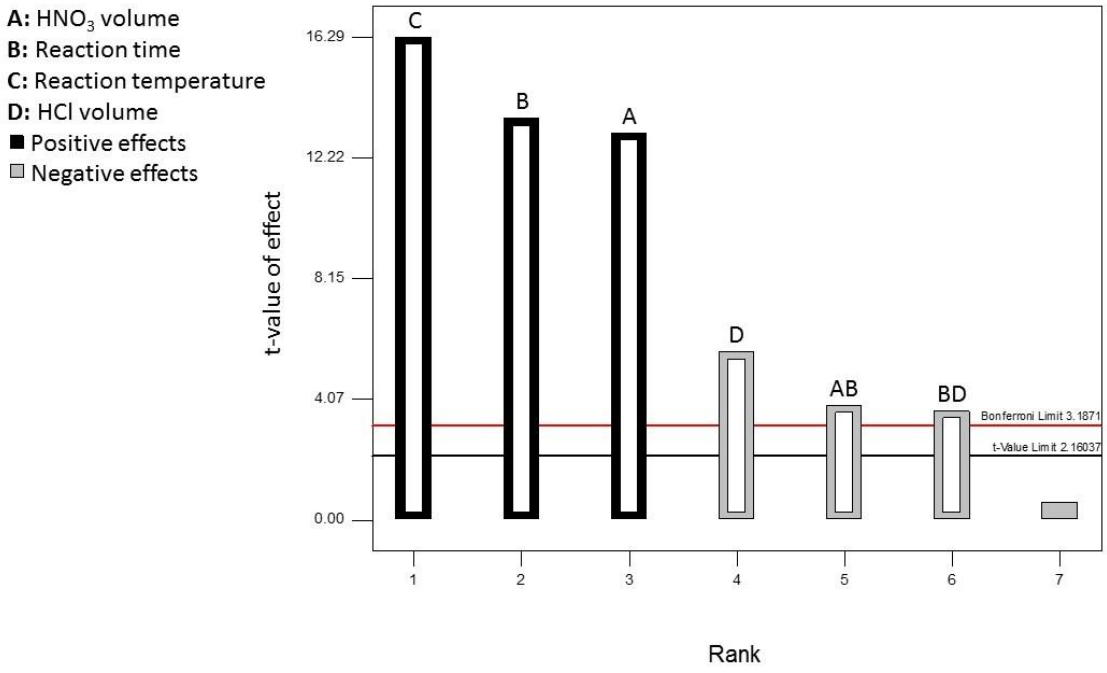

Figure 24. Pareto chart of the effect of the four variables tested in the two-level factorial design (HNO_3 volume, HCl volume, reaction time and reaction temperature).

IV.4.2 Method Optimization Using CCD

Twenty-one experiments were carried out with the significant variables selected from the screening experiment: HNO_3 volume (A), reaction time (B), reaction temperature (C) and HCl volume (D). The sum of Pd and Pt content in the in-house material was used as the response for the CCD experiment. The generated models were validated by two common diagnostic residuals, the R^2 and Q^2. Typical values that indicate adequate models are $R^2 > 0.75$ and $Q^2 > 0.60$. In this study, the predicted R^2 and the adjusted R^2 values were 0.97 and 0.98, respectively, and the Q^2 value was 0.97, evidencing the goodness of the model. The adequate precision, measured as a signal-to-noise ratio, was 33.8 (a ratio > 4 is desirable), indicating the adequacy of the present model. As shown in **Table 10**, the F value was 97.3, which indicates that the regression model is statistically significant ($p < 0.0001$) at a 99% confidence level. The terms A, B, C, D, AC, AD, BC, CD, A^2, B^2, C^2 and D^2 showed p-values < 0.05, proving the significance of the model terms. The lack-of-fit was 0.22 as desired and, thus, non-significant relative to the pure error. Therefore, the quadratic model could be considered valid.

Table 10. Analysis of variance (ANOVA) for the response surface model.

Source	Sum of squares	Degrees of freedom	Mean square	F value	Probability > F	Remarks
Model	15.86	14	1.13	97.3	< 0.0001	significant
A – HNO_3 volume	4.68	1	4.68	401.5	< 0.0001	significant
B – Reaction time	0.25	1	0.25	21.8	0.0003	significant
C – Reaction temperature	8.55	1	8.55	733.6	< 0.0001	significant
D – HCl volume	0.16	1	0.16	13.7	0.0021	significant
AB	0.017	1	0.017	1.44	0.2491	not significant
AC	0.31	1	0.31	26.3	0.0001	significant
AD	0.11	1	0.11	9.51	0.0076	significant
BC	0.33	1	0.33	28.6	< 0.0001	significant
BD	0.0005	1	0.0005	0.046	0.8332	not significant
CD	0.078	1	0.078	6.66	0.0209	significant
A^2	0.16	1	0.16	14.0	0.0019	significant
B^2	0.40	1	0.40	34.6	< 0.0001	significant
C^2	0.51	1	0.51	44.1	< 0.0001	significant
D^2	0.26	1	0.26	22.3	0.0003	significant
Residual	0.17	15	0.012			
Lack of Fit	0.053	10	0.0053	0.22	0.9811	not significant
Pure Error	0.12	5	0.024			
Total	16.1	29				

Three-dimensional surface and contour plots were drawn to demonstrate the interactive effect of two factors in the selected response (**Figure 25**). **Figure 25a** shows the combined effect of the variables HNO_3 volume and reaction temperature. **Figure 25b** shows the combined effect of HNO_3 volume and HCl volume, while **Figure 25c** shows the combined effect of reaction time and reaction temperature. Lastly, **Figure 25d** shows the combined effect of reaction temperature and HCl volume.

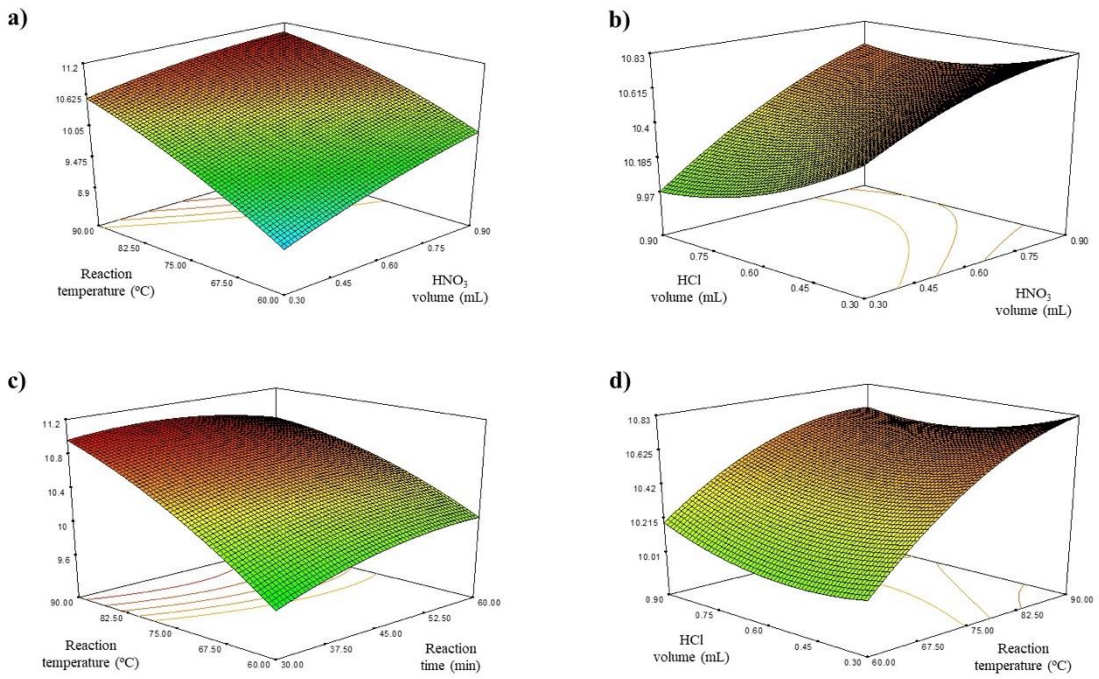

Figure 25. Three-dimensional surface and contour plots for the CCD: (**a**) HNO_3 volume vs reaction temperature, (**b**) HNO_3 volume vs HCl volume, (**c**) Reaction time vs reaction temperature, (**d**) Reaction temperature vs HCl volume.

To complete the CCD optimization, the desirability index (DI) was applied. In short, DI is a method for multicriteria optimization used to quantify how desirable certain outcomes are on an absolute scale (*i.e.*, [0,1]). In this particular case, all factors (variables) were left at their default values of the experimental range and the response was maximized. The following optimal conditions (DI = 1) were obtained: HNO_3 volume – 0.9 mL, reaction time – 60 min, reaction temperature – 90 ºC and HCl volume – 0.3 mL.

IV.4.3 Method Performance

The linearity, limits of detection (LODs), limits of quantification (LOQs), precision and accuracy of the developed method as well as matrix effects are summarized in **Table 11** to **Table 14.** The calibration curves showed good linearity in the range 0.025 to 10 µg/L for both Pd and Pt with coefficients of determination (r^2) of 0.9999 and 0.9998, respectively. The LODs were respectively 0.0009 µg/L and 0.0011 µg/L, whereas the LOQs were 0.0033 µg/L and 0.0025 µg/L (**Table 11**).

Table 11. Linear dynamic range, coefficient of determination (r^2), limit of detection (LOD) and limit of quantification (LOQ).

Element	Isotope	Linear dynamic range (µg/L)	r^2	LOD (µg/L)	LOQ (µg/L)
Palladium	^{108}Pd	0.025 − 10	0.9999	0.0009	0.0033
Platinum	^{195}Pt	0.025 − 10	0.9998	0.0011	0.0025

The procedure repeatability and the between-run precision in ICP-MS analysis were determined for all the matrices (solid tissues and biofluids) (**Table 12**). The results showed good repeatability and between-run precision with CV < 1.9% and CV < 1.5%, respectively.

Table 12. Repeatability and between-run precision for Pd and Pt content in the different tissues and biofluids under study.

Tissue/biofluid	Repeatability[a] (n=2)		Between-run precision[a] (n=3)	
	^{108}Pd	^{195}Pt	^{108}Pd	^{195}Pt
Whole blood	0.21	0.56	0.58	0.79
Blood serum	0.19	0.51	0.87	0.57
Liver	0.81	0.30	0.72	0.63
Brain	0.19	0.22	1.53	1.06
Heart	1.32	0.02	0.99	1.07
Lungs	0.03	0.11	0.74	0.88
Kidney	0.78	1.91	0.67	1.14
Spleen	0.86	0.15	0.97	0.52
Muscle	1.18	0.85	0.81	0.79
Testis	0.16	0.68	0.62	0.89
Adipose tissue	0.85	0.91	0.61	0.87

[a]data expressed as percent coefficient of variation (%CV).

Concerning the accuracy of the developed method, results obtained from sample solutions prepared by microwave-assisted acid digestion were considered as reference values. For all the tissues and biofluids, the Pd/Pt contents obtained by the newly developed procedure were within good agreement limits, ranging between 83.5 to 105.1%, as summarized in **Table 13**. With the exception of adipose tissue, the developed method showed excellent accuracy for all tested tissues and biofluids, higher than 95% when 50 mg of sample was used. As anticipated, the adipose tissue was the most challenging matrix for digestion due to its high lipid content, requiring a tissue mass reduction to 25 mg, which led to improved accuracy of 98.1–100.3%.

Table 13. Accuracy results for Pd and Pt quantification in different tissues and biofluids under study.

Tissue/biofluid	Sample quantity	Sample dilution	Method	Within-run accuracy (n=2)				Between-run accuracy (n=3)			
				^{108}Pd		^{195}Pt		^{108}Pd		^{195}Pt	
				Mean ± SD (µg/g)	Accuracy (%)	Mean ± SD (µg/g)	Accuracy (%)	Mean ± SD (µg/g)	Accuracy (%)	Mean ± SD (µg/g)	Accuracy (%)
Whole blood	50 µL	5	Developed	0.52 ± 0.001	100.0	0.51 ± 0.005	96.9	0.52 ± 0.003	99.3	0.51 ± 0.005	96.6
			Reference	0.52 ± 0.002		0.52 ± 0.002		0.53 ± 0.004		0.52 ± 0.005	
Blood serum	50 µL	5	Developed	0.54 ± 0.001	105.1	0.52 ± 0.003	97.2	0.54 ± 0.005	105.0	0.52 ± 0.003	98.3
			Reference	0.52 ± 0.001		0.54 ± 0.001		0.51 ± 0.004		0.53 ± 0.009	
Liver	50 mg	5	Developed	1.32 ± 0.011	100.6	4.29 ± 0.013	100.6	1.32 ± 0.009	100.4	4.27 ± 0.027	99.8
			Reference	1.32 ± 0.001		4.26 ± 0.027		1.31 ± 0.010		4.28 ± 0.019	
Brain	50 mg	5	Developed	0.07 ± 0.001	98.4	0.14 ± 0.001	100.1	0.07 ± 0.001	96.7	0.14 ± 0.002	96.3
			Reference	0.07 ± 0.001		0.14 ± 0.001		0.07 ± 0.002		0.15 ± 0.004	
Heart	50 mg	5	Developed	0.57 ± 0.008	97.8	1.96 ± 0.001	98.9	0.57 ± 0.006	96.6	1.94 ± 0.021	95.6
			Reference	0.58 ± 0.006		1.99 ± 0.010		0.59 ± 0.009		2.03 ± 0.035	
Lungs	50 mg	5	Developed	1.05 ± 0.001	102.5	3.83 ± 0.004	100.2	1.05 ± 0.008	100.1	3.80 ± 0.033	97.8
			Reference	1.03 ± 0.002		3.82 ± 0.012		1.04 ± 0.014		3.88 ± 0.058	
Kidney	50 mg	50	Developed	39.89 ± 0.312	96.2	29.34 ± 0.561	95.8	39.90 ± 0.269	99.2	29.21 ± 0.332	98.7
			Reference	41.48 ± 0.080		30.64 ± 0.329		40.21 ± 0.986		29.60 ± 0.840	
Spleen	50 mg	5	Developed	2.40 ± 0.021	99.4	3.88 ± 0.006	98.0	2.38 ± 0.023	97.4	3.86 ± 0.020	96.6
			Reference	2.41 ± 0.022		3.96 ± 0.041		2.44 ± 0.025		3.99 ± 0.043	
Muscle	50 mg	5	Developed	1.73 ± 0.020	100.8	4.34 ± 0.037	100.3	1.74 ± 0.014	100.7	4.31 ± 0.034	98.2
			Reference	1.72 ± 0.003		4.33 ± 0.003		1.73 ± 0.014		4.39 ± 0.064	
Testis	50 mg	5	Developed	0.66 ± 0.001	100.6	1.08 ± 0.007	98.9	0.66 ± 0.004	98.4	1.07 ± 0.010	97.6
			Reference	0.66 ± 0.002		1.09 ± 0.003		0.67 ± 0.010		1.10 ± 0.010	
Adipose tissue	50 mg	5	Developed	1.49 ± 0.013	84.3	1.18 ± 0.011	87.1	1.48 ± 0.009	83.5	1.17 ± 0.010	85.9
			Reference	1.76 ± 0.002		1.35 ± 0.013		1.77 ± 0.010		1.37 ± 0.021	
Adipose tissue	25 mg	5	Developed	2.02 ± 0.178	98.1	1.49 ± 0.149	100.3	ND		ND	
			Reference	2.06 ± 0.146		1.49 ± 0.163					

In general, a high concentration of matrix elements may result in the suppression or enhancement of the analyte signal. Therefore, these matrix effects were studied in each type of biologic matrix, by spiking sample solutions resulting from its digestion. The mean recoveries ranged from 92.4 to 114.7%, showing a marginal effect of the elemental matrix composition on the analyte signal (**Table 14**).

Table 14. Evaluation of matrix effect in the Pd and Pt determination for each type of tissue and biofluid digests.

Tissue/biofluid	**Matrix effect (n=2)**	
	^{108}Pd	**^{195}Pt**
Whole blood	99.1	97.7
Blood serum	99.1	98.2
Liver	99.2	105.9
Brain	95.0	95.2
Heart	97.2	97.0
Lungs	96.1	99.0
Kidney	89.7	106.4
Spleen	100.5	98.6
Muscle	101.2	114.6
Testis	95.4	92.4
Adipose tissue	95.4	100.5

[a]data expressed as recovery (%) of spiked concentration.

Furthermore, the agreement between the results obtained from the newly developed method and the reference method (microwave-assisted digestion) was assessed using a Bland–Altman plot (**Figure 26**). The mean bias of 0.0147 µg/L and its 95% confidence interval includes the line of the equality, suggesting the agreement between the two methods. Furthermore, uniformly scattered differences demonstrated no proportional bias originating from the measurements.

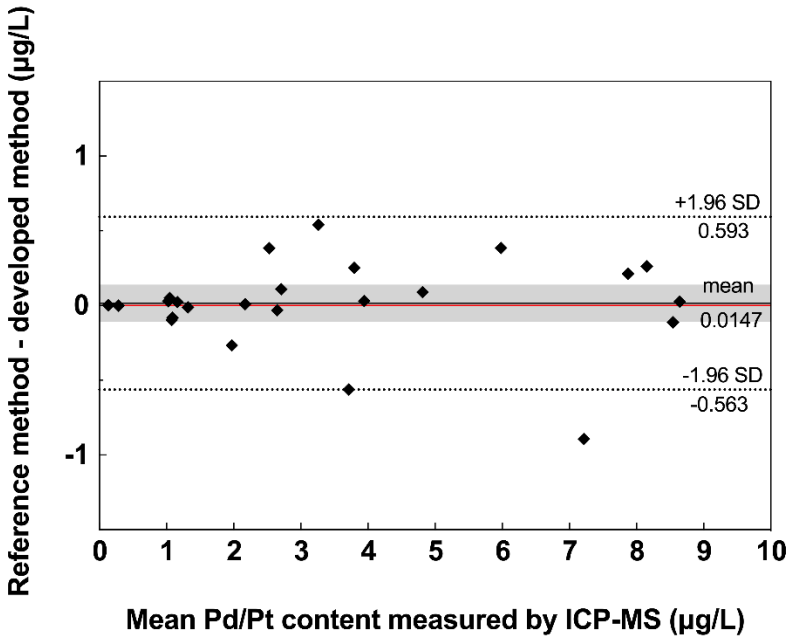

Figure 26. Bland–Altman plot of differences between the methods (vertical axis) against the average of the methods (horizontal axis) with 95% limits of agreement (dotted lines).

The mean bias 0.0147 µg/L (black continuous line) is represented with corresponding 95% confidence interval limits (shaded area) that include the line of equality (red continuous line), evidencing the agreement between the two methods. The plot shows uniformly scattered differences (homoscedasticity) along the line of equality with no proportional bias.

IV.4.4 Application to Real Samples from Biodistribution Studies

Lyophilization of solid tissues and their subsequent pulverization are common procedures for removing water to preserve animal samples and to increase digestion efficiency for ICP-MS analysis when hundreds of samples with distinct biologic compositions are needed to be analysed. However, the reduction of tissue weight by lyophilization also leads to an increased concentration of the analyte (Pd and Pt content), which is commonly expressed *per* tissue weight. During pharmacokinetic studies, the area under the curve (AUC) defines the drug systemic exposure that can be determined for each of the organs. Thus, to obtain biologically meaningful data, it is important to express the drug content in tissues in terms of natural tissue weight (prior to lyophilization). This can be achieved using conversion factors established from the weight of natural tissues *versus* dry tissue weight (**Table 15**). As shown in **Figure 27**, the analyte concentration can be overestimated ~4–7 times in tissues with an abundant water content—such as testis, lungs, heart, spleen and brain—when expressed *per* lyophilized tissue weight. Therefore, pharmacokinetic studies that aim to quantify drug biodistribution in a variety of organs

should collect the weights of both the natural tissue and the lyophilized one for data analysis. Furthermore, it is also noteworthy that in a case of small rodents (such as mice or hamster), a successful digestion of whole lyophilized tissues/organs weighting ≤ 50 mg can be achieved without prior pulverization of tissues.

Table 15. Conversion of Pd and Pt content in dry tissue to natural tissue weight.

Tissue	Natural weight after dissection (g)	Dried weight after lyophilization (g)	Tissue water content (%)	To convert Pd/Pt in dry tissue (µg/g) to Pd/Pt in natural tissue (µg/g), divide by
Body weight	466 ± 51.07			
Liver	13.12 ± 1.06	4.11 ± 0.33	68.69 ± 0.20	**3.192**
Brain	1.91 ± 0.21	0.44 ± 0.05	76.67 ± 0.38	**4.341**
Heart	1.07 ± 0.09	0.24 ± 0.02	77.22 ± 0.70	**4.458**
Lungs	1.98 ± 0.24	0.35 ± 0.05	81.85 ± 4.09	**5.657**
Kidney	2.23 ± 0.23	0.59 ± 0.05	73.52 ± 1.05	**3.780**
Spleen	0.72 ± 0.13	0.18 ± 0.03	75.03 ± 1.03	**4.000**
Muscle	2.45 ± 0.84	0.75 ± 0.31	69.99 ± 2.54	**3.267**
Testis	3.40 ± 0.63	0.51 ± 0.03	84.56 ± 2.79	**6.667**
Adipose tissue	3.67 ± 0.34	3.26 ± 0.33	11.10 ± 4.12	**1.126**

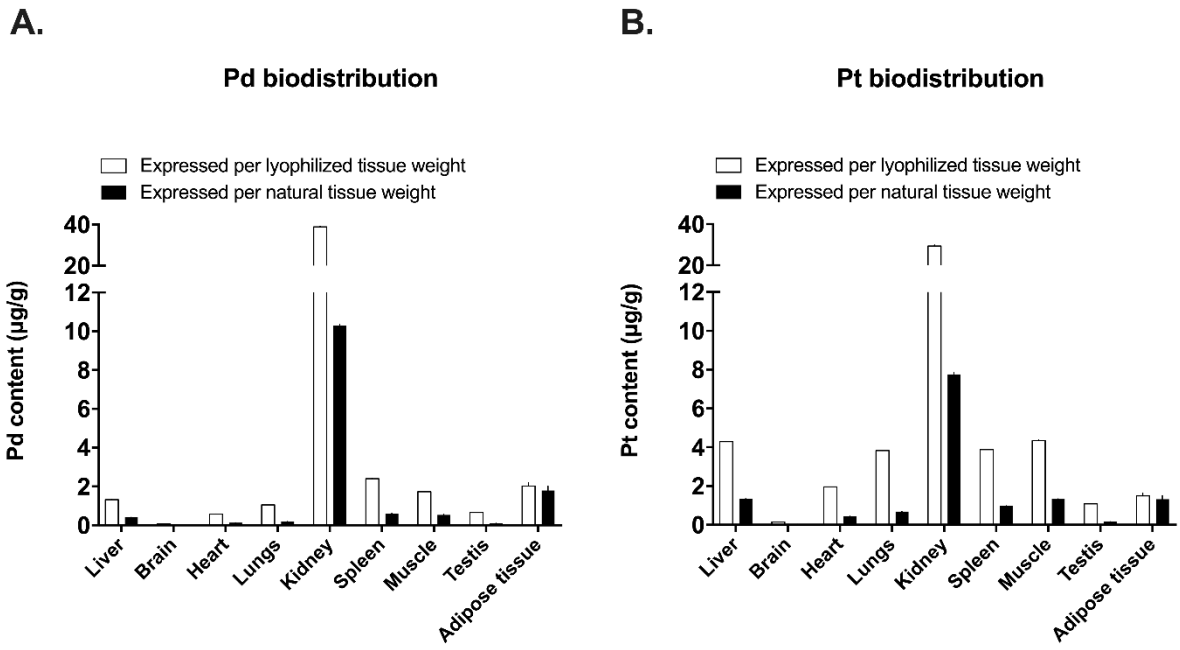

Figure 27. Comparison of Pd/Pt biodistribution profiles (mean ± SD) expressed per lyophilized tissue weights and natural tissue weights: (**a**) Pd biodistribution profile, (**b**) Pt biodistribution profile.

IV.4.5 Final Remarks

The present study offers a fast, reliable, and cost-effective alternative to microwave-assisted digestion for ICP-MS quantification of the Pd and/or Pt content in animal tissues and biofluids. The method was developed and validated using in-house materials with intracellular incorporation of Pd/Pt in biologic matrices. Optimal conditions for complete digestion of animal samples (50 mg) were 3:1 (v/v) mixture of nitric acid (900 µL) with hydrochloric acid (300 µL) during 60 min in a 90 °C water bath, which was achieved by two-level factorial and central composite design.

The method showed LODs of 0.001 µg/L, linear dynamic range between 0.025 and 10 µg/L with R^2 = 0.9999 for Pd and R^2 = 0.9998 for Pt, and good repeatability (0.02–1.9%) as well as intermediate precision (0.52–1.5%) for both metals. The accuracy ranged from 83.5 to 105.1% considering microwave-assisted digestion as reference method. Except for adipose tissue, the developed method showed accuracy > 95% for all biologic matrices when 50 mg of sample was used. As anticipated, high lipid content of white adipose tissue was the most challenging matrix for digestion—requiring tissue mass reduction to 25 mg, which led to improved accuracy of 98.1–100.3%. Finally, Bland–Altman plot confirmed the validated method as a reliable alternative to microwave-assisted digestion. This method allows to prepare hundreds of samples per hour in closed conical bottom centrifuge tubes with a screw cap, using a standard laboratory water bath, small tissue amounts and small volume of acids. Herein, the novel method showed to be very suitable for *in vivo* pharmaco-toxicokinetic and biodistribution studies of Pd and/or Pt-based drugs in a wide variety of animal tissues (e.g. adipose tissue, muscle, liver, kidney, spleen, testis, heart, lungs and brain) as well as in biofluids (such as blood and serum).

IV.5 *In Vivo* Effects – Pharmacokinetics

IV.5.1 Serum and Serum Ultrafiltrate Analysis

The concentrations of Pd and Pt in serum (total Pd/Pt) and serum ultrafiltrate (free Pd/Pt) after a single intraperitoneal bolus injection of Pd_2Spm 3 mg/kg or cisplatin 3.5 mg/kg, in healthy female Balb/c mice, were measured by ICP-MS, the corresponding serum concentration–time profiles of Pd (from Pd_2Spm) and Pt (from cisplatin) are shown in **Figure 28**. The decrease in Pd and Pt concentrations in serum and serum ultrafiltrate showed a biphasic kinetic behaviour with a rapid initial distribution phase followed by a prolonged first-order elimination phase in both Pd_2Spm- and cisplatin-treated animals (see **Figure 28**).

Even though the doses of Pd_2Spm (3 mg/kg) and cisplatin (3.5 mg/kg) used in this study were somewhat similar, the actual dose of Pd administered to the animals was only half of the dose of Pt owing to the difference in the metal composition in each compound (dinuclear versus mononuclear in Pd_2Spm and cisplatin, respectively; please see section **III.4.3.5. Pharmacokinetic Analysis***,* for further clarification). Therefore, to obtain biologically meaningful comparisons of relative metal kinetics, the mean Pd and Pt concentrations were normalized to the administered metal dose (**Figure 28b**). Regarding the metal dose-normalized concentration–time profiles in serum ultrafiltrate, a higher concentration of free Pd than Pt was found during the 0.5–12 h period, reaching equivalent concentrations for both metals during the 24–48 h period. The dose normalization also revealed that animals treated with Pd_2Spm reached a 3- and a 4.2-fold higher C_{max} in serum and serum ultrafiltrate, respectively, compared to cisplatin. Additionally, considering the dose-normalized areas under the curve (AUCs), Pd_2Spm administration resulted in a 1.2- ($p > 0.05$) and a 4.3-fold ($p < 0.001$) higher AUC for Pd in serum and serum ultrafiltrate when compared to cisplatin, respectively.

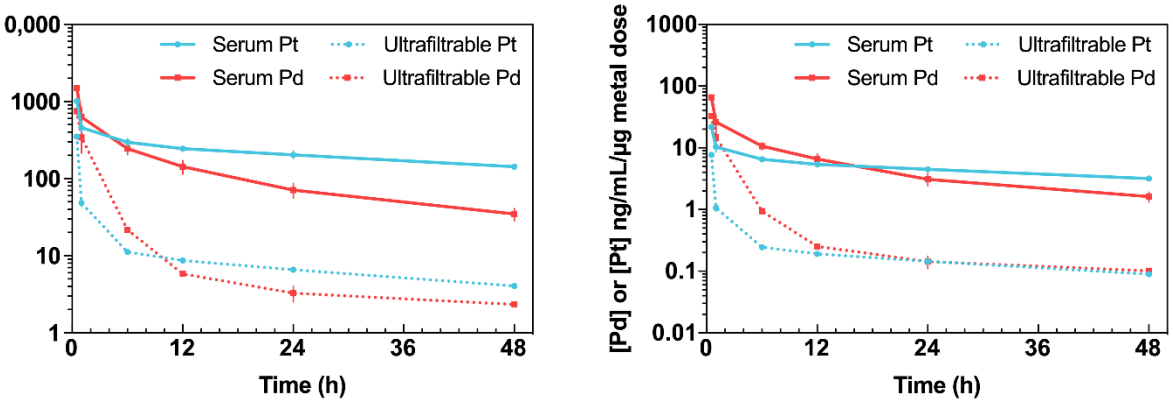

(a) (b)

Figure 28. Kinetic profiles of Pd (from Pd_2Spm, 3 mg/kg bw) and Pt (from cisplatin, 3.5 mg/kg bw) in serum and serum ultrafiltrate after single intraperitoneal bolus injection in Balb/c mice.

(**a**) Concentration–time plot of mean Pd or Pt levels in serum and serum ultrafiltrate. (**b**) Concentration–time plot of mean Pd or Pt levels in serum and serum ultrafiltrate normalized to administered metal dose. (**a,b**) Data are expressed as mean ± SEM (*n* = 5 animals per time point).

The kinetic profiles of Pd (from Pd_2Spm, 3 mg/kg bw) and Pt (from cisplatin, 3.5 mg/kg bw) were also analysed with non-compartment analysis yielding pharmacokinetic parameters summarized in **Table 16**.

Table 16. Pharmacokinetic parameters of total Pd and Pt in serum and serum ultrafiltrate following intraperitoneal bolus injection of Pd_2Spm (3 mg/kg bw) and cisplatin (3.5 mg/kg bw) in Balb/c mice.

Pharmacokinetic Parameter (unit)	Pd_2Spm		Cisplatin	
	Total Pd in Serum	Free Pd in Ultrafiltrate	Total Pt in Serum	Free Pt in Ultrafiltrate
Half-life (h)	20.7	35.5	43.3	31.5
λ_z (1/h)	0.034	0.019	0.016	0.022
T_{max} (h)	0.5	0.5	0.5	0.5
C_{max} (ng/mL)	1499.4 ± 38.5	749.0 ± 120.6	1009.6 ± 64.2	350.7 ± 16.8
C_{max}/Dose (ng/mL/µg)	65.9 ± 4.2	32.7 ± 5.3	21.9 ± 1.9	7.7 ± 0.4
$AUC_{0–48\ h}$ (h × ng/mL)	6490.2	1219.7	10867.5	567.2
$AUC_{0–48\ h}$/Dose (h × ng/mL/µg)	285.0	53.2	240.5	12.5
$AUC_{0–\infty}$ (h × ng/mL)	7523.9	1339.1	19,758.5	751.5
Vz/F (mL/kg)	4555.0	43,992.0	7202.8	143,864.7
CL/F (mL/h/kg)	152.8	858.8	115.4	2989.9

λz = elimination rate constant; T_{max} = time to reach C_{max}; C_{max} = mean maximum concentration ± SEM; $AUC_{0-48\ h}$ = area under curve from time zero to 48 h; $AUC_{0-\infty}$ = area under the curve from time zero to infinity; Vz/F = volume of distribution at terminal phase; CL/F = body clearance.

Pd_2Spm administration (3 mg/kg bw) resulted in mean serum Pd concentrations within the range of 34.7 to 1499.4 ng/mL. The maximum concentration (C_{max}), 1499.4 ± 38.5 ng/mL, declined rapidly within the first hour and decreased steadily during the terminal elimination phase. In serum, Pd was found to display an elimination half-life of 20.7 h and a clearance (CL/F) of 152.8 mL/h/kg. Its volume of distribution (Vz/F: 4555.0 mL/kg) in mice was greater than total body water, suggesting the widespread distribution of Pd in tissues. Free Pd reached C_{max} = 749.0 ± 120.6 ng/mL, with an elimination half-life of 35.5 h and CL/F = 858.8 mL/h/kg. At 48 h, the concentration of free Pd in serum ultrafiltrate was 2.3 ng/mL.

Administration of cisplatin (3.5 mg/kg) resulted in mean serum Pt concentrations within the range 142.4 to 1009.6 ng/mL. The C_{max} 1009.6 ± 64.2 ng/mL decreased steadily with a terminal half-life of 43.3 h and a CL/F of 115.4 mL/h/kg. The volume of distribution was 7202.8 mL/kg. Free Pt in serum peaked at a maximum concentration of C_{max} = 350.7 ± 16.8 ng/mL, with an elimination half-life of 31.5 h, a volume of distribution equal to 143,864.7 mL/kg and CL/F = 2989.9 mL/h/kg. At 48 h, the concentration of free Pt was found to be 4.1 ng/mL.

Since the maximum concentration (c_{max}) for both Pd and Pt in plasma was reached immediately at the first sampling time-point, 0.5 h (T_{max}), the Pd/Pt concentration during the preceding period (<30 min post-injection) may be higher.

Even though the terminal half-life of Pd (from Pd_2Spm) in serum was found to be 20.7 h, in contrast with 43.3 h for Pt (from cisplatin), the free Pd in serum ultrafiltrate had a higher terminal half-life than Pt (35.5 h *versus* 31.5 h, respectively), which suggests a longer persistence of free Pd in blood circulation during the terminal elimination phase. The analysis of serum ultrafiltrate has particular relevance since this biological matrix contains free drug and its low molecular weight metabolite(s) (< 30 kDa in this study prepared with cut-off 30K NMWL filter), which are both responsible for exerting pharmacological effects [195]. Upon systemic administration, the drug occurs in plasma in different forms: (i) as a free, intact molecule that was administered *in vivo*; (ii) free hydrolyzed species and/or low molecular weight metabolites; and (iii) a plasma protein-bound drug (either *via* reversible or irreversible bonds with different affinities and kinetics).

IV.5.2 Binding to Plasma Proteins

The analysis of Pd and Pt concentrations in serum ultrafiltrate showed different profiles of plasma protein binding. At 0.5 and 1 h following Pd_2Spm administration, only ca. 50% of Pd from Pd_2Spm was bound to plasma proteins and 91.0% at 6 h, reaching the maximum protein plasma binding of 95.9% at 12 h post-administration (**Figure 29**). At 48 h, 92.8% of Pd_2Spm was bound to plasma proteins. For cisplatin, in turn, a faster binding was determined—65.5% at 0.5 h and 89.5% at 1 h, reaching a maximum of ca. 97% at 6 h (i.e., virtually twice as fast relative to Pd_2Spm). A comparative analysis revealed significantly lower Pd binding (from Pd_2Spm) to plasma proteins than Pt (from cisplatin) during the 0.5–6 h period after drug administration. Additionally, while at 12 and 24 h, Pd and Pt showed similar binding to plasma proteins (ca. 96–97%), at 48 h, the fraction of Pd bound to plasma proteins presented a 3.1% decrease compared to the preceding period.

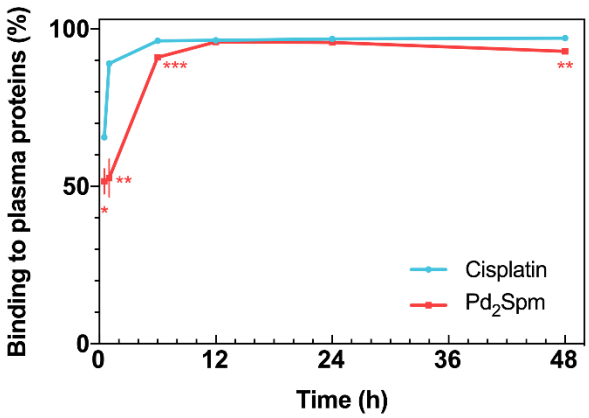

Figure 29. Drug binding to plasma proteins versus time, for cisplatin and Pd_2Spm.

Data are expressed as mean ± SEM (n = 5 animals per time point) and were compared with Student's t-test. * $p < 0.05$, ** $p < 0.01$, *** $p < 0.001$.

The drug binding to plasma proteins (namely albumin, α1-acid glycoprotein, and lipoproteins) is an unavoidable effect that influences the pharmacokinetic and pharmacodynamic properties of all systemically administered drugs. In general, drug´s high binding to plasma proteins results in the drug´s lower tissue permeability, a small volume of distribution, decreased metabolism, slower clearance, and prolonged half-life. In turn, considering the widely accepted free the drug theory, the concentration of the free drug in plasma correlates more accurately with drug´s pharmacological effects and toxicity than the total plasma concentration (free drug plus protein-bound drug), as only the free drug can reach its target in tissues and exert therapeutic effects. The free drug theory also stipulates

that when a steady-state equilibrium is reached in the plasma, the free drug concentration in plasma reflects the pharmacologically relevant amount of the free drug at the target site (*i.e*., tissues) [196]. Regarding conventional Pt(II)-agents (cisplatin, carboplatin, and oxaliplatin), previous *in vivo* studies in rodents have shown different interactions of these drugs with plasma proteins; at 3 h post-administration > 85% of cisplatin and oxaliplatin were bound to albumin mostly *via* irreversible covalent bonds, while only 20 to 50% of carboplatin was reversibly bound to plasma proteins [197–199]. Indeed, Pt-based chemotherapeutics undergo both aquation reactions and biologic transformation in blood, which allow binding of a drug's metal centre to cysteine and methionine residues of amino acids that constitute plasma proteins (mostly *via* covalent bonds that inactivate Pt agents) [200]. This process is highly time-dependent and differs between different Pt drugs, depending on the stability of its ligands and leaving groups [201]. In the present work, the analysis of serum ultrafiltrate samples showed that 1 h post-administration, only *ca.* 50% of Pd_2Spm was bound to plasma proteins compared to *ca.* 90% for cisplatin, revealing different affinities of Pd_2Spm and cisplatin towards plasma proteins. Since most cisplatin is bound to plasma proteins *via* irreversible bonds, only a small fraction of administered cisplatin is available to cross cell membranes and exert pharmacological effects. Pd_2Spm, on the other hand, showed a lower affinity to coordinate to plasma proteins, which indicates that following the administration, the majority of Pd_2Spm is initially present in the plasma as a free unbound drug, which may more easily reach its targets in the tissues and exert pharmacological effects. These results are further supported with 4.3-fold ($p < 0.001$) higher AUC and longer elimination half-life (35.5 h) of free Pd in serum ultrafiltrate, which suggests a higher availability and persistence of free Pd than free Pt in blood circulation.

IV.5.3 Tissue Biodistribution

Accumulation of Pd (from Pd_2Spm) and Pt (from cisplatin) in mice kidney, liver, lungs, heart, adipose tissue, mammary gland, brain and ovaries was determined by ICP-MS, and the corresponding $AUC_{0-48\,h}$ for each tissue is presented in **Figure 30a.** Except for the brain, Pd was widely distributed in the tested tissues, and the primary accumulation was found in the kidney, followed by the liver, lungs, ovaries, adipose tissue and mammary glands. Excluding the kidney, the animals treated with a single cisplatin dose showed a higher accumulation of Pt in all the organs than the Pd levels found in the organs of Pd_2Spm-treated animals. In the kidney, similar Pd and Pt concentrations were found (when comparing cisplatin- and Pd_2Spm-treated mice), suggesting a similar accumulation of metals in renal tissue when doses of 3 mg/kg of Pd_2Spm and 3.5 mg/kg of cisplatin are administered.

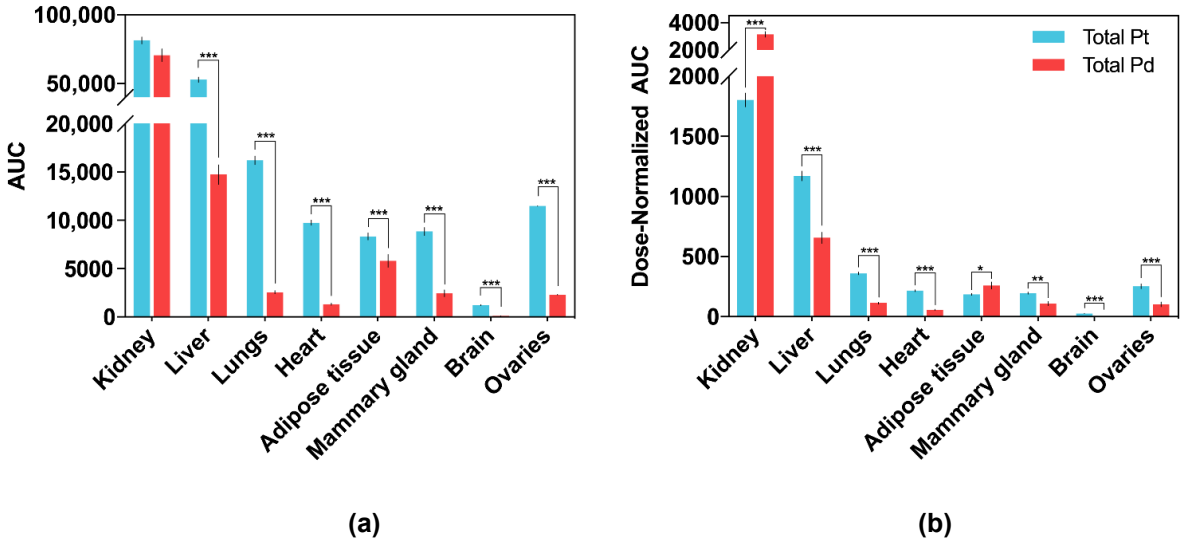

Figure 30. Biodistribution of total Pd (from Pd2Spm, 3 mg/kg bw) and Pt (from cisplatin, 3.5 mg/kg bw) in tissues after single intraperitoneal bolus injection in Balb/c mice.

Values are expressed as mean ± SEM (n = 5 animals per time point) and were compared with Student's t-test. * $p < 0.05$, ** $p < 0.01$, *** $p < 0.001$. (**a**) $AUC_{0\text{-}48h}$ (area under the Pd/Pt concentration–time curve); (**b**) metal dose-normalized $AUC_{0–48\ h}$ (area under the Pd/Pt concentration–time curve).

The corresponding kinetic profiles of Pd and Pt concentrations in tissues are also available in **Figure 31**. Since these metal concentrations at 12 h post-administration of either drug—Pd_2Spm (**Figure 31a**) or cisplatin (**Figure 31b**) did not show a substantial decrease during the sampling period of 48 h, the pharmacokinetic parameters for each tissue could not be estimated. The normalization of AUCs to the administered metal dose evidenced 1.7- and 1.4-fold higher exposures to Pd versus Pt in kidney and adipose tissues, respectively, suggesting a higher relative accumulation of Pd_2Spm. In turn, the dose-normalized AUCs for Pd in liver, lungs, heart, ovaries and mammary tissue were lower compared to Pt exposure; Pd was decreased by 43.9% in liver, 68.4% in lungs, 73% in heart, 44.1% in mammary tissue and 59.4% in ovaries as compared to Pt. The brain was the least exposed studied tissue, evidencing 82.7% lower accumulation of Pd than Pt, which indicates a reduced permeability of the blood–brain barrier to Pd_2Spm than to cisplatin; thus, this agent is highly unlikely to affect the central nervous system. Corresponding dose-normalized kinetic profiles for Pd and Pt in tissues are shown in **Figure 32a** and **Figure 32b**, respectively.

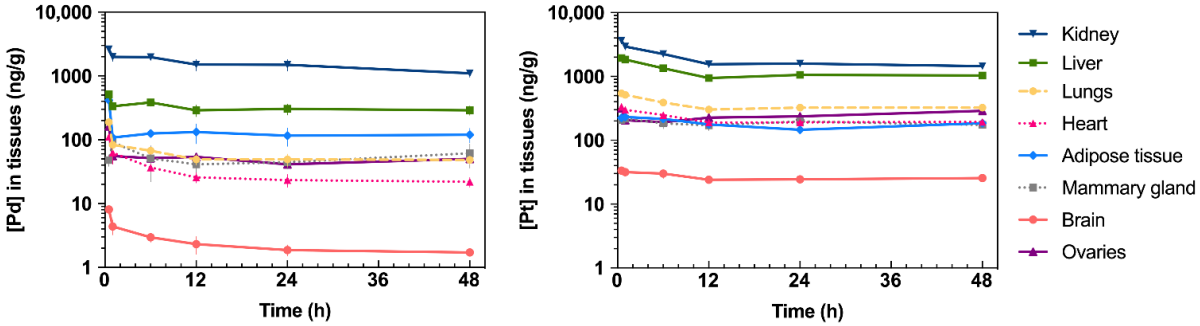

Figure 31. Kinetic profiles of Pd (from Pd_2Spm, 3 mg/kg bw) and Pt (from cisplatin, 3.5 mg/kg bw) in tissues after single intraperitoneal bolus injection in Balb/c mice.

(**a**) Concentration–time plot of mean Pd levels in tissues. (**b**) Concentration–time plot of mean Pt levels in tissues. (**a,b**) Data are expressed as mean ± SEM (n = 5 animals per time point). Units: ng/g of tissue.

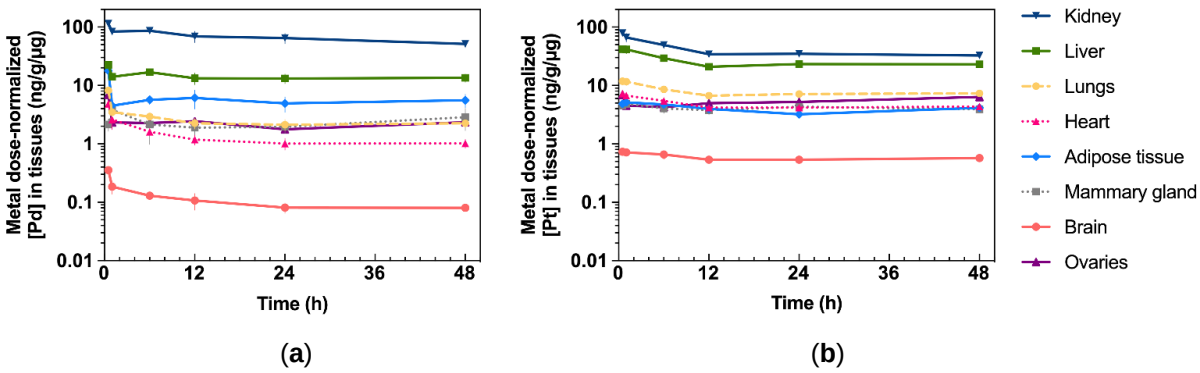

Figure 32. Metal dose-normalized kinetic profiles of Pd (from Pd_2Spm, 3 mg/kg bw) and Pt (from cisplatin, 3.5 mg/kg bw) in tissues after single intraperitoneal bolus injection in Balb/c mice.

(**a**) Concentration–time plot of mean Pd levels (normalized to administered metal dose) in tissues. (**b**) Concentration–time plot of mean Pt levels (normalized to administered metal dose) in tissues.(**a,b**) Data are expressed as mean ± SEM (n = 5 animals per time point). Units: ng/g per µg of metal dose.

Therefore, owing to its limited accumulation, Pd_2Spm is expected to be well tolerated, without noteworthy deleterious effects in liver, heart, lung and brain. In turn, a 74.2% higher accumulation of Pd (from Pd_2Spm) relative to Pt (from cisplatin) was determined in the kidney. This very large disparity in the accumulation of Pd and Pt in the kidney compared to the other organs was an expected outcome, which agrees with previous reports for several Pt-based compounds [202–204]. The dose-dependent nephrotoxicity of Pt-based

drugs results from the binding of the drug´s Pt centre to thiol-containing renal enzymes (*e.g.,* metallothioneins) [205] but, as shown for oxaliplatin and carboplatin, which displayed a higher and lower renal accumulation than cisplatin, respectively [206], the total content of Pt accumulated in the kidney is an unreliable biomarker of nephrotoxicity, and attention should be paid to specific interactions between the drug/its metabolites and renal biomolecules likely to be responsible for functional deviation and associated toxicity [199,206,207]. Several authors have anticipated lower nephrotoxicity elicited by Pd-based compounds owing to their decreased reactivity towards sulfhydryl groups of proteins in the kidney; however, it still remains to be yet fully understood under *in vivo* conditions [208,209]. Accordingly, since we have observed the highest exposure to Pd_2Spm (and cisplatin) in the kidney and liver, the metabolic impact of Pd_2Spm and cisplatin on these organs had already been the subject of our parallel work aiming to determine possible deleterious alterations [210,211]. Using an identical experimental design, the metabolomics results evidenced that Pd_2Spm treatment triggered rapid and short-term changes with almost complete recovery to control levels in liver (both polar and lipid metabolites) and kidney (polar metabolites), while cisplatin induced distinctive and more persistent deviations [210]. In general, these metabolic results provided encouraging evidence that Pd_2Spm treatment may induce lower negative effects compared to the treatment with cisplatin [211] despite considerable Pd accumulation in the kidney and liver.

IV.5.4 Final Remarks

This work reported, for the first time, an *in vivo* pharmacokinetic study of a dinuclear Pd(II)-polyamine anticancer agent (Pd_2Spm) after intraperitoneal bolus injection in healthy Balb/c mice. Using ICP-MS, the tissue biodistribution and several pharmacokinetic parameters were obtained and compared with those measured for cisplatin, taken as a reference drug.

Pd_2Spm showed appropriate pharmacokinetics regarding its potential therapeutic application. In addition, it displayed a slower plasma protein binding and a higher terminal half-life of free Pd in serum as compared to cisplatin. Since the overall accumulation of Pd in tissues was lower than Pt (in Pd_2Spm- and cisplatin-treated mice, respectively), it is expected that Pd(II)-agent might present decreased systemic adverse effects. This study provides valuable insights into the *in vivo* pharmacokinetic profile and biodistribution of Pd_2Spm, allowing further research and preclinical development of this promising compound. In addition, the results thus gathered constitute a reliable scientific basis for future pharmacokinetics studies of other Pd-based potential anticancer agents.

IV.6 *In Vivo* Effects – Proof-of-Concept for Efficacy and Safety

IV.6.1 Tumour Growth Inhibition in Xenografted Mice

To validate the *in vitro* anticancer effects of Pd_2Spm, we have studied the effects of *in vivo* administration of Pd_2Spm (5 mg/kg/day, for 5 consecutive days) on the growth of subcutaneously implanted MDA-MB-231 cancer cells in female nude mice. The cisplatin-treated mice (2 mg/kg/day, for 5 consecutive days) were used as a reference treatment group. The selection of doses of Pd_2Spm and cisplatin used *in vivo* took into consideration the doses we used previously for pharmacokinetic and tissue biodistribution studies. The average tumour volumes in mice treated with either Pd_2Spm or cisplatin for 5 consecutive days were significantly lower compared to vehicle-treated control mice ($p < 0.05$; **Figure 33**). At the end of the experiment, the tumour growth reduction (versus the vehicle group) was 43.3% and 56.6% for Pd_2Spm- and cisplatin-treated animals, respectively.

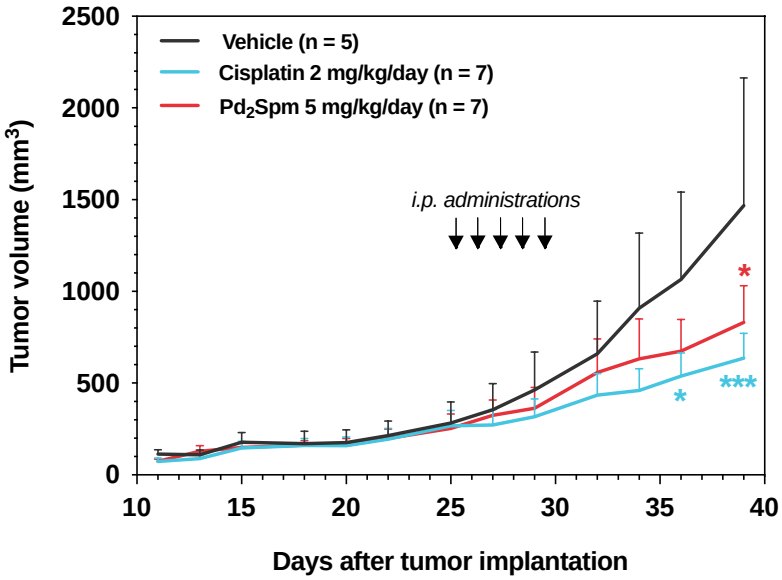

Figure 33. Effect of Pd_2Spm treatment (5 mg/kg/day), cisplatin treatment (2 mg/kg/day) or vehicle (PBS + 0.5% DMSO) on growth of MDA-MB-231 tumours in mice.

Drugs were administered intraperitoneally for 5 consecutive days in CBA nude female mice bearing subcutaneously implanted MDA-MB-231 triple-negative human breast cancer tumours. Data are expressed as mean tumour volume (mm^3) ± SEM and analysed with two-way ANOVA followed by Tukey's multiple comparison test. * $p < 0.05$ Pd_2Spm versus vehicle; *** $p < 0.001$ cisplatin versus vehicle.

The *in vivo* anticancer activity of Pd(II)-based compounds against TNBC is still largely unexplored, and to date, there are only a few *in vivo* studies in rodents regarding Ehrlich ascites carcinoma (EAC), which is an undifferentiated murine mammary adenocarcinoma sensitive to chemotherapy and not classified as TNBC [115,118]. The Pd complex of terpyridine with saccharinate, also known as [Pd(sac)(terpy)](sac)·4H_2O, administered intraperitoneally at a dose of 2 mg/kg (two injections per week for 2 weeks, up to a cumulative dose of 8 mg/kg) was found to reduce tumour volume by 67.5%, but one mouse died during treatment (1 of 10), indicating the toxicity and poor tolerability of this compound [118]. Another study focused on the similar derivative [PdCl(terpy)](sac)·2H_2O found that at a dose of 3 mg/kg (two injections per week for 2 weeks, up to a cumulative dose of 12 mg/kg), it reduced tumour volume by 69.8%, and one mouse died during treatment (1 of 9) [115]. Additionally, mice treated with 4 mg/kg of cisplatin (two injections per week for 2 weeks up to a cumulative dose of 16 mg/kg) showed 36.4% tumour volume reduction in a first study with two associated deaths [118] and a in 46.7% tumour volume reduction in a second study with no associated deaths [115]. When compared to the present results, it is clear that Pd_2Spm shows a good ability to effectively reduce the growth of TNBC tumours by 43.3% at a cumulative dose of 25 mg/kg (5 mg/kg/day of Pd_2Spm for 5 consecutive days) with no associated deaths, while cisplatin reduced the tumour growth by 56.6% at a cumulative dose of 10 mg/kg (2 mg/kg/day of cisplatin for 5 consecutive days). The selection of the 5 mg/kg/day dose of Pd_2Spm accounted for Pd_2Spm's pharmacokinetics and differential accumulation of Pd in cancer cells that were explored in previous studies [212]. Moreover, the dose selection also reflected the different molar ratios of Pd and Pt atoms in Pd_2Spm and cisplatin molecules, respectively (i.e., 5 mg/kg/day of Pd_2Spm corresponded to 1.91 mg/kg/day of the administered dose of Pd, and 2 mg/kg of cisplatin corresponded to 1.3 mg/kg/day of the administered dose of Pt) [212].

IV.6.2 Histopathological Analysis and Immunohistochemistry

All study animals developed malignant neoplasms characterized by a dense population of polyhedral epithelial cells arranged in a solid pattern. Neoplastic lesions exhibited an infiltrative behaviour, infiltrating surrounding muscle and adipose tissue, with large central necrotic areas. Neoplastic cells exhibited marked anisocytosis and anisokaryosis, and multinucleated cells and aberrant nuclear shapes were found (**Figure 34a—H&E**). Tumours treated with the vehicle showed highly dense cancer cells with atypical nuclei, evidencing intense mitosis. The mitotic count of vehicle-treated animals was significantly increased compared to cisplatin- and Pd_2Spm-treated groups (**Figure 34b**). In order to evaluate whether Pd_2Spm-mediated suppression of tumour growth occurred with a

decrease in cell proliferation and/or DNA damage induction, the Ki-67 proliferation index (a well-accepted marker of cellular proliferation, [213]) and the TUNEL assay (marker of DNA damage) were used. Immunoreactivity for Ki-67 in tumour sections from the groups of animals under study (Pd_2Spm, cisplatin or vehicle) are shown in **Figure 4a.** The Ki-67 index of tumours was significantly decreased in animals treated with Pd_2Spm when compared to animals treated with the vehicle. Tumours from cisplatin-treated animals also showed a significant decrease in Ki-67 relative to the vehicle-treated mice (**Figure 34c**). Analysis of DNA damage showed a significant increase in TUNEL-positive cells in tumours obtained from animals treated with Pd_2Spm and cisplatin when compared to tumours from vehicle-treated animals (**Figure 34d**).

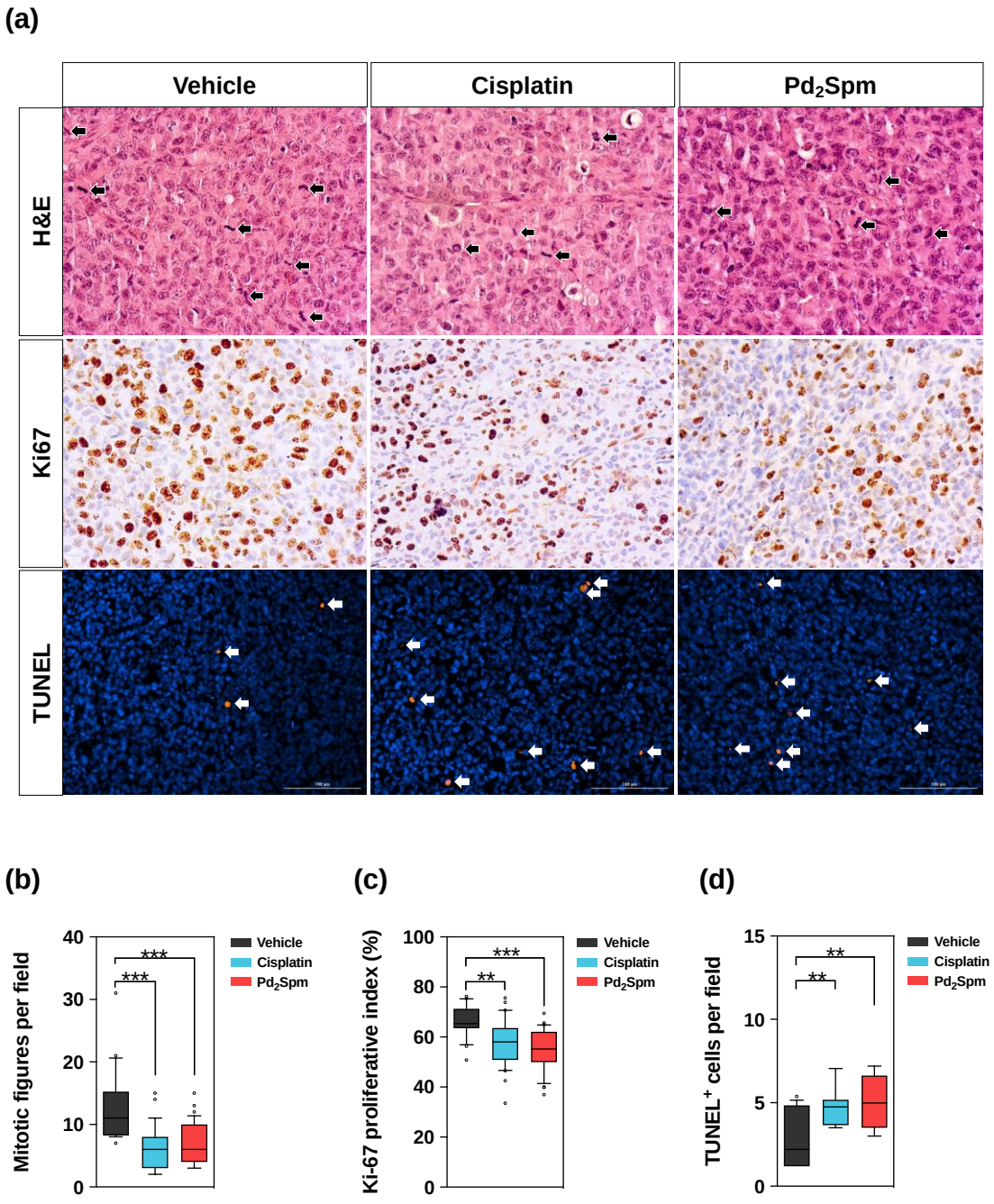

Figure 34. Representative photomicrographs of MDA-MB-231 breast cancer tumours.

(**a**) hematoxylin–eosin (H&E, black arrows show mitotic figures), Ki-67 nuclear staining and TUNEL assay staining (white arrows show TUNEL positive cells). (**b**) Quantitative analysis of mitotic figures. (**c**) Ki-67 proliferative index and (**d**) TUNEL-positive cells. **(b-d)** Data are shown as box plots with medians analysed with Kruskal–Wallis test followed by Dunn's multiple comparisons test. ** $p < 0.01$, *** $p < 0.001$. Five random fields per tumour with at least 600 cells/field were analysed. Pd_2Spm 5 mg/kg/day ($n = 7$), cisplatin 2 mg/kg/day ($n = 7$), vehicle ($n = 5$). **(a)** Scale bar = 100 µm.

Overall, these results evidenced that Pd_2Spm administration inhibited the growth of MDA-MB-231 xenografts *in vivo* by reducing tumour cell proliferation and inducing DNA damage and cell death. Our data also showed that 5-day treatment of tumour-bearing mice with 5 mg/kg/day of Pd_2Spm or 2 mg/kg/day of cisplatin results in comparable anticancer effects when (i) tumour volume reduction, (ii) tumour proliferative activity decrease (Ki-67 and mitotic count) and (iii) tumour DNA damage increase are compared in Pd_2Spm- versus cisplatin-treated animals. This may be explained in part by the similarity in the pharmacokinetics of Pd_2Spm and cisplatin [212], as well as by the similarity in the amounts of administered metals (1.91 mg/kg/day of Pd administered from 5 mg/kg/day of Pd_2Spm, and 1.3 mg/kg/day of Pt administered from 2 mg/kg/day of cisplatin).

IV.6.3 Tolerability and Systemic Toxicity

IV.6.3.1 Body Weight

As body weight can be considered a marker of general systemic toxicity, we performed a daily monitoring of the mice's weight in all groups. A five-day treatment administration induced notable changes in mice's body weight (**Figure 35**): during the initial three days of the treatment, a body weight loss was observed in all study groups, and this trend continued in cisplatin-treated animals also after the administration period. A progressive recovery of the body weight was observed in all groups, and at the end of the experiment, the body weight of all animals was higher compared to the starting value. The cisplatin group demonstrated a slower body weight recovery compared to Pd_2Spm- and vehicle-treated groups. There was no significant difference in body weight between groups at the end of the procedure.

In addition to body weight decrease, cisplatin-treated animals showed signs of general toxicity, such as decreased movement/activity, transient dehydration and diarrhoea. In turn, no such adverse effects were observed in animals treated with either Pd_2Spm or the vehicle.

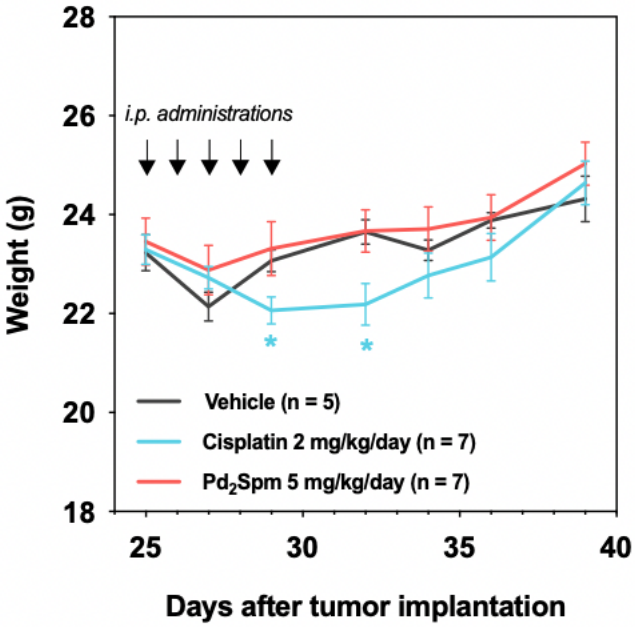

Figure 35. Impact of Pd_2Spm, cisplatin or vehicle treatment on the body weight of MDA-MB-231 breast tumour-bearing mice.

Body weight changes of tumour-bearing mice treated intraperitoneally with either Pd_2Spm (5 mg/kg/day), cisplatin (2 mg/kg/day) or vehicle (PBS + 0.5% DMSO) for 5 consecutive days. Data are expressed as mean weight (g) ± SEM. Two-way ANOVA followed by Tukey's multiple comparisons test was used to analyse weight change in groups over the time, $*p < 0.05$ cisplatin versus vehicle.

The treatment of animals with Pd_2Spm, cisplatin or vehicle did not impact the relative weight of the liver, heart, lungs, spleen or brain, with no significant differences being detected among the studied groups (**Table 17**). On the other hand, the relative weight of the kidneys in cisplatin-treated animals was lower compared to animals treated with the vehicle or Pd_2Spm. Histopathological evaluation showed a decreased perirenal adipose tissue in cisplatin-treated compared to vehicle-treated animals, which may further support a reduction in the relative weight of the kidneys in cisplatin-treated animal **Figure 36**. No other histopathological changes were observed during histological analysis of the kidneys (data not shown). Regarding the liver, histopathological analysis allowed us to conclude that cisplatin-treated animals exhibited a swollen, pale and finely vacuolated cytoplasm due to intracellular accumulation of glycogen **Figure 36**, as confirmed by periodic acid–Schiff

(PAS). This glycogen accumulation was not observed in the livers of vehicle- and Pd_2Spm-treated animals.

Table 17. Relative organ weight after treatment with either Pd_2Spm, cisplatin or vehicle.

Organ	Relative Organ Weight (%) [a]		
	Vehicle	**Cisplatin 2 mg/kg/day**	**Pd_2Spm 5 mg/kg/day**
	(*n* = 5)	**(*n* = 7)**	**(*n* = 7)**
Liver	6.08 ± 0.55	6.50 ± 0.34	6.14 ± 0.29
Heart	0.53 ± 0.06	0.53 ± 0.06	0.53 ± 0.06
Lungs	0.73 ± 0.11	0.77 ± 0.08	0.77 ± 0.08
Spleen	0.31 ± 0.10	0.33 ± 0.08	0.32 ± 0.11
Brain	1.85 ± 0.10	1.79 ± 0.14	1.79 ± 0.16
Kidneys	1.46 ± 0.05	1.29 ± 0.10 *	1.43 ± 0.10

[a] The relative organ weight (mean % ± SEM) was calculated as organ weight (g)/body weight (g) × 100%. Data analysed with one-way ANOVA followed by Dunnett's multiple comparisons *t*-test. * $p < 0.05$ cisplatin versus vehicle.

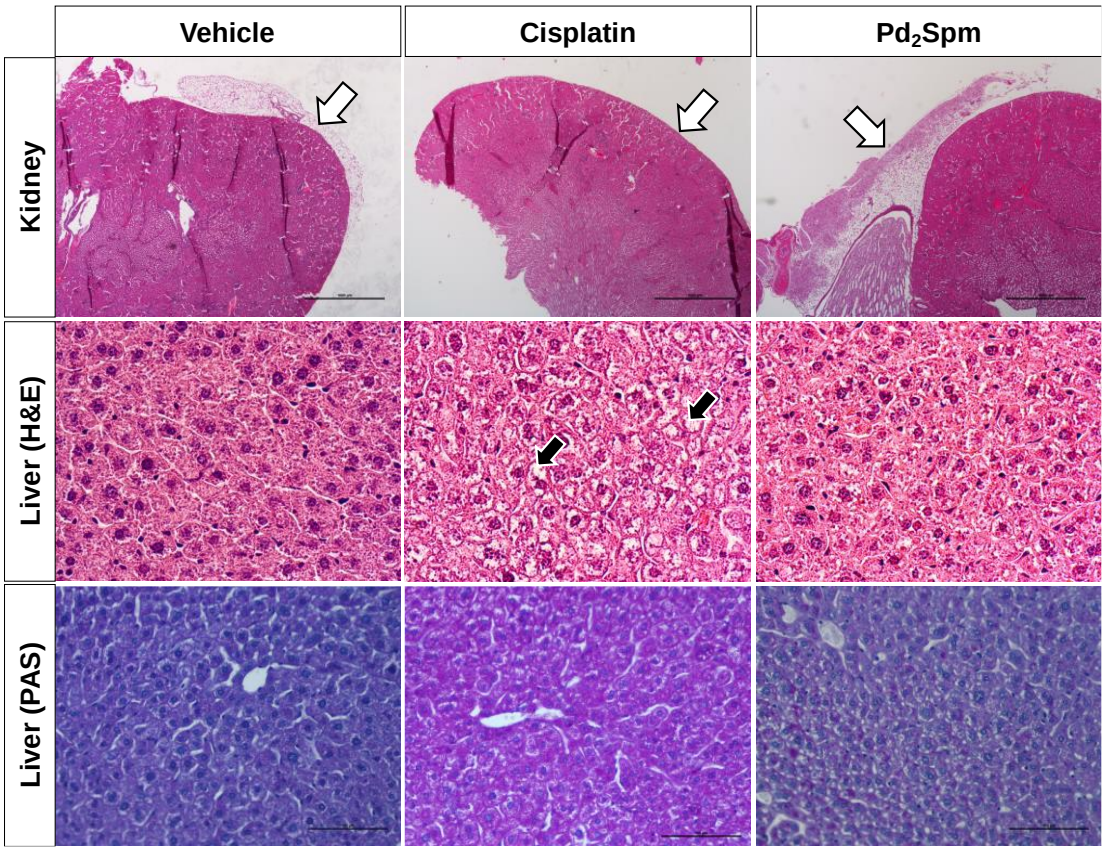

Figure 36. Representative microphotographs of kidney and liver from animals treated with Pd_2Spm, cisplatin or vehicle, showing absence of perirenal adipose tissues (white arrows) in cisplatin-treated animals.

Hepatocytes of cisplatin-treated animals showing marked cytoplasmic vacuolization and hepatocellular glycogen deposits (black arrows). Scale bar (kidney) = 1000 µm. Scale bar (liver) = 100 µm.

IV.6.3.2 Haematological and Biochemical Parameters

Haematological analysis of animals treated with Pd_2Spm revealed no significant deviations from the animals treated with the vehicle (**Figure 37a**). Cisplatin-treated animals, in turn, showed a decrease in red blood cells (RBC), haemoglobin (Hb) and haematocrit (Htc), accompanied by an increase in the mean corpuscular volume (MCV), as compared to vehicle-treated animals. Plasma biochemical analysis (urea, creatinine, glucose, AST, ALT, total proteins, triglycerides and total cholesterol) in Pd_2Spm-treated animals did not reveal changes relative to vehicle-treated animals (**Figure 37b**). For cisplatin treatment, a

decrease in total proteins and an increase in triglycerides were observed as compared to the vehicle-treated group.

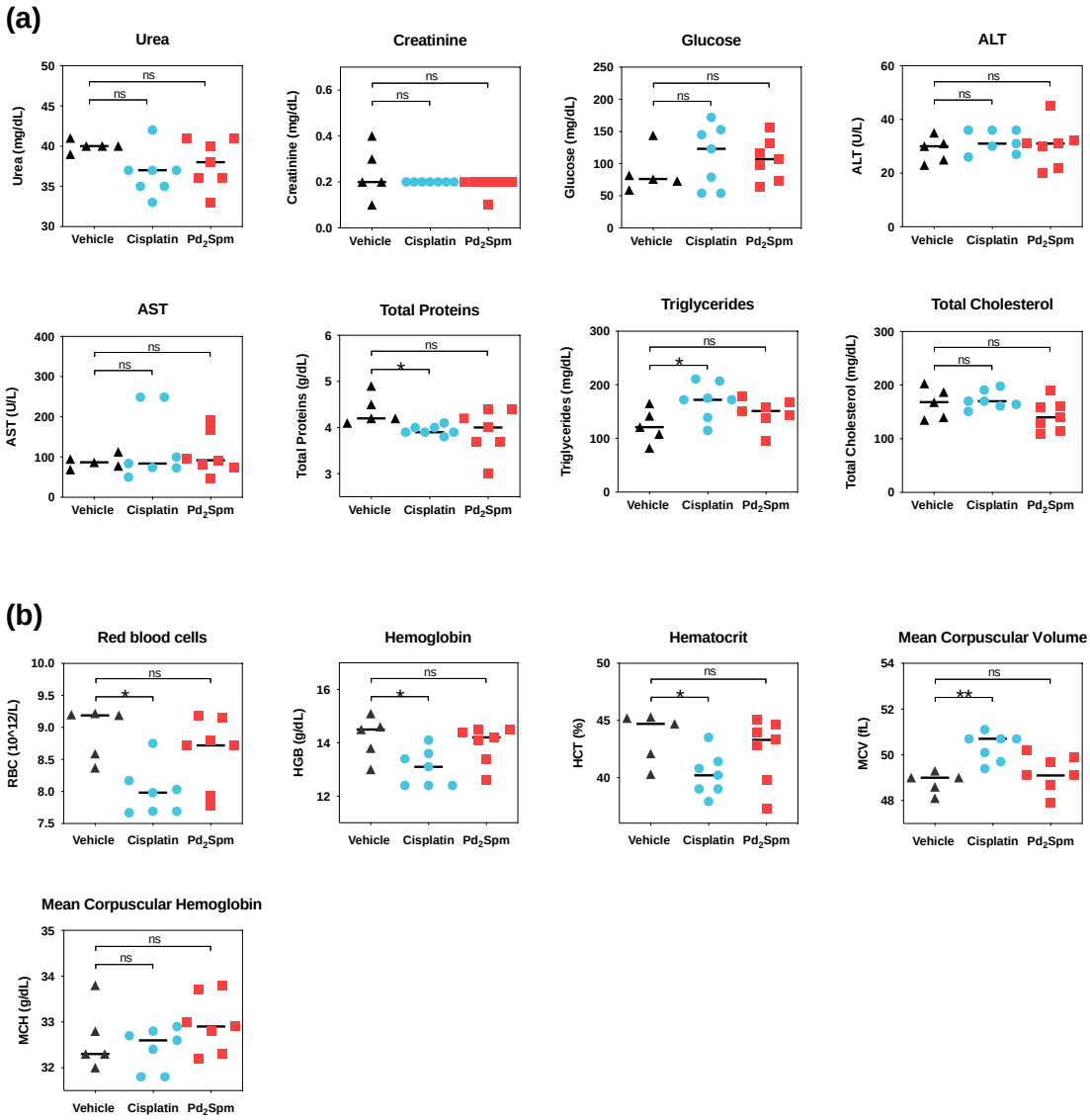

Figure 37. (a) Haematological and **(b)** biochemical analysis and of mice bearing MDA-MB-231 breast cancer tumours xenografts treated with either Pd_2Spm (5 mg/kg/day), cisplatin (2 mg/kg/day) or vehicle (PBS + 0.5% DMSO).

Values are shown as individual values with medians, analysed with Kruskal–Wallis test followed by Dunn's multiple comparisons test. * $p < 0.05$, ** $p < 0.01$, ns = not significant. Pd_2Spm ($n = 7$), cisplatin ($n = 5$), vehicle ($n = 5$).

Pd_2Spm administration did not result in significant variations regarding haematological and biochemical parameters when compared to cisplatin-treated animals that evidenced signs of macrocytic anaemia (decrease in red blood cells, haemoglobin and

haematocrit together with an increase in mean corpuscular volume). The cisplatin-induced changes in body weight, diarrhoea and haematotoxicity were previously described [214,215] and are generally considered as surrogates for the drug's systemic toxicity. Furthermore, these results support the reduced off-target effects and low toxicity elicited by Pd_2Spm treatment compared to cisplatin. Interestingly, besides a decrease in the total serum proteins and an increase in serum triacylglycerides, no other parameters related to renal or hepatic functions were altered in cisplatin-treated animals. In contrast, Pd_2Spm treatment did not trigger any of these changes.

IV.6.4 Final Remarks

This study constitutes the first proof-of-concept regarding the *in vivo* activity of Pd_2Spm as a potential candidate chemotherapeutic for TNBC treatment. The *in vivo* administration of Pd_2Spm in TNBC tumour-bearing mice resulted in tumour growth inhibition to a similar extent to that in animals treated with cisplatin. Furthermore, the systemic toxicity (haematotoxicity, weight loss, diarrhoea and biochemical alterations) observed in cisplatin-treated animals was not verified in Pd_2Spm-treated mice. Here we have provided encouraging evidence of the selective activity of Pd_2Spm towards TNBC with minimal effects to non-cancerous breast cells, both *in vitro* and *in vivo*. Therefore, Pd_2Spm may become a promising potential Pd(II) drug candidate for the treatment of TNBC.

CHAPTER V: GENERAL DISCUSSION

CHAPTER V – GENERAL DISCUSSION

The development of new chemotherapeutic agents for the treatment of TNBC is essential due to the limited effectivity and associated toxicity of current treatment options involving Pt-based compounds. The use of Pd-based compounds has emerged as a promising approach for the development of new treatments with improved properties compared to Pt-based drugs.

The main objective of the present thesis was to evaluate TNBC therapeutic potential of Pd_2Spm and/or Pd_3Spd_2 compared to cisplatin in four main areas (i) selectivity and anticancer potency (ii) ability to circumvent Pt resistance of TNBC cells, (iii) biodistribution and pharmacokinetics and (iv) mechanism of action.

Both Pd_2Spm and Pd_3Spd_2 showed similar *in vitro* activity in TNBC cells sensitive and resistant to Pt drugs. However, Pd_2Spm has shown superior selectivity towards cancer cells than Pd_3Sp_2, thus Pd_2Spm was a focus of further work. Low activity of Pd_2Spm in non-neoplastic MCF-12A cells suggested that this compound may present minimal off-target toxicity responsible for adverse events and contrasted with indiscriminatory effects of cisplatin that showed similar antiproliferative activity both in cancer and non-neoplastic cells. A successful suppression of TNBC tumour growth in mice treated with Pd_2Spm confirmed that this compound remains active *in vivo* and can yield comparable effects to cisplatin. In addition to reduction in tumour volume, treatment with Pd_2Spm also reduced the number of mitoses in the tumour; decreased in the proliferative index measured with immunohistochemical marker Ki67; and increased in TUNEL-positive cells (in the tumour), which are indicative of increased DNA damage to similar extent than cisplatin. Additionally, animals treated with Pd_2Spm did not show signs of systemic toxicity observed in cisplatin-treated animals (such as weight reduction if biochemical and haematological alterations that were), therefore superior tolerability profile of Pd_2Spm was also confirmed and corroborated previous *in vitro* data (i.e. low activity towards non-neoplastic cells). Anticancer effects in Pt-resistant MDA-MB-231/R cells have shown that Pd_2Spm surpasses activity of cisplatin and carboplatin in these cells and indicated that the mechanism of cross-resistance is not shared for Pt- versus Pd-based drugs under the study. Altogether, Pd_2Spm showed promising *in vitro* and *in vivo* anticancer activity, selectivity, and ability to overcome Pt-resistance.

To study pharmacokinetics and biodistribution of Pd_2Spm, we have verified the need for a validated and time-/cost-efficient method for Pd/Pt analysis in animal samples and biofluids. Thus, we have first developed and validated a single ICP-MS method for Pd/Pt analysis that allowed to process hundreds of multi-organ biologic samples simultaneously, with low reagent and sample consumption.

CHAPTER V – GENERAL DISCUSSION

Pd_2Spm showed superior pharmacokinetic properties compared to cisplatin, having 4.3-fold ($p < 0.001$) higher AUC and longer elimination half-life (35.5 h) of free (unbound) Pd in serum ultrafiltrate suggestive of higher availability and persistence of free Pd_2Spm than cisplatin in blood circulation. This was explained by lower affinity of Pd_2Spm to plasma proteins than cisplatin, since 1 h post-administration, only *ca.* 50% of Pd_2Spm was bound to plasma proteins compared to *ca.* 90% protein-bound cisplatin at the same time. Cisplatin forms irreversible bonds with plasma proteins, and only small fraction remains free to cross cell membranes and exert pharmacological effects. As a majority of Pd_2Spm is initially present in the plasma as a free/unbound drug, this may allow time to reach its targets in the tissues and exert pharmacological effects.

The highest accumulation of Pd in healthy mice was found in the kidney, followed by the liver, lungs, heart, and brain, with the latter being the least exposed organ. This biodistribution pattern in 5 major organs was also observed for cisplatin, however, significantly lower exposures to Pd (from Pd_2Spm) were detected in the liver, lungs, heart, and brain compared to Pt (from cisplatin). In kidney, even though higher Pd than Pt accumulation was found, our parallel work has shown that the metabolomic impact remains low compared to cisplatin that induced more profound deviations [210,211].

In comparing the *in vitro* potency of Pd_2Spm and cisplatin, the initial studies estimated approximately 8-fold lower potency of Pd_2Spm than cisplatin with antiproliferative activity in low micromolar range (<10 μM). However, pharmacokinetics and biodistribution studies in healthy mice have also shown lower relative accumulation of Pd_2Spm compared to cisplatin. Therefore, a 47% higher dose of Pd_2Spm (than cisplatin was used for *in vivo* efficacy study to avoid the necessity of more animals that would be needed for different concentration levels. This dose correction (1.91 mg/kg/day of Pd administered from 5 mg/kg/day of Pd_2Spm, and 1.3 mg/kg/day of Pt administered from 2 mg/kg/day of cisplatin) effectively compensated for the differences in drug potencies, and both Pd_2Spm and cisplatin yielded comparable anticancer effects in regard to tumour growth inhibition, DNA damage, and decrease in mitotic figures and Ki-67 staining. These results also demonstrated that differences in potencies observed *in vitro* are not direct surrogates for equally lower *in vivo* activity.

Pd_2Spm has shown ability to modulate angiogenesis and cell migration that are significant contributors to TNBC pathogenesis, particularly regarding its metastatic potential and aggressive biology. The development of agents able to suppress cancer cell proliferation, migration and angiogenesis are highly desired. In this study, Pd_2Spm: (i) inhibited the migration of MDA-MB-231 cells; (ii) inhibited angiogenesis in CAM; and (iii)

suppressed VEGF secretion by MDA-MB-231 cells with similar potency to cisplatin. These results are in line with previous reports that revealed that cisplatin's anti-migratory and antiangiogenic effects, although the underlying mechanism(s) are still largely unknown [216,217]. Regarding the effects of Pd(II) compounds, there is limited information in the literature describing their ability to suppress angiogenesis and cell migration. So far, studies with the mononuclear Pd(II) saccharinate complex of terpyridine [PdCl(terpy)](sac)·2H_2O have shown inhibition of the migration of endothelial cells (HUVEC) in the range of 12.5–50 µM and have also shown inhibition of angiogenesis in CAM assay at a concentration of 5 mg/mL [218]. In the current study, Pd_2Spm significantly inhibited angiogenesis at an 8 µM concentration (corresponding to 4.46 µg/mL of Pd_2Spm), impacting both early and late steps of angiogenesis and further supporting the previous reports [82]. Nevertheless, the mechanism behind this activity is still unexplored and requires further study.

This study has also provided the first clues that Pd_2Spm and cisplatin may not share identical mechanism of action. First, *in vitro* drug uptake studies have shown higher accumulation of cisplatin than Pd_2Spm in TNBC cells when same concentration of drugs were applied. This result was not unexpected, since Pd_2Spm has initially shown lower potency than cisplatin in TNBC cells. However, non-neoplastic cells accumulated higher amounts of Pd_2Spm than TNBC cells, while cisplatin´s quantity in non-neoplastic cells was close to the quantities observed in TNBC cells. These results contradict to general expectations that higher drug accumulation translates directly into higher effects. While cisplatin´s accumulation follows this theory both regarding to higher potency in TNBC compared to Pd_2Spm (more accumulated drug causing higher effects) as well as relatively to the indiscriminatory cisplatin´s effects in non-neoplastic cells owing to similar quantities being accumulated in both cell lines. These observations are also in line with obtained IC_{50} values since cisplatin has shown almost identical IC_{50} values in TNBC and non-neoplastic cells. On the other hand, higher accumulation of Pd_2Spm was observed in non-neoplastic cells compared to TNBC cells, and in theory this should indicate higher impact on these cells. However, antiproliferative herein obtained show at least 11.64-fold lower sensitive of non-neoplastic cells to Pd_2Spm than TNBC cells. Thus, higher accumulation of Pd_2Spm in non-neoplastic cells seems not to impact proliferation of non-neoplastic cells and suggest different intracellular processing of Pd_2Spm by non-neoplastic cells than cisplatin. Secondly, putative involvement of polyamine pathway has been observed when exogenous addition of putrescine decreased the effects of Pd_2Spm in TNBC cells. Since these effects were not observed for cisplatin, we theorize that different intracellular mechanisms are involved in processing of Pd_2Spm and cisplatin. Putative involvement of polyamine pathway in mechanism of action of Pd-polyamine complexes was also probed by others but no definite

conclusions were obtained so far [219]. Nevertheless, the results herein obtained suggested different intracellular behaviour and that Pd_2Spm may have a different spectrum of targets compared to cisplatin, which may explain its superior selectivity and ability to overcome Pt resistance. Since typical features of apoptosis and caspase-3 cleavage were not detected in cells treated with Pd_2Spm, further investigation has led to identification that autophagic activation may be involved in the mechanism of cell death triggered by Pd_2Spm. This finding contrasted with the effects elicited by cisplatin that triggered apoptosis and induced lower activation of autophagy. Additionally, the differential activation of NF-κB and ERK 1/2 pathways by Pd_2Spm and cisplatin provided further clues on Pd_2Spm's targets and indicated that these two metal-based compounds do not trigger the same transduction vias and, most probably, do not share the same molecular targets. Indeed, in TNBC, contrasting to cisplatin, Pd_2Spm does not seem to trigger NF-κB pathway but strongly interfere with ERK pathway promoting ERK1/2 phosphorylation, a process that is even more accentuated in Pt-resistant cells.

Given the limited information on *in vivo* effects of Pd-based compounds that is currently available, this thesis provided the first proof-of-concept of Pd_2Spm's efficacy to decrease tumour growth with minimal systemic toxicity. Overall, the study established strong therapeutic potential of Pd_2Spm as a novel chemotherapeutic for TNBC and laid foundations for further investigation and development of Pd compounds with biogenic polyamines for the treatment of TNBC and its Pt-resistant forms. The development of new treatments for TNBC is crucial, and our findings may contribute to the development of new therapies for the treatment of this aggressive form of breast cancer. Future studies may be focused on a further increase in therapeutic outcomes using different treatment schedules and/or higher Pd_2Spm concentrations.

CHAPTER VI: CONCLUSIONS AND FUTURE PERSPECTIVES

CHAPTER VI – CONCLUSION AND FUTURE PERSPECTIVES

The development of new effective cancer treatments with reduced toxicity and the ability to overcome resistance is crucial for improving outcomes of TNBC patients and surpassing the limitations of currently used Pt-based compounds. Under the scope of this thesis, experimental work was conducted with *in vitro*, *in ovo* and *in vivo* models to evaluate the therapeutic potential of two Pd-based compounds with polyamines Pd_2Spm and Pd_3Spd_2 as promising drug candidates for TNBC.

A successful in-house development of TNBC cell line with Pt-resistance (resistant to common Pt drugs such as cisplatin, carboplatin and oxaliplatin) allowed us to screen the *in vitro* antiproliferative activity of new Pd compounds in a total of three cell lines (Pt-sensitive TNBC, Pt-resistant TNBC, and non-neoplastic breast cells) and compare their effects to cisplatin, a reference Pt-drug in the clinic. The *in vitro* screening studies demonstrated that both Pd_2Spm and Pd_3Spd_2 showed similar antiproliferative effects in TNBC cells sensitive and resistant to Pt drugs in the low micromolar range. Cisplatin had inferior activity in Pt-resistant cells, whereas Pd-based compounds evidenced the ability to overcome resistance mechanisms that limit the effectiveness of Pt drugs in the clinics (namely cisplatin and carboplatin). Moreover, the *in vitro* studies pointed to superior selectivity of the dinuclear chelate Pd_2Spm than the trinuclear chelate Pd_3Spd_2, since Pd_2Spm presented lower toxicity to non-neoplastic breast cells than Pd_3Spd_2, which justifies the further focus of this work on Pd_2Spm.

To perform pharmacokinetic study of Pd_2Spm and compare it with that of cisplatin, an accurate, fast and cost-effective ICP-MS method was developed and validated. This method overcame the absence of a validated micro-methodology that enables simultaneous detection of Pd/Pt in high quantities of samples, which includes hundreds of animal tissues and biofluids. The pharmacokinetics of Pd_2Spm in mice was determined for the first time and showed similar kinetic behaviour compared to cisplatin, indicating that Pd_2Spm could be administered using similar intravenous scheduling regimens as cisplatin. Moreover, Pd_2Spm was able to inhibit tumour growth in TNBC-bearing mice with similar efficacy as cisplatin but without the general toxicity that was observed in mice treated with cisplatin (i.e. weight loss and haematotoxicity).

Finally, even though Pd_2Spm and cisplatin can produce similar reduction in cancer invasiveness and *in vivo* tumour growth, the two compounds seem not share same mechanism of action. Rather than apoptosis, Pd_2Spm seems to involve autophagy with ERK1/2 pathway activation in the mechanism of a cell death both in sensitive and resistant TNBC cells.

CHAPTER VI – CONCLUSIONS AND FUTURE PERSPECTIVES

The findings obtained in this work are significant because they constitute the very first evidence of *in vivo* anticancer activity of Pd_2Spm. These results may constitute the basis for further optimization of this compound to offer an effective and less toxic treatment option for patients with TNBC, and may also provide foundation for further investigation of Pd-based compounds with polyamines and development of new treatment options for resistant TNBC forms.

Despite the promising results, there are some limitations and areas for future research that should be considered. Firstly, more detailed studies focused on autophagic cell death could provide further understanding of Pd_2Spm *in vivo* and its impact on overcoming the Pt-resistance in TNBC. Secondly, the mechanisms of resistance that Pd_2Spm overcomes are not yet fully understood and further research will be needed to identify potential biomarkers of treatment response using proteomics and metabolomics studies. Moreover, current research has focused on preclinical studies and the validation of anticancer effects of Pd-polyamine chelates in humans is currently unknown.

In conclusion, the Pd-based compound Pd_2Spm has shown great promise in present preclinical studies as an alternative to cisplatin for the treatment of TNBC. The drug has demonstrated selectivity, efficacy, and reduced toxicity compared to cisplatin, and has the potential to overcome resistance mechanisms that limit the effectiveness of cisplatin. The results of this work provide evidence of therapeutic potential of Pd_2Spm and highlight the importance of continued efforts to develop novel metal-based compounds for TNBC.

REFERENCES

REFERENCES

1. Sung H, Ferlay J, Siegel RL, et al. Global Cancer Statistics 2020: GLOBOCAN Estimates of Incidence and Mortality Worldwide for 36 Cancers in 185 Countries. *CA: A Cancer Journal for Clinicians*. 2021;71(3):209-249. doi:10.3322/CAAC.21660

2. Torre L, Rebecca Siegel AJ. Global Cancer Facts & Figures 3rd Edition. *American Cancer Society*. 2015;(800):1-64. doi:10.1002/ijc.27711

3. Cancer - Our World in Data. Accessed March 12, 2023. https://ourworldindata.org/cancer#cancer-survival-rates

4. Dent R, Trudeau M, Pritchard KI, et al. Triple-negative breast cancer: clinical features and patterns of recurrence. *Clinical cancer research : an official journal of the American Association for Cancer Research*. 2007;13(15 Pt 1):4429-4434. doi:10.1158/1078-0432.CCR-06-3045

5. Cardoso F, Costa A, Norton L, et al. 1st International consensus guidelines for advanced breast cancer (ABC 1). *The Breast*. 2012;21(3):242-252. doi:10.1016/j.breast.2012.03.003

6. Zeichner SB, Terawaki H, Gogineni K. A Review of Systemic Treatment in Metastatic Triple-Negative Breast Cancer. *Breast cancer : basic and clinical research*. 2016;10:25-36. doi:10.4137/BCBCR.S32783

7. Lobbezoo DJA, van Kampen RJW, Voogd AC, et al. Prognosis of metastatic breast cancer: are there differences between patients with de novo and recurrent metastatic breast cancer? *British journal of cancer*. 2015;112(9):1445-1451. doi:10.1038/bjc.2015.127

8. Sanguinetti A, Polistena A, Lucchini R, et al. Male breast cancer, clinical presentation, diagnosis and treatment: Twenty years of experience in our Breast Unit. *International journal of surgery case reports*. 2016;20S(Suppl):8-11. doi:10.1016/j.ijscr.2016.02.004

9. Mills D, Gomberawalla A, Gordon EJ, et al. Examination of Duct Physiology in the Human Mammary Gland. *PloS one*. 2016;11(4):e0150653. doi:10.1371/journal.pone.0150653

10. PDQ Adult Treatment Editorial Board. Breast Cancer Treatment (PDQ®): Patient Version. In: *PDQ Cancer Information Summaries*. National Cancer Institute (US); 2002. Accessed May 17, 2023. http://www.ncbi.nlm.nih.gov/books/NBK65969/

11. Tiede B, Kang Y. From milk to malignancy: the role of mammary stem cells in development, pregnancy and breast cancer. *Cell research*. 2011;21(2):245-257. doi:10.1038/cr.2011.11

12. Visvader JE, Stingl J. Mammary stem cells and the differentiation hierarchy: current status and perspectives. *Genes & development*. 2014;28(11):1143-1158. doi:10.1101/gad.242511.114

13. Visvader JE. Keeping abreast of the mammary epithelial hierarchy and breast tumorigenesis. *Genes and Development*. 2009;23(22):2563-2577. doi:10.1101/gad.1849509

14. Neri A, Marrelli D, Megha T, et al. Clinical significance of multifocal and multicentric breast cancers and choice of surgical treatment: a retrospective study on a series of 1158 cases. *BMC Surgery*. 2015;15(1):1. doi:10.1186/1471-2482-15-1

REFERENCES

15. Guiu S, Wolfer A, Jacot W, et al. Invasive lobular breast cancer and its variants: How special are they for systemic therapy decisions? *Critical Reviews in Oncology/Hematology*. 2014;92(3):235-257. doi:10.1016/j.critrevonc.2014.07.003

16. Sinn HP, Kreipe H. A Brief Overview of the WHO Classification of Breast Tumors, 4th Edition, Focusing on Issues and Updates from the 3rd Edition. *Breast care (Basel, Switzerland)*. 2013;8(2):149-154. doi:10.1159/000350774

17. Zardavas D, Irrthum A, Swanton C, Piccart M. Clinical management of breast cancer heterogeneity. *Nature Reviews Clinical Oncology*. 2015;12(7):381-394. doi:10.1038/nrclinonc.2015.73

18. Amin MB, Edge SB, American Joint Committee on Cancer. *AJCC Cancer Staging Manual*.

19. Maajani K, Jalali A, Alipour S, Khodadost M, Tohidinik HR, Yazdani K. The Global and Regional Survival Rate of Women With Breast Cancer: A Systematic Review and Meta-analysis. *Clin Breast Cancer*. 2019;19(3):165-177. doi:10.1016/j.clbc.2019.01.006

20. Rakha EA, Reis-Filho JS, Baehner F, et al. Breast cancer prognostic classification in the molecular era: the role of histological grade. *Breast cancer research : BCR*. 2010;12(4):207. doi:10.1186/bcr2607

21. Elston CW, Ellis IO. Pathological prognostic factors in breast cancer. I. The value of histological grade in breast cancer: experience from a large study with long-term follow-up. *Histopathology*. 1991;19(5):403-410.

22. Tao ZQ, Shi A, Lu C, Song T, Zhang Z, Zhao J. Breast Cancer: Epidemiology and Etiology. *Cell Biochemistry and Biophysics*. 2015;72(2):333-338. doi:10.1007/s12013-014-0459-6

23. Dai X, Li T, Bai Z, et al. Breast cancer intrinsic subtype classification, clinical use and future trends. *American Journal of Cancer Research*. 2015;5(10):2929-2943.

24. Guiu S, Michiels S, André F, et al. Molecular subclasses of breast cancer: How do we define them? The IMPAKT 2012 working group statement. *Annals of Oncology*. 2012;23(12):2997-3006. doi:10.1093/annonc/mds586

25. Hon JDC, Singh B, Sahin A, et al. Breast cancer molecular subtypes: From TNBC to QNBC. *American Journal of Cancer Research*. 2016;6(9):1864-1872. doi:2156-6976/ajcr0025739

26. Perou CM, Sùrlie T, Eisen MB, et al. Molecular portraits of human breast tumours. *Nature*. 2000;533(May):747-752. doi:10.1038/35021093

27. Perou CM. Molecular stratification of triple-negative breast cancers. *The oncologist*. Published online 2010:61-70. doi:10.1634/theoncologist.2011-S1-61

28. Prat A, Perou CM. Deconstructing the molecular portraits of breast cancer. *Molecular Oncology*. 2011;5(1):5-23. doi:10.1016/j.molonc.2010.11.003

29. Gnant M, Harbeck N, Thomssen C. St. Gallen 2011: Summary of the consensus discussion. *Breast Care*. 2011;6(2):136-141. doi:10.1159/000328054

30. Sabatier R, Finetti P, Guille A, et al. Claudin-low breast cancers: clinical, pathological, molecular and prognostic characterization. *Molecular cancer*. 2014;13:228. doi:10.1186/1476-4598-13-228

31. Diessner J, Wischnewsky M, Blettner M, et al. Do Patients with Luminal A Breast Cancer Profit from Adjuvant Systemic Therapy? A Retrospective Multicenter Study. *PloS one*. 2016;11(12):e0168730. doi:10.1371/journal.pone.0168730

32. Prat A, Pineda E, Adamo B, et al. Clinical implications of the intrinsic molecular subtypes of breast cancer. *Breast*. 2015;24:S26-S35. doi:10.1016/j.breast.2015.07.008

33. Parker JS, Mullins M, Cheang MCU, et al. Supervised risk predictor of breast cancer based on intrinsic subtypes. *Journal of clinical oncology : official journal of the American Society of Clinical Oncology*. 2009;27(8):1160-1167. doi:10.1200/JCO.2008.18.1370

34. Prat A, Adamo B, Cheang MCU, Anders CK, Carey LA, Perou CM. Molecular Characterization of Basal-Like and Non-Basal-Like Triple-Negative Breast Cancer. *The Oncologist*. 2013;18(2):123-133. doi:10.1634/theoncologist.2012-0397

35. Gown AM, Goldstein LC, Barry TS, et al. High concordance between immunohistochemistry and fluorescence in situ hybridization testing for HER2 status in breast cancer requires a normalized IHC scoring system. *Modern Pathology*. 2008;21(10):1271-1277. doi:10.1038/modpathol.2008.83

36. Kulkarni A, Kelkar DA, Parikh N, Shashidhara LS, Koppiker CB, Kulkarni M. Meta-Analysis of Prevalence of Triple-Negative Breast Cancer and Its Clinical Features at Incidence in Indian Patients With Breast Cancer. *JCO Glob Oncol*. 2020;6:GO.20.00054. doi:10.1200/GO.20.00054

37. Haffty BG, Yang Q, Reiss M, et al. Locoregional relapse and distant metastasis in conservatively managed triple negative early-stage breast cancer. *Journal of clinical oncology : official journal of the American Society of Clinical Oncology*. 2006;24(36):5652-5657. doi:10.1200/JCO.2006.06.5664

38. Oualla K, El-Zawahry HM, Arun B, et al. Novel therapeutic strategies in the treatment of triple-negative breast cancer. *Therapeutic Advances in Medical Oncology*. 2017;9(7):493-511. doi:10.1177/1758834017711380

39. Hudis CA, Gianni L. Triple-negative breast cancer: an unmet medical need. *The oncologist*. Published online 2011:1-11. doi:10.1634/theoncologist.2011-S1-01

40. Zagami P, Carey LA. Triple negative breast cancer: Pitfalls and progress. *npj Breast Cancer*. 2022;8(1):1-10. doi:10.1038/s41523-022-00468-0

41. Lehmann BD, Bauer JA, Chen X, et al. Identification of human triple-negative breast cancer subtypes and preclinical models for selection of targeted therapies. *The Journal of Clinical Investigation*. 2011;121(7):2750. doi:10.1172/JCI45014DS1

42. Prat A, Parker JS, Karginova O, et al. Phenotypic and molecular characterization of the claudin-low intrinsic subtype of breast cancer. *Breast cancer research : BCR*. 2010;12(5):R68. doi:10.1186/bcr2635

REFERENCES

43. Khosravi-Shahi P, Cabezón-Gutiérrez L, Custodio-Cabello S. Metastatic triple negative breast cancer: Optimizing treatment options, new and emerging targeted therapies. *Asia-Pacific Journal of Clinical Oncology*. 2018;14(1):32-39. doi:10.1111/ajco.12748

44. Kuchenbaecker KB, Hopper JL, Barnes DR, et al. Risks of Breast, Ovarian, and Contralateral Breast Cancer for BRCA1 and BRCA2 Mutation Carriers. *JAMA*. 2017;317(23):2402. doi:10.1001/jama.2017.7112

45. Minami CA, Chung DU, Chang HR. Management options in triple-negative breast cancer. *Breast Cancer: Basic and Clinical Research*. 2011;5(1):175-199. doi:10.4137/BCBCR.S6562

46. Gupta GK, Collier AL, Lee D, et al. Perspectives on Triple-Negative Breast Cancer: Current Treatment Strategies, Unmet Needs, and Potential Targets for Future Therapies. *Cancers*. 2020;12(9):2392. doi:10.3390/cancers12092392

47. Minotti G, Menna P, Salvatorelli E, Cairo G, Gianni L. Anthracyclines: molecular advances and pharmacologic developments in antitumor activity and cardiotoxicity. *Pharmacological reviews*. 2004;56(2):185-229. doi:10.1124/pr.56.2.6

48. Abal M, Andreu JM, Barasoain I. Taxanes: microtubule and centrosome targets, and cell cycle dependent mechanisms of action. *Current cancer drug targets*. 2003;3(3):193-203. doi:10.2174/1568009033481967

49. Liedtke C, Mazouni C, Hess KR, et al. Response to Neoadjuvant Therapy and Long-Term Survival in Patients With Triple-Negative Breast Cancer. *Journal of Clinical Oncology*. 2008;26(8):1275-1281. doi:10.1200/JCO.2007.14.4147

50. Omarini C, Guaitoli G, Pipitone S, et al. Neoadjuvant treatments in triple-negative breast cancer patients: where we are now and where we are going. *Cancer management and research*. 2018;10:91-103. doi:10.2147/CMAR.S146658

51. von Minckwitz G, Schneeweiss A, Loibl S, et al. Neoadjuvant carboplatin in patients with triple-negative and HER2-positive early breast cancer (GeparSixto; GBG 66): a randomised phase 2 trial. *The Lancet Oncology*. 2014;15(7):747-756. doi:10.1016/S1470-2045(14)70160-3

52. Joensuu H, Gligorov J. Adjuvant treatments for triple-negative breast cancers. *Annals of Oncology*. 2012;23(suppl 6):vi40-vi45. doi:10.1093/annonc/mds194

53. Rosenberg B, Van Camp L, Krigas T. Inhibition of cell division in Escherichia coli by electrolysis products from a platinum electrode. *Nature*. 1965;205(4972):698-699. doi:10.1038/205698a0

54. Wheate NJ, Walker S, Craig GE, et al. The status of platinum anticancer drugs in the clinic and in clinical trials. *Dalton Transactions*. 2010;39(35):8113. doi:10.1039/c0dt00292e

55. Lin C, Cui J, Peng Z, et al. Efficacy of platinum-based and non-platinum-based drugs on triple-negative breast cancer: meta-analysis. *European Journal of Medical Research*. 2022;27. doi:10.1186/s40001-022-00839-0

56. Lu F, Hou Y, Chen Z, et al. Efficacy and Safety of Platinum-Based Chemotherapy as First-Line Therapy for Metastatic Triple-Negative Breast Cancer: A Meta-Analysis of

Randomized Controlled Trials. *Technology in Cancer Research & Treatment*. 2021;20. doi:10.1177/15330338211016369

57. Dasari S, Tchounwou PB. Cisplatin in cancer therapy: molecular mechanisms of action. *European journal of pharmacology*. 2014;740:364-378. doi:10.1016/j.ejphar.2014.07.025

58. Siddik ZH. Cisplatin: mode of cytotoxic action and molecular basis of resistance. *Oncogene*. 2003;22:7265-7279. doi:10.1038/sj.onc.1206933

59. Marques MPM. Platinum and Palladium Polyamine Complexes as Anticancer Agents: The Structural Factor. *ISRN Spectroscopy*. 2013;2013(Ii):1-29. doi:10.1155/2013/287353

60. Saif MW, Reardon J. Management of oxaliplatin-induced peripheral neuropathy. *Therapeutics and Clinical Risk Management*. 2005;1(4):249.

61. Stordal B, Pavlakis N, Davey R. Oxaliplatin for the treatment of cisplatin-resistant cancer: a systematic review. *Cancer Treat Rev*. 2007;33(4):347-357. doi:10.1016/j.ctrv.2007.01.009

62. Tomao F, Papa A, Zaccarelli E, et al. Triple-negative breast cancer: New perspectives for targeted therapies. *OncoTargets and Therapy*. 2015;8:177-193. doi:10.2147/OTT.S67673

63. Carey LA, Loirat D, Punie K, et al. Sacituzumab govitecan as second-line treatment for metastatic triple-negative breast cancer-phase 3 ASCENT study subanalysis. *NPJ Breast Cancer*. 2022;8(1):72. doi:10.1038/s41523-022-00439-5

64. Schlam I, Tolaney SM, Tarantino P. The efficacy of trastuzumab-deruxtecan for the treatment of patients with advanced pretreated HER2-low breast cancer. *Expert Rev Anticancer Ther*. Published online 2023. doi:10.1080/14737140.2023.2171993

65. Rizzo A, Cusmai A, Acquafredda S, Rinaldi L, Palmiotti G. Ladiratuzumab vedotin for metastatic triple negative cancer: preliminary results, key challenges, and clinical potential. *Expert Opinion on Investigational Drugs*. 2022;31(6):495-498. doi:10.1080/13543784.2022.2042252

66. Chen YF, Xu Y ying, Shao ZM, Yu KD. Resistance to antibody-drug conjugates in breast cancer: mechanisms and solutions. *Cancer Communications*. 2023;43(3):297-337. doi:10.1002/cac2.12387

67. Abdou Y, Goudarzi A, Yu JX, Upadhaya S, Vincent B, Carey LA. Immunotherapy in triple negative breast cancer: beyond checkpoint inhibitors. *npj Breast Cancer*. 2022;8(1):1-10. doi:10.1038/s41523-022-00486-y

68. Synnott NC, Murray A, McGowan PM, et al. Mutant p53: a novel target for the treatment of patients with triple-negative breast cancer? *International Journal of Cancer*. 2017;140(1):234-246. doi:10.1002/ijc.30425

69. Synnott NC, Bauer MR, Madden S, et al. Mutant p53 as a therapeutic target for the treatment of triple-negative breast cancer: Preclinical investigation with the anti-p53 drug, PK11007. *Cancer Letters*. 2018;414:99-106. doi:10.1016/J.CANLET.2017.09.053

REFERENCES

70. Shu S, Lin CY, He HH, et al. Response and resistance to BET bromodomain inhibitors in triple-negative breast cancer. *Nature*. 2016;529(7586):413-417. doi:10.1038/nature16508

71. Ocaña A, Nieto-Jiménez C, Pandiella A. BET inhibitors as novel therapeutic agents in breast cancer. *Oncotarget*. 2017;8(41):71285-71291. doi:10.18632/oncotarget.19744

72. Miranda M, Rozali E, Khanna KK, Al-Ejeh F. MEK5-ERK5 pathway associates with poor survival of breast cancer patients after systemic treatments. *Oncoscience*. 2015;2(2):99-101. doi:10.18632/oncoscience.135

73. Ortiz-Ruiz MJ, Álvarez-Fernández S, Parrott T, et al. Therapeutic potential of ERK5 targeting in triple negative breast cancer. *Oncotarget*. 2014;5(22):11308-11318. doi:10.18632/oncotarget.2324

74. Bukowski K, Kciuk M, Kontek R. Mechanisms of Multidrug Resistance in Cancer Chemotherapy. *International Journal of Molecular Sciences 2020, Vol 21, Page 3233*. 2020;21(9):3233. doi:10.3390/IJMS21093233

75. Vasan N, Baselga J, Hyman DM. A view on drug resistance in cancer. *Nature*. 2019;575(7782):299-309. doi:10.1038/s41586-019-1730-1

76. Housman G, Byler S, Heerboth S, et al. Drug Resistance in Cancer: An Overview. *Cancers 2014, Vol 6, Pages 1769-1792*. 2014;6(3):1769-1792. doi:10.3390/CANCERS6031769

77. Haider T, Pandey V, Banjare N, Gupta PN, Soni V. Drug resistance in cancer: mechanisms and tackling strategies. *Pharmacological Reports 2020 72:5*. 2020;72(5):1125-1151. doi:10.1007/S43440-020-00138-7

78. Marques MPM, Gianolio D, Cibin G, et al. A molecular view of cisplatin's mode of action: interplay with DNA bases and acquired resistance. *Phys Chem Chem Phys*. 2015;17(7):5155-5171. doi:10.1039/C4CP05183A

79. Acosta-Casique A, Montes-Alvarado JB, Barragán M, et al. ERK activation modulates invasiveness and Reactive Oxygen Species (ROS) production in triple negative breast cancer cell lines. *Cellular Signalling*. 2023;101:110487. doi:10.1016/J.CELLSIG.2022.110487

80. Godwin P, Baird AM, Heavey S, Barr MP, O'Byrne KJ, Gately K. Targeting nuclear factor-kappa B to overcome resistance to chemotherapy. *Frontiers in Oncology*. 2013;3 MAY:120. doi:10.3389/FONC.2013.00120/BIBTEX

81. Ma J, Dong C, Cao YZ, Ma BL. Dual Target of EGFR and mTOR Suppresses Triple-Negative Breast Cancer Cell Growth by Regulating the Phosphorylation of mTOR Downstream Proteins. *Breast Cancer: Targets and Therapy*. 2023;15:11-24. doi:10.2147/BCTT.S390017

82. Batista de Carvalho ALM, Medeiros PSC, Costa FM, et al. Anti-Invasive and Anti-Proliferative Synergism between Docetaxel and a Polynuclear Pd-Spermine Agent. Ahmad A, ed. *PLOS ONE*. 2016;11(11):e0167218. doi:10.1371/journal.pone.0167218

83. Braga SS, Marques J, Fernandes JA, et al. Supramolecular adducts of native and permethylated β-cyclodextrins with (2,2′-dipyridylamine)chlorido(1,4,7-

trithiacyclononane)ruthenium(II) chloride: solid-state and biological activity studies. *Chemical Papers*. 2017;71(7):1235-1248. doi:10.1007/s11696-016-0117-0

84. Marques J, Fernandes JA, Almeida Paz FA, Marques MPM, Braga SS. Isolation, crystal structure, and cytotoxicity on osteosarcoma of a ruthenium(III) complex with coordinated acetonitrile. *Journal of Coordination Chemistry*. 2012;65(14):2489-2499. doi:10.1080/00958972.2012.696624

85. Braga SS, Mokal V, Paz FAA, et al. Synthesis, Characterisation and Antiproliferative Studies of Allyl(dicarbonyl)(cyclopentadienyl)molybdenum Complexes and Cyclodextrin Inclusion Compounds. *European Journal of Inorganic Chemistry*. 2014;(29):5034-5045. doi:10.1002/ejic.201402540

86. van Rijt SH, Sadler PJ. Current applications and future potential for bioinorganic chemistry in the development of anticancer drugs. *Drug discovery today*. 2009;14(23-24):1089-1097. doi:10.1016/j.drudis.2009.09.003

87. Zhang P, Sadler PJ. Redox-Active Metal Complexes for Anticancer Therapy. *European Journal of Inorganic Chemistry*. 2017;(12):1541-1548. doi:10.1002/ejic.201600908

88. Frezza M, Hindo S, Chen D, et al. Novel metals and metal complexes as platforms for cancer therapy. *Current pharmaceutical design*. 2010;16(16):1813-1825. doi:10.2174/138161210791209009

89. Alam MN, Huq F. Comprehensive review on tumour active palladium compounds and structure-activity relationships. *Coordination Chemistry Reviews*. 2016;316:36-67. doi:10.1016/j.ccr.2016.02.001

90. Tookad | European Medicines Agency. Accessed March 5, 2023. https://www.ema.europa.eu/en/medicines/human/EPAR/tookad

91. Pooyan M, Shariatinia Z, Mohammadpanah F, et al. Spectral studies, crystal structures, DNA binding, and anticancer potentials of Pd(II) complexes with iminophosphine ligands: Experimental and computational methods. *Inorganica Chimica Acta*. 2023;547:121368. doi:10.1016/j.ica.2022.121368

92. Luo M, Zhang JC, Yin H, et al. Palladium (II), platinum (II) and silver (I) complexes with oxazolines: Their synthesis, characterization, DFT calculation, molecular docking and antitumour effects. *Journal of Inorganic Biochemistry*. 2023;239:112048. doi:10.1016/j.jinorgbio.2022.112048

93. Kordestani N, Rudbari HA, Correia I, et al. Heteroleptic enantiopure Pd(II)-complexes derived from halogen-substituted Schiff bases and 2-picolylamine: synthesis, experimental and computational characterization and investigation of the influence of chirality and halogen atoms on the anticancer activity. *New Journal of Chemistry*. 2021;45(20):9163-9180. doi:10.1039/D1NJ01491A

94. Miklášová N, Herich P, Dávila-Becerril JC, et al. Evaluation of Antiproliferative Palladium(II) Complexes of Synthetic Bisdemethoxycurcumin towards In Vitro Cytotoxicity and Molecular Docking on DNA Sequence. *Molecules*. 2021;26(14):4369. doi:10.3390/molecules26144369

95. A van N, A B, S K, et al. DNA-binding affinity and molecular docking studies of the PEGylated binuclear palladacycle, BTC2, an efficient metallodrug against triple-

negative breast cancer. *Journal of inorganic biochemistry*. 2023;243. doi:10.1016/j.jinorgbio.2023.112191

96. Kazimir A, Schwarze B, Lönnecke P, et al. Metallodrugs against Breast Cancer: Combining the Tamoxifen Vector with Platinum(II) and Palladium(II) Complexes. *Pharmaceutics*. 2023;15(2):682. doi:10.3390/pharmaceutics15020682

97. Haribabu J, Srividya S, Mahendiran D, et al. Synthesis of Palladium(II) Complexes via Michael Addition: Antiproliferative Effects through ROS-Mediated Mitochondrial Apoptosis and Docking with SARS-CoV-2. *Inorganic Chemistry*. 2020;59(23):17109-17122. doi:10.1021/acs.inorgchem.0c02373

98. Fabra D, Matesanz AI, Herrero JM, et al. Two Different Thiosemicarbazone Tauto-Conformers Coordinate to Palladium (II). Stability and Biological Studies of the Final Complexes. *European Journal of Inorganic Chemistry*. 2021;2021(11):1041-1049. doi:10.1002/ejic.202001066

99. Alqatati A, S. Hamad Elgazwy AS, Aliwaini S. Newly Synthesized Palladium (II) Complex ASH10 Induces Apoptosis and Autophagy in Breast Cancer Cells. *International Journal of Cancer Research*. 2020;16(2):40-47. doi:10.3923/ijcr.2020.40.47

100. Matilla A, Tercero JM, Niclós-Gutiérrez J, et al. cis-Dichloro-palladium(II) complexes with diaminosuccinic acid and its diethyl ester: Synthesis, molecular structure, and preliminary DNA-binding and antitumor studies. *Journal of Inorganic Biochemistry*. 1994;55(4):235-247. doi:10.1016/0162-0134(94)85008-9

101. Stojković DL, Jevtić VV, Radić GP, et al. Stereospecific ligands and their complexes. XXII. Synthesis and antitumor activity of palladium(II) complexes with some esters of (S,S)-ethylenediamine-N,N′-di-(2,2′-di(4-hydroxy-benzyl))-acetic acid. *Journal of Inorganic Biochemistry*. 2015;143:111-116. doi:10.1016/j.jinorgbio.2014.12.001

102. Vujic J, Kaluderovic G, Stanojkovic T, Antic J, Trifunovic S. In Vitro Antitumoral Activity of Palladium(II) and Platinum(II) Complexes with O,O'-Dialkyl Esters of Ethylene-bis(S)-Leucine. *Letters in Drug Design & Discovery*. 2014;11(4):387-394. doi:10.2174/15701808113106660092

103. Navarro-Ranninger C, Zamora F, López-Solera I, et al. Palladium(II) salt and complexes of spermidine with a six-member chelate ring. Synthesis, characterization, and initial DNA-binding and antitumor studies. *Journal of Inorganic Biochemistry*. 1992;46(4):267-279. doi:10.1016/0162-0134(92)80037-V

104. Navarro-Ranninger C, Zamora F, Masaguer JR, Pérez JM, González VM, Alonso C. Palladium(II) compounds of putrescine and spermine. Synthesis, characterization, and DNA-binding and antitumor properties. *Journal of Inorganic Biochemistry*. 1993;52(1):37-49. doi:10.1016/0162-0134(93)85621-E

105. Fiuza SM, Holy J, Batista de Carvalho LAE, Marques MPM. Biologic Activity of a Dinuclear Pd(II)-Spermine Complex Toward Human Breast Cancer. *Chemical Biology & Drug Design*. 2011;77(6):477-488. doi:10.1111/j.1747-0285.2011.01081.x

106. Silva TM, Fiuza SM, Marques MPM, Persson L, Oredsson S. Increased breast cancer cell toxicity by palladination of the polyamine analogue N1,N11-bis(ethyl)norspermine. *Amino Acids*. 2014;46(2):339-352. doi:10.1007/s00726-013-1621-y

107. Silva TM, Andersson S, Sukumaran SK, Marques MP, Persson L, Oredsson S. Norspermidine and Novel Pd(II) and Pt(II) Polynuclear Complexes of Norspermidine as Potential Antineoplastic Agents Against Breast Cancer. Katz E, ed. *PLoS ONE*. 2013;8(2):e55651. doi:10.1371/journal.pone.0055651

108. Navarro-Ranninger C, López-Solera I, González VM, et al. Cyclometalated Complexes of Platinum and Palladium with N-(4-Chlorophenyl)-α-benzoylbenzylideneamine. In Vitro Cytostatic Activity, DNA Modification, and Interstrand Cross-Link Studies. *Inorg Chem*. 1996;35(11):5181-5187. doi:10.1021/ic960050y

109. Karami K, Kharat MH, Sadeghi-Aliabadi H, Lipkowski J, Mirian M. Dinuclear bridged biphosphinic and mononuclear cyclopalladated complexes of benzylamines: Synthesis, structural characterization and antitumor activity. *Polyhedron*. 2013;50(1):187-192. doi:10.1016/j.poly.2012.11.002

110. Albert J, García S, Granell J, et al. Cyclopalladated benzophenone imines: Synthesis, cytotoxicity against human breast adenocarcinoma cell lines and DNA interaction. *Journal of Organometallic Chemistry*. 2013;724:289-296. doi:10.1016/j.jorganchem.2012.11.034

111. Albert J, Bosque R, Crespo M, et al. Cyclopalladated primary amines: A preliminary study of antiproliferative activity through apoptosis induction. *European Journal of Medicinal Chemistry*. 2014;84:530-536. doi:10.1016/j.ejmech.2014.07.046

112. Albert J, Granell J, Qadir R, et al. Cyclopalladated benzophenone imines: Synthesis, antitumor activity, cell accumulation, dna interaction, and cathepsin b inhibition. *Organometallics*. 2014;33(24):7284-7292. doi:10.1021/om501060f

113. Aliwaini S, Peres J, Kröger WL, et al. The palladacycle, AJ-5, exhibits anti-tumour and anti-cancer stem cell activity in breast cancer cells. *Cancer Letters*. 2015;357(1):206-218. doi:10.1016/j.canlet.2014.11.027

114. Akdi K, Vilaplana RA, Kamah S, Navarro JAR, Salas JM, González-Vílchez F. Study of the biological effects and DNA damage exerted by a new dipalladium-Hmtpo complex on human cancer cells. *Journal of Inorganic Biochemistry*. 2002;90(1-2):51-60. doi:10.1016/S0162-0134(02)00370-7

115. Ari F, Cevatemre B, Armutak EII, Aztopal N, Yilmaz VT, Ulukaya E. Apoptosis-inducing effect of a palladium(II) saccharinate complex of terpyridine on human breast cancer cells in vitro and in vivo. *Bioorganic and Medicinal Chemistry*. 2014;22(17):4948-4954. doi:10.1016/j.bmc.2014.06.039

116. Kacar O, Adiguzel Z, Yilmaz VT, et al. Evaluation of the molecular mechanisms of a palladium(II) saccharinate complex with terpyridine as an anticancer agent. *Anti-Cancer Drugs*. 2014;25(1):17-29. doi:10.1097/CAD.0b013e328364c6ad

117. Kacar O, Cevatemre B, Hatipoglu I, et al. The role of cell cycle progression for the apoptosis of cancer cells induced by palladium(II)-saccharinate complexes of terpyridine. *Bioorganic and Medicinal Chemistry*. 2017;25(6):1770-1777. doi:10.1016/j.bmc.2017.01.033

118. Ulukaya E, Ari F, Dimas K, Ikitimur EI, Guney E, Yilmaz VT. Anti-cancer activity of a novel palladium(II) complex on human breast cancer cells in vitro and in vivo.

European Journal of Medicinal Chemistry. 2011;46(10):4957-4963. doi:10.1016/j.ejmech.2011.07.055

119. Adiguzel Z, Baykal AT, Kacar O, Yilmaz VT, Ulukaya E, Acilan C. Biochemical and proteomic analysis of a potential anticancer agent: Palladium(II) saccharinate complex of terpyridine acting through double strand break formation. *Journal of Proteome Research*. 2014;13(11):5240-5249. doi:10.1021/pr5006718

120. Cetin Y, Adiguzel Z, Polat HU, et al. A palladium(II)-saccharinate complex of terpyridine exerts higher anticancer potency and less toxicity than cisplatin in a mouse allograft model. *Anti-Cancer Drugs*. 2017;28(8):898-910. doi:10.1097/CAD.0000000000000531

121. Quirante J, Ruiz D, Gonzalez A, et al. Platinum(II) and palladium(II) complexes with (N,N′) and (C,N,N′)-ligands derived from pyrazole as anticancer and antimalarial agents: Synthesis, characterization and in vitro activities. *Journal of Inorganic Biochemistry*. 2011;105(12):1720-1728. doi:10.1016/j.jinorgbio.2011.09.021

122. Deepthi SB, Trivedi R, Sujitha P, Kumar CG, Sridhar B, Bhargava SK. Synthesis, characterization and cytotoxic activity of palladium (II) carbohydrate complexes. *Journal of Chemical Sciences*. 2012;124(6):1405-1413. doi:10.1007/s12039-012-0340-3

123. Ari F, Ulukaya E, Sarimahmut M, Yilmaz VT. Palladium(II) saccharinate complexes with bis(2-pyridylmethyl)amine induce cell death by apoptosis in human breast cancer cells in vitro. *Bioorganic and Medicinal Chemistry*. 2013;21(11):3016-3021. doi:10.1016/j.bmc.2013.03.073

124. El-Asmy HA, Butler IS, Mouhri ZS, Jean-Claude BJ, Emmam MS, Mostafa SI. Zinc(II), ruthenium(II), rhodium(III), palladium(II), silver(I), platinum(II) and MoO 2 2 + complexes of 2-(2′-hydroxy-5′- methylphenyl)-benzotriazole as simple or primary ligand and 2,2′- bipyridyl, 9,10-phenanthroline or triphenylphosphine as secondary. *Journal of Molecular Structure*. 2014;1059(1):193-201. doi:10.1016/j.molstruc.2013.11.039

125. Deepthi SB, Trivedi R, Giribabu L, Sujitha P, Kumar CG. Palladium(II) carbohydrate complexes of alkyl, aryl and ferrocenyl esters and their cytotoxic activities. *Inorganica Chimica Acta*. 2014;416:164-170. doi:10.1016/j.ica.2014.03.018

126. Chukwu JU, López C, González A, et al. Pd(II) complexes with N-substituted pyrazoles as ligands. the influence of the R group [OMe versus NMe2] of [1-{R-(CH2)2-}-3,5-Ph2-(C3HN2)] on their cytotoxic activity on breast cancer cell lines. *Journal of Organometallic Chemistry*. 2014;766:13-21. doi:10.1016/j.jorganchem.2014.04.034

127. Reddy ER, Trivedi R, Sarma AVS, et al. Sugar-boronate ester scaffold tethered pyridyl-imine palladium(II) complexes: Synthesis and their in vitro anticancer evaluation. *Dalton Transactions*. 2015;44(40):17600-17616. doi:10.1039/c5dt03266k

128. McNeill SM, Preston D, Lewis JEM, et al. Biologically active $[Pd_2L_4]^{4+}$ quadruply-stranded helicates: stability and cytotoxicity. *Dalton Trans*. 2015;44(24):11129-11136. doi:10.1039/C5DT01259G

129. Živanović M, Košarić J, Šmit B, Šeklić D, Pavlivić R, Marković S. Novel seleno-hydantoin palladium(II) complex – antimigratory, cytotoxic and prooxidative potential

on human colon HCT-116 and breast MDA-MB-231 cancer cells Marko. *General Physiology and Biophysics*. 2017;36:187-196. doi:10.4149/gpb

130. Hung FF, Wu SX, To WP, et al. Palladium(II) Acetylide Complexes with Pincer-Type Ligands: Photophysical Properties, Intermolecular Interactions, and Photo-cytotoxicity. *Chemistry - An Asian Journal*. 2017;12(1):145-158. doi:10.1002/asia.201601414

131. Ćoćić D, Jovanović S, Nišavić M, et al. New dinuclear palladium(II) complexes: Studies of the nucleophilic substitution reactions, DNA/BSA interactions and cytotoxic activity. *Journal of Inorganic Biochemistry*. 2017;175(April):67-79. doi:10.1016/j.jinorgbio.2017.07.009

132. Plutín AM, Mocelo R, Alvarez A, et al. On the cytotoxic activity of Pd(II) complexes of N,N-disubstituted- N′-acyl thioureas. *Journal of Inorganic Biochemistry*. 2014;134:76-82. doi:10.1016/j.jinorgbio.2014.01.022

133. Navarro M, Peña NP, Colmenares I, González T, Arsenak M, Taylor P. Synthesis and characterization of new palladium-clotrimazole and palladium-chloroquine complexes showing cytotoxicity for tumor cell lines in vitro. *Journal of Inorganic Biochemistry*. 2006;100(1):152-157. doi:10.1016/j.jinorgbio.2005.10.013

134. Campanella NC, da Silva Demartini M, Torres C, De Almeida ET, Gouvêa CMCP. The cytotoxic and growth inhibitory effects of palladium(ii) complexes on MDA-MB-435 cells. *Genetics and Molecular Biology*. 2012;35(1):159-163. doi:10.1590/S1415-47572012005000016

135. Pruchnik H, Lis T, Latocha M, Zielińska A, Pruchnik FP. Palladium(II) complexes with tris(2-carboxyethyl)phosphine, structure, reactions and cytostatic activity. *Journal of Inorganic Biochemistry*. 2016;156:14-21. doi:10.1016/j.jinorgbio.2015.12.001

136. Padhye S, Afrasiabi Z, Sinn E, Fok J, Mehta K, Rath N. Antitumor metallothiosemicarbazonates: Structure and antitumor activity of palladium complex of phenanthrenequinone thiosemicarbazone. *Inorganic Chemistry*. 2005;44(5):1154-1156. doi:10.1021/ic048214v

137. Kovala-Demertzi D, Boccarelli A, Demertzis MA, Coluccia M. In vitro antitumor activity of 2-acetyl pyridine 4N-ethyl thiosemicarbazone and its platinum(II) and palladium(II) complexes. *Chemotherapy*. 2007;53(2):148-152. doi:10.1159/000099986

138. Jagadeesh M, Rashmi HK, Subba Rao Y, et al. Synthesis and spectroscopic characterization of 3,4-difluoroacetophenone- thiosemicarbazone and its palladium(II) complex: Evaluation of antimicrobial and antitumour activity. *Spectrochimica Acta - Part A: Molecular and Biomolecular Spectroscopy*. 2013;115:583-587. doi:10.1016/j.saa.2013.06.071

139. Bakalova A, Buyukliev R, Momekov G. Palladium complexes with 3-substituted derivatives of 5-methyl-5-(4-pyridyl)hydantoins. Synthesis, study and in vitro cytotoxicity. *Croatica Chemica Acta*. 2014;87(3):195-199. doi:10.5562/cca2360

140. Wu N, Zhang J, Zhao J, et al. Precision medicine based on tumorigenic signaling pathways for triple-negative breast cancer. *Oncology letters*. 2018;16(4):4984-4996. doi:10.3892/ol.2018.9290

REFERENCES

141. Koff J, Ramachandiran S, Bernal-Mizrachi L. A Time to Kill: Targeting Apoptosis in Cancer. *International Journal of Molecular Sciences*. 2015;16(2):2942-2955. doi:10.3390/ijms16022942

142. Pitts TM, Davis SL, Eckhardt SG, Bradshaw-Pierce EL. Targeting nuclear kinases in cancer: Development of cell cycle kinase inhibitors. *Pharmacology & Therapeutics*. 2014;142(2):258-269. doi:10.1016/J.PHARMTHERA.2013.12.010

143. Somasundaram V, Nadhan R, K. Hemalatha S, Kumar Sengodan S, Srinivas P. Nitric oxide and reactive oxygen species: Clues to target oxidative damage repair defective breast cancers. *Critical Reviews in Oncology/Hematology*. 2016;101:184-192. doi:10.1016/J.CRITREVONC.2016.03.004

144. Bertheloot D, Latz E, Franklin BS. Necroptosis, pyroptosis and apoptosis: an intricate game of cell death. *Cellular & Molecular Immunology*. 2021;18(5):1106-1121. doi:10.1038/s41423-020-00630-3

145. Ulukaya E, Frame FM, Cevatemre B, et al. Differential Cytotoxic Activity of a Novel Palladium-Based Compound on Prostate Cell Lines, Primary Prostate Epithelial Cells and Prostate Stem Cells. *PLOS ONE*. 2013;8(5):e64278. doi:10.1371/JOURNAL.PONE.0064278

146. Cocco S, Leone A, Piezzo M, et al. Targeting Autophagy in Breast Cancer. *International Journal of Molecular Sciences*. 2020;21(21):7836. doi:10.3390/ijms21217836

147. Verzella D, Pescatore A, Capece D, et al. Life, death, and autophagy in cancer: NF-κB turns up everywhere. *Cell Death & Disease 2020 11:3*. 2020;11(3):1-14. doi:10.1038/s41419-020-2399-y

148. Nikoletopoulou V, Markaki M, Palikaras K, Tavernarakis N. Crosstalk between apoptosis, necrosis and autophagy. *Biochimica et Biophysica Acta (BBA) - Molecular Cell Research*. 2013;1833(12):3448-3459. doi:10.1016/j.bbamcr.2013.06.001

149. Jung S, Jeong H, Yu SW. Autophagy as a decisive process for cell death. *Experimental & Molecular Medicine*. 2020;52(6):921-930. doi:10.1038/s12276-020-0455-4

150. Škubník J, Svobodová Pavlíčková V, Ruml T, Rimpelová S. Autophagy in cancer resistance to paclitaxel: Development of combination strategies. *Biomedicine & Pharmacotherapy*. 2023;161:114458. doi:10.1016/j.biopha.2023.114458

151. Agostinelli E, Marques MPM, Calheiros R, et al. Polyamines: Fundamental characters in chemistry and biology. *Amino Acids*. 2010;38(2):393-403. doi:10.1007/s00726-009-0396-7

152. Nowotarski SL, Woster PM, Casero RA, Jr. Polyamines and cancer: implications for chemotherapy and chemoprevention. *Expert reviews in molecular medicine*. 2013;15:e3. doi:10.1017/erm.2013.3

153. Murray-Stewart TR, Woster PM, Casero RA. Targeting polyamine metabolism for cancer therapy and prevention. *Biochemical Journal*. 2016;473(19). doi:10.1042/BCJ20160383

154. Palmer AJ, Wallace HM. The polyamine transport system as a target for anticancer drug development. *Amino Acids*. 2010;38(2):415-422. doi:10.1007/s00726-009-0400-2

155. Batista de Carvalho ALM, Pilling M, Gardner P, et al. Chemotherapeutic response to cisplatin-like drugs in human breast cancer cells probed by vibrational microspectroscopy. *Faraday Discussions*. 2016;187(0):273-298. doi:10.1039/C5FD00148J

156. Fiuza SM, Amado AM, Parker SF, Marques MPM, Batista de Carvalho LAE. Conformational insights and vibrational study of a promising anticancer agent: the role of the ligand in Pd(II)–amine complexes. *New Journal of Chemistry*. 2015;39(8):6274-6283. doi:10.1039/C5NJ01088H

157. Corduneanu O, Chiorcea-Paquim AM, Diculescu V, Fiuza SM, Marques MPM, Oliveira-Brett AM. DNA Interaction with Palladium Chelates of Biogenic Polyamines Using Atomic Force Microscopy and Voltammetric Characterization. *Analytical Chemistry*. 2010;82(4):1245-1252. doi:10.1021/ac902127d

158. Linsalata M, Orlando A, Ruso F. Pharmacological and dietary agents for colorectal cancer chemoprevention: Effects on polyamine metabolism (Review). *International Journal of Oncology*. 2014;45(5):1802-1812. doi:10.3892/ijo.2014.2597

159. Codina G, Caubet A, López C, Moreno V, Molins E. Palladium(II) and Platinum(II) Polyamine Complexes: X-Ray Crystal Structures of (SP-4-2)-Chloro{N-[(3-amino-κN)propyl]propane-1,3-diamine-κN,κN′}palladium(1+) Tetrachloropalladate (2-) (2 : 1) and (R,S)-Tetrachloro[μ-(spermine)]dipalladium(II) (={μ-{N,N′-Bis[(3-amino-κN)propyl]butane-1,4-diamine-κN:κN′}}tetrachlorodipalladium). *Helvetica Chimica Acta*. 1999;82(7):1025-1037. doi:10.1002/(SICI)1522-2675(19990707)82:7<1025::AID-HLCA1025>3.0.CO;2-1

160. Batista de Carvalho LAE, Marques MPM, Martin C, Parker SF, Tomkinson J. Inelastic Neutron Scattering Study of Pt ^{II} Complexes Displaying Anticancer Properties. *ChemPhysChem*. 2011;12(7):1334-1341. doi:10.1002/cphc.201001067

161. Navarro-Ranninger C, Ochoa PA, Pérez JM, González VM, Masaguer JR, Alonso C. Platinum (II) and (IV) spermidine complexes. Synthesis, characterization, and biological studies. *Journal of Inorganic Biochemistry*. 1994;53(3):177-190. doi:10.1016/0162-0134(94)80003-0

162. Zhang T, Cai S, Forrest WC, Mohr E, Yang Q, Forrest ML. Development and validation of an inductively coupled plasma mass spectrometry (ICP-MS) method for quantitative analysis of platinum in plasma, urine, and tissues. *Applied Spectroscopy*. 2016;70(9):1529-1536. doi:10.1177/0003702816662607

163. Zimmermann S, Menzel CM, Berner Z, et al. Trace analysis of platinum in biological samples: A comparison between sector field ICP-MS and adsorptive cathodic stripping voltammetry following different digestion procedures. *Analytica Chimica Acta*. 2001;439(2):203-209. doi:10.1016/S0003-2670(01)01041-8

164. Rudolph E, Hann S, Stingeder G, Reiter C. Ultra-trace analysis of platinum in human tissue samples. *Analytical and Bioanalytical Chemistry*. 2005;382(7):1500-1506. doi:10.1007/s00216-005-3370-6

REFERENCES

165. Van Stralen KJ, Jager KJ, Zoccali C, Dekker FW. Agreement between methods. *Kidney International*. 2008;74(9):1116-1120. doi:10.1038/ki.2008.306

166. Azar HA, Hansen CT, Costa J. N:NIH(S)II-nu/nu Mice With Combined Immunodeficiency: A New Model for Human Tumor Heterotransplantation. *JNCI: Journal of the National Cancer Institute*. 1980;65(2):421-430. doi:https://doi.org/10.1093/jnci/65.2.421

167. Carlsson G, Gullberg B, Hafström L. Estimation of liver tumor volume using different formulas-An experimental study in rats. *Journal of Cancer Research and Clinical Oncology*. 1983;105(1):20-23. doi:10.1007/BF00391826

168. Law AMK, Yin JXM, Castillo L, et al. Andy's Algorithms: New automated digital image analysis pipelines for FIJI. *Scientific Reports*. 2017;7(1):1-11. doi:10.1038/s41598-017-15885-6

169. Ribatti D, Vacca A, Roncali L, Dammacco F. The Chick Embryo Chorioallantoic Membrane as a Model for in vivo Research on Anti-Angiogenesis. *Current Pharmaceutical Biotechnology*. 2000;1(1):73-82. doi:10.2174/1389201003379040

170. Carpentier G, Martinelli M, Courty J, Cascone I. Angiogenesis Analyzer for ImageJ. In: *4th ImageJ User and Developer Conference Proceedings.* Mondorf-les-Bains,; 2012:198-201.

171. Ribatti D, Nico B, Ruggieri S, Tamma R, Simone G, Mangia A. Angiogenesis and Antiangiogenesis in Triple-Negative Breast cancer. *Translational oncology*. 2016;9(5):453-457. doi:10.1016/J.TRANON.2016.07.002

172. Liu B, Han M, Sun RH, et al. ABL-N-induced apoptosis in human breast cancer cells is partially mediated by c-Jun NH2-terminal kinase activation. *Breast Cancer Research*. 2010;12(1):R9. doi:10.1186/bcr2475

173. Ji X, Wang R, Tang H, et al. Necroptosis of osteoblasts was induced by breast cancer cells in vitro. *Translational Cancer Research*. 2020;9(2):500-507. doi:10.21037/TCR.2019.11.32

174. Rodrigues EG, Silva LS, Fausto DM, et al. Cyclopalladated compounds as chemotherapeutic agents: Antitumor activity against a murine melanoma cell line. *International Journal of Cancer*. 2003;107(3):498-504. doi:10.1002/IJC.11434

175. Frik M, Fernández-Gallardo J, Gonzalo O, et al. Cyclometalated Iminophosphorane Gold(III) and Platinum(II) Complexes. A Highly Permeable Cationic Platinum(II) Compound with Promising Anticancer Properties. *Journal of Medicinal Chemistry*. 2015;58(15):5825-5841. doi:10.1021/ACS.JMEDCHEM.5B00427

176. Xi H, Wang S, Wang B, et al. The role of interaction between autophagy and apoptosis in tumorigenesis (Review). *Oncology Reports*. 2022;48(6):1-16. doi:10.3892/OR.2022.8423/HTML

177. McAleese CE, Butcher NJ, Minchin RF. Arylamine N-acetyltransferase 1 deficiency inhibits drug-induced cell death in breast cancer cells: switch from cytochrome C-dependent apoptosis to necroptosis. *Breast Cancer Research and Treatment*. 2022;195(3):223-236. doi:10.1007/S10549-022-06668-3

178. Flamme M, Cressey PB, Lu C, et al. Induction of Necroptosis in Cancer Stem Cells using a Nickel(II)-Dithiocarbamate Phenanthroline Complex. *Chemistry – A European Journal*. 2017;23(40):9674-9682. doi:10.1002/CHEM.201701837

179. Polloni L, Seni Silva AC de, Teixeira SC, et al. Action of copper(II) complex with β-diketone and 1,10-phenanthroline (CBP-01) on sarcoma cells and biological effects under cell death. *Biomedicine & Pharmacotherapy*. 2019;112:108586. doi:10.1016/J.BIOPHA.2019.01.047

180. Verwey M, Nolte EM, Joubert AM, Theron AE. Autophagy induced by a sulphamoylated estrone analogue contributes to its cytotoxic effect on breast cancer cells. *Cancer Cell International*. 2016;16(1):1-17. doi:10.1186/S12935-016-0367-5

181. Koubkova L, Vyzula R, Karban J, et al. Evaluation of cytotoxic activity of titanocene difluorides and determination of their mechanism of action in ovarian cancer cells. *Investigational New Drugs*. 2015;33(5):1123-1132. doi:10.1007/S10637-015-0274-Y

182. Sun L, Liu N, Liu SS, et al. Beclin-1-independent autophagy mediates programmed cancer cell death through interplays with endoplasmic reticulum and/or mitochondria in colbat chloride-induced hypoxia. *American Journal of Cancer Research*. 2015;5(9):2626.

183. Jiang Y, Ji F, Liu Y, et al. Cisplatin-induced autophagy protects breast cancer cells from apoptosis by regulating yes-associated protein. *Oncology Reports*. 2017;38(6):3668-3676. doi:10.3892/OR.2017.6035

184. Chang H, Zou Z. Targeting autophagy to overcome drug resistance: further developments. *Journal of Hematology & Oncology 2020 13:1*. 2020;13(1):1-18. doi:10.1186/S13045-020-01000-2

185. Sui X, Kong N, Ye L, et al. p38 and JNK MAPK pathways control the balance of apoptosis and autophagy in response to chemotherapeutic agents. *Cancer Letters*. 2014;344(2):174-179. doi:10.1016/J.CANLET.2013.11.019

186. Brouwers EE, Tibben MM, Rosing H, et al. Sensitive inductively coupled plasma mass spectrometry assay for the determination of platinum originating from cisplatin, carboplatin, and oxaliplatin in human plasma ultrafiltrate. *Journal of Mass Spectrometry*. 2006;41(August):1186-1194. doi:10.1002/jms

187. Ducoulombier-Crépineau C, Feidt C, Rychen G. Platinum and Palladium transfer to milk, organs and tissues after a single oral administration to lactating goats. *Chemosphere*. 2007;68(4):712-715. doi:10.1016/j.chemosphere.2007.01.029

188. Zhao D, Zhang Y, Xu C, et al. Pharmacokinetics, tissue distribution, and plasma protein binding study of platinum originating from dicycloplatin, a novel antitumor supramolecule, in rats and dogs by ICP-MS. *Biological Trace Element Research*. 2012;148(2):203-208. doi:10.1007/s12011-012-9364-2

189. Bettinelli M. ICP-MS determination of Pt in biological fluids of patients treated with antitumor agents: Evaluation of analytical uncertainty. *Microchemical Journal*. 2005;79(1-2):357-365. doi:10.1016/j.microc.2004.08.003

190. Lemoine L, Thijssen E, Noben JP, Adriaensens P, Carleer R, Speeten KV der. A validated inductively coupled plasma mass spectrometry (ICP-MS) method for the quantification of total platinum content in plasma, plasma ultrafiltrate, urine and

peritoneal fluid. *Journal of Pharmaceutical and Biomedical Analysis*. 2018;152:39-46. doi:10.1016/j.jpba.2018.01.033

191. Bettinelli M, Spezia S, Ronchi A, Minoia C. Determination of Pt in biological fluids with ICP-MS: Evaluation of analytical uncertainty. *Atomic Spectroscopy*. 2004;25(3):103-111.

192. Morrison JG, White P, Mcdougall S, et al. Validation of a highly sensitive ICP-MS method for the determination of platinum in biofluids. *Journal of Pharmaceutical and Biomedical Analysis*. 2000;24:1-10.

193. Breda M, Maffini M, Mangia A, Mucchino C, Musci M. Development and validation of an inductively coupled plasma mass spectrometry method with optimized microwave-assisted sample digestion for the determination of platinum at ultratrace levels in plasma and ultrafiltrate plasma. *Journal of Pharmaceutical and Biomedical Analysis*. 2008;48(2):435-439. doi:10.1016/j.jpba.2008.04.013

194. Ding H, Goldberg MM, Raymer JH, Holmes J, Stanko J, Chaney SG. Determination of platinum in rat dorsal root ganglion using ICP-MS. *Biological Trace Element Research*. 1999;67(1):1-11. doi:10.1007/BF02784270

195. Hanada K, Ninomiya K, Ogata H. Pharmacokinetics and Toxicodynamics of Cisplatin and Its Metabolites in Rats: Relationship between Renal Handling and Nephrotoxicity of Cisplatin. *Journal of Pharmacy and Pharmacology*. 2000;52(11):1345-1353. doi:10.1211/0022357001777496

196. Bohnert T, Gan LS. Plasma protein binding: From discovery to development. *Journal of Pharmaceutical Sciences*. 2013;102(9):2953-2994. doi:10.1002/jps.23614

197. Ueda T, Yasumasu T, Uozumi J. Experimental studies on the pharmacokinetics and nephrotoxicity of carboplatin (cis-diammine-1, 1-cyclobutane dicarboxylate platinum II) in rats. *Journal of Toxicological Sciences*. 1991;16(3):101-109. doi:10.2131/jts.16.101

198. Kato R, Sato T, Iwamoto A, et al. Interaction of platinum agents, cisplatin, carboplatin and oxaliplatin against albumin *in vivo* rats and *in vitro* study using inductively coupled plasma-mass spectrometory. *Biopharmaceutics & Drug Disposition*. 2019;40(7):242-249. doi:10.1002/bdd.2197

199. Yasumasu T, Ueda T, Uozumi J, Mihara Y, Kumazawa J. Comparative Study of Cisplatin and Carboplatin on Pharmacokinetics, Nephrotoxicity and Effect on Renal Nuclear DNA Synthesis in Rats. *Pharmacology & Toxicology*. 1992;70(2):143-147. doi:10.1111/j.1600-0773.1992.tb00445.x

200. Will J, Wolters DA, Sheldrick WS. Characterisation of cisplatin binding sites in human serum proteins using hyphenated multidimensional liquid chromatography and ESI tandem mass spectrometry. *ChemMedChem*. 2008;3(11):1696-1707. doi:10.1002/cmdc.200800151

201. Sooriyaarachchi M, Narendran A, Gailer J. Comparative hydrolysis and plasma protein binding of cis-platin and carboplatin in human plasma in vitro. *Metallomics*. 2011;3(1):49-55. doi:10.1039/c0mt00058b

202. Li Y, Meng F, Chen Z, et al. Pharmacokinetics and tissue distribution in rats of a novel anticancer platinum compound LLC-1903. *Xenobiotica*. 2020;50(8):980-987. doi:10.1080/00498254.2020.1728421

203. Zhao J, Wen Y, Zhang W, et al. Investigation on pharmacokinetics, tissue distribution and excretion of a novel platinum anticancer agent in rats by Inductively Coupled Plasma Mass Spectrometry (ICP-MS). *Xenobiotica*. 2014;44(8):757-762. doi:10.3109/00498254.2014.889333

204. Navolotskii DV, Ivanenko NB, Solovyev ND, Fedoros EI, Panchenko AV. Pharmacokinetics and tissue distribution of novel platinum containing anticancer agent BP-C1 studied in rabbits using sector field inductively coupled plasma mass spectrometry. *Drug Testing and Analysis*. 2015;7(9):737-744. doi:10.1002/dta.1824

205. Perše M, Veceric-Haler Z. Cisplatin-Induced Rodent Model of Kidney Injury : Characteristics and Challenges. *BioMed Research International*. 2018;2018:1-29. doi:10.1155/2018/1462802

206. Esteban-Fernández D, Verdaguer JM, Ramírez-Camacho R, Palacios MA, Gómez-Gómez MM. Accumulation, fractionation, and analysis of platinum in toxicologically affected tissues after cisplatin, oxaliplatin, and carboplatin administration. *Journal of Analytical Toxicology*. 2008;32(2):140-146. doi:10.1093/jat/32.2.140

207. Wang X, Au-Yeung SCF, Ho YP. Pharmacokinetics and tissue distribution of novel traditional Chinese medicine-platinum anticancer agents in rats. *Journal of Inorganic Biochemistry*. 2007;101(6):909-917. doi:10.1016/j.jinorgbio.2007.02.007

208. Jahromi EZ, Divsalar A, Saboury AA, Khaleghizadeh S, Mansouri-Torshizi H, Kostova I. Palladium complexes: New candidates for anti-cancer drugs. *Journal of the Iranian Chemical Society*. 2016;13(5):967-989. doi:10.1007/s13738-015-0804-8

209. Divsalar A, Saboury AA, Ahadi L, et al. Biological evaluation and interaction of a newly designed anti-cancer pd(II) complex and human serum albumin. *Journal of Biomolecular Structure and Dynamics*. 2011;29(2):283-296. doi:10.1080/07391102.2011.10507385

210. Carneiro TJ, Araújo R, Vojtek M, et al. Multi-organ NMR metabolomics to assess in vivo overall metabolic impact of cisplatin in mice. *Metabolites*. 2019;9(11). doi:10.3390/metabo9110279

211. Carneiro TJ, Araújo R, Vojtek M, et al. Novel Insights into Mice Multi-Organ Metabolism upon Exposure to a Potential Anticancer Pd(II)-Agent. *Metabolites*. 2021;11(2):114. doi:10.3390/metabo11020114

212. Vojtek M, Gonçalves-Monteiro S, Pinto E, et al. Preclinical Pharmacokinetics and Biodistribution of Anticancer Dinuclear Palladium(II)-Spermine Complex (Pd2Spm) in Mice. *Pharmaceuticals 2021, Vol 14, Page 173*. 2021;14(2):173. doi:10.3390/PH14020173

213. Sun X, Kaufman PD. Ki-67: more than a proliferation marker. *Chromosoma*. 2018;127(2):175-186. doi:10.1007/S00412-018-0659-8

214. Perše M. Cisplatin Mouse Models: Treatment, Toxicity and Translatability. *Biomedicines 2021, Vol 9, Page 1406*. 2021;9(10):1406. doi:10.3390/BIOMEDICINES9101406

215. Yamamoto N, Murata K, Fuke H, et al. Macrocytic Anemia during Low-dose Cisplatin and 5-Fluorouracil through Implanted Infusion Port for Unresectable Hepatobilliary Malignancies. *Anticancer Research*. 2005;25(2B).

REFERENCES

216. Fei L, Huimei H, Dongmin C. Pivalopril improves anti-cancer efficiency of cDDP in breast cancer through inhibiting proliferation, angiogenesis and metastasis. *Biochemical and Biophysical Research Communications*. 2020;533(4):853-860. doi:10.1016/J.BBRC.2020.07.059

217. Duyndam MCA, van Berkel MPA, Dorsman JC, Rockx DAP, Pinedo HM, Boven E. Cisplatin and doxorubicin repress Vascular Endothelial Growth Factor expression and differentially down-regulate Hypoxia-inducible Factor I activity in human ovarian cancer cells. *Biochemical pharmacology*. 2007;74(2):191-201. doi:10.1016/J.BCP.2007.04.003

218. Aydinlik S, Uvez A, Kiyan HT, et al. Palladium (II) complex and thalidomide intercept angiogenic signaling via targeting FAK/Src and Erk/Akt/PLCγ dependent autophagy pathways in human umbilical vein endothelial cells. *Microvascular Research*. 2021;138:104229. doi:10.1016/J.MVR.2021.104229

219. Tummala R, Diegelman P, Fiuza SM, et al. Characterization of Pt-, Pd-spermine complexes for their effect on polyamine pathway and cisplatin resistance in A2780 ovarian carcinoma cells. *Oncology reports*. 2010;24(1):15-24. doi:10.3892/or_00000823

ANNEX – SUPPLEMENTARY MATERIAL

Appendix A

Table A1.Reagents.

Description	Supplier
1:1 mixture of Dulbecco's Modified Eagle's Medium and Ham's F12 cell growth medium (DMEM/F12 1:1)	Sigma-Aldrich Chemical S.A., Sintra, Portugal
3-methyladenine	Sigma-Aldrich Chemical S.A., Sintra, Portugal
Acetic acid glacial (99.7%)	Sigma-Aldrich Chemical S.A., Sintra, Portugal
AlphaScreen SureFire pERK1/2 Kit	PerkinElmer, I.L.C., Lisboa, Portugal
AlphaScreen SureFire pNF-κB Kit	PerkinElmer, I.L.C., Lisboa, Portugal
Bovine insulin (10 mg/mL insulin in 25 mM HEPES, pH 8.2)	Sigma-Aldrich Chemical S.A., Sintra, Portugal
Carboplatin (cis-Diammine(1,1-cyclobutanedicarboxylato)platinum(II), ≥99%)	Tocris – Biogen Científica, Madrid, Spain
Cholera toxin from Vibrio cholerae	Sigma-Aldrich Chemical S.A., Sintra, Portugal
Cisplatin (cis-dichlorodiammine platinum(II), 99.9%)	Sigma-Aldrich Chemical S.A., Sintra, Portugal
Dimethyl-sulphoxide (DMSO)	Sigma-Aldrich Chemical S.A., Sintra, Portugal
Dulbecco's Modi-fied Eagle's Medium—high-glucose cell growth medium (DMEM-HG)	Sigma-Aldrich Chemical S.A., Sintra, Portugal
Ethanol (99.8%)	Sigma-Aldrich S.A., Sintra, Portugal
Ethylenediaminetetraacetic acid (EDTA) (≥ 98.5%)	Sigma-Aldrich S.A., Sintra, Portugal
Euthasol® solution (400 mg/mL pentobarbital sodium)	Le Vet, Oudewater, Netherlands
Fetal bovine serum (EU approved, South America)	Gibco, Thermo Fisher Scientific, Inc., Waltham, MA, USA.
Hanks' Balanced solution 1X	Sigma-Aldrich Chemical S.A., Sintra, Portugal
Horse serum (New Zealand)	Gibco, Thermo Fisher Scientific, Inc., Waltham, MA, USA.
Human epidermal growth factor (hEGF; recombinant, expressed in E. coli)	Sigma-Aldrich Chemical S.A., Sintra, Portugal
Human VEGF Quantikine ELISA Kit	R&D Systems Inc., Minneapolis, MN, USA
Hydrochloric acid (HCl, TraceSELECT™, ≥ 30%)	Honeywell Fluka™, Düsseldorf, Germany.
Hydrocortisone	Sigma-Aldrich Chemical S.A., Sintra, Portugal
In Situ Cell Death Detection Kit	Roche Diagnostics GmbH, Mannheim, Germany
Internal standard solution ICP-MS-200.8-IS-1 (100 mg/L of Sc, Y, In, Tb, Bi)	AccuStandard®, New Haven, CT, USA

ANNEX

Description	Supplier
IsoFlo®, 100% isoflurane	Abbott, Berkshire, UK
Monodansylcadaverine	Sigma-Aldrich Chemical S.A., Sintra, Portugal
Multi-element standard solution TraceCERT® (100 mg/L), ICH Q3D oral, Standard 2 solution	Merck KGaA, Darmstadt, Germany
Necrostatin-1	R&D Systems Inc., Minneapolis, MN, USA
Nitric acid (HNO3, TraceSELECT™, ≥ 69.0%)	Honeywell Fluka™, Düsseldorf, Germany.
Novex ECL Chemiluminescent kit	Invitrogen, Life Technologies, Madrid, Spain
Novolink Polymer Detection Systems	Leica Biosystems Inc., Buffalo Grove, IL, USA
Oxaliplatin ((Oxalato[(1R-trans)-1,2-cyclohexanediamine]platinum(II), ≥99%)	Tocris – Biogen Científica, Madrid, Spain
Pd ICP-MS standard solution (palladium(II) nitrate) 1000 mg/L	Merck KGaA, Darmstadt, Germany
Polarity-sensitive probe pSIVA-IANBD	Bio-Rad, Lisbon, Portugal
Potassium chloride	Sigma-Aldrich S.A., Sintra, Portugal
Potassium tetrachloropalladate (II) (K2PdCl4, 98%)	Sigma-Aldrich Chemical S.A., Sintra, Portugal
Pt ICP-MS standard solution (hydrogen hexachloroplatinate(IV)) 1000 mg/L	Merck KGaA, Darmstadt, Germany
Rabbit anti-caspase-3, cleaved antibody	Abcam, London, UK
rabbit anti-LC3B antibody	Merck, Lisbon, Portugal
RIPA buffer supplemented with protease inhibitors cocktail	Abcam, London, UK
SDS–PAGE using 12% TGX Stain-free gels	Bio-Rad, Lisbon, Portugal
Sodium bicarbonate (NaHCO3, ≥99.0%)	Sigma-Aldrich Chemical S.A., Sintra, Portugal
Sodium chloride (99.0%)	Sigma-Aldrich S.A., Sintra, Portugal
Sodium hydroxide	Sigma-Aldrich S.A., Sintra, Portugal
Sodium phosphate dibasic (≥ 99.0%)	Sigma-Aldrich S.A., Sintra, Portugal
Spermidine (N1-(3-Aminopropyl)butane-1,4-diamine, 99%)	Sigma-Aldrich Chemical S.A., Sintra, Portugal
Spermine (N,N'-bis(3-aminopropyl)-1,4-diaminobutane, 99%)	Sigma-Aldrich Chemical S.A., Sintra, Portugal
Trypan blue (0.4% w/v)	Sigma-Aldrich Chemical S.A., Sintra, Portugal
Trypsin-EDTA (1×)	Gibco-Life Technologies, Porto, Portugal
Z-VAD-FMK	R&D Systems Inc., Minneapolis, MN, USA

Table A2. Materials

Description	**Supplier**
12-well cell culture plate	TPP Techno Plastic Products AG, Trasadingen, Switzerland
23G needles	BD Falcon, Enzifarma, Portugal
5 mL syringes	BD Falcon, Enzifarma, Portugal
96-well cell culture plate	TPP Techno Plastic Products AG, Trasadingen, Switzerland
Amicon Ultra-0.5mL Centrifugal Filters with 30K NMWL	Merck KGaA, Darmstadt, Germany
Cell culture flask, T-25	Sarstedt, Nümbrecht, Germany
Cell culture flask, T-75	Sarstedt, Nümbrecht, Germany
Polypropylene 10 mL tubes with high-density polyethylene screw caps (Ref# 62.9924.284)	Sarstedt, Nümbrecht, Germany
Screw cap tube 15 mL	Sarstedt, Nümbrecht, Germany
Screw cap tube 50 mL	Sarstedt, Nümbrecht, Germany

Table A3. Equipment and Software.

Description	**Supplier**
ABX Micros 60 automated analyser	ABX Horiba diagnostics, Montpellier, France
Analytical balance (Toledo AB54)	Mettler, Rotoquímica, Portugal
Angiogenesis Analyser package	Paris, France
Arium® pro water purification system (ultrapure water: 18.2 MΩ.cm at 25 °C)	Sartorius, Goettingen, Germany
Automated analyser Pentra 400	ABX Horiba diagnostics, Montpellier, France
ChemiDoc MP Imaging System	Bio-Rad, Lisbon, Portugal
ChemiDoc™ Imaging Systems with Image Lab™ Software Instrument	Bio-Rad, Lisbon, Portugal
Contrast-phase microscope	Motic® AE200 inverted microscope, Spectra Services, VWR International
Design Expert Trial Version 10 software	Stat-Ease, Inc., MN, USA
Eppendorf, Centrifuge 5810 R	Eppendorf, Madrid, Spain
Gen 5 Image Analysis software	BioTek, Winooski, VT, USA
GraphPad Prism 7 Software	San Diego, CA, USA
Heracell 150 CO2 Incubator	Thermo Fisher Scientific, Bremen, Germany
iCAPTM Q ICP-MS	Thermo Fisher Scientific, Bremen, Germany
Laboratory Freeze Dryer CRYODOS	Telstar®, Barcelona, Spain
LionheartFX automated microscope	BioTek, Winooski, VT, USA

ANNEX

Description	Supplier
MLS 1200 Mega high-performance microwave digestion unit equiped with HPR-1000/10 S rotor	Milestone, Sorisole, Italy
MSC-Advantage Class II Biological Safety Cabinet	Thermo Fisher Scientific, Bremen, Germany
Multipette E3	Eppendorf, Madrid, Spain
pH-meter (Basic 20 +)	Crison, Rotoquímica, Portugal
Phoenix WinNonlin v8.3.1.5014 (free student license)	Certara USA Inc., Princeton, NJ, USA
Precellys® Evolution tissue homogenizer	Bertin-Instruments, Montigny-le-Bretonneux, France
Synergy HT Microplate reader	BioTek, Winooski, VT, USA
Vortex Mixer ZX3	Velp Scientifica, Italy